Investigations on novel polymer nano composites and bio-compatible manganese doped ZnS nanocrystals for photonic and bio-imaging applications

Thesis Submitted to
Cochin University of Science and Technology
In partial fulfillment of the requirements
for the award of the degree of
Doctor of Philosophy

By

SAJIMOL AUGUSTINE. M

Department of Physics
Cochin University of Science and Technology
Cochin-22

December 2012

Investigations on novel polymer nano composites and bio-compatible manganese doped ZnS nanocrystals for photonic and bio-imaging applications

Ph.D thesis in the field of material science

Author:

Sajimol Augustine. M
Division for Research in Advanced Materials
Department of Physics
Cochin University of Science and Technology
Cochin-682022, Kerala, India
Email: sajimollazar@gmail.com

Supervisor:

Dr. S.Jayalekshmi
Professor,
Division for Research in Advanced Materials
Department of Physics
Cochin University of Science and Technology
Cochin-682022, Kerala, India
Email: jayalekshmi@cusat.ac.in

December 2012

Department of Physics
Cochin University of Science and Tecnology
***Cochin* - 682022**

Dr. S. Jayalekshmi
Professor

Certificate

Certified that the work presented in the thesis entitled **"Investigations on novel polymer nano composites and bio-compatible manganese doped ZnS nanocrystals for photonic and bio-imaging applications"** is based on the original work done by Mrs. Sajimol Augustine.M, under my guidance and supervision at the Department of Physics, Cochin University of Science and Technology, Cochin-22, India and has not been included in any other thesis submitted previously for the award of any degree.

Cochin - 22
20-12-2012

Prof.S.Jayalekshmi
(Supervising Guide)

Declaration

Certified that the work presented in the proposed thesis entitled **"Investigations on novel polymer nano composites and bio-compatible manganese doped ZnS nanocrystals for photonic and bio-imaging applications"** is based on the original work done by me under the guidance of Dr. S Jayalekshmi, Professor, Department of Physics, Cochin University of Science and Technology, Cochin–22, India and it has not been included in any other thesis submitted previously for the award of any degree.

Cochin – 22
20-12-2012

Sajimol Augustine. M

ACKNOWLEDGEMENT

At this moment of accomplishment, it is a pleasure to express my sincere thanks to all those who have contributed in many ways to the successful completion of my efforts.

I would like to express my sincere gratitude to my supervising guide, Dr. S. Jayalekshmi, Professor, Department of Physics, CUSAT, for initiating in me the drive, motivation and enthusiasm to pursue a research oriented Physics carrier. Her guidance with valuable suggestions helped me all through the course of the PhD programme. I take this opportunity to sincerely thank her for giving me the opportunity to work under her guidance. I have been fortunate to experience her constant support, encouragement and more importantly her friendship, throughout my research career.

I am grateful to Prof. B. Pradeep, Head of the Department of Physics, CUSAT and Prof. M. R. Anantharaman, the former Head, for extending all the necessary facilities and co-operation. I am indebted to Prof. M .K. Jayaraj, Doctoral committee member for the consideration shown throughout the research period. I take this opportunity to thank sincerely all the faculty members of the Department of Physics, especially Prof. K. P. Vijayakumar and Prof. C. Sudha Kartha, for their support and encouragement.

I am extremely thankful to Dr. Sarita. G. Bhat, Associate Professor and Head, Department of Biotechnology, CUSAT, for introducing me to the beautiful and intriguing biological concepts and helping generously to bring the physics related biotechnology work to a successful completion.

I would like to thank Dr. Abdulaziz Anas, Scientist, National Institute of Oceanography, Kochi and Dr. Ani. V. Das, Scientist, Rajiv Gandhi Centre for Biotechnology, Thiruvananthapuram, for the collaboration and help extended.

I would like to thank the office, library and laboratory staff of the Department of Physics for the services extended throughout my research period.

I take this opportunity to express my sincere thanks to Prof.V.P.N Nampoori, Prof. P. Radhakrishnan and Dr. Reethamma Thomas of International School of Photonics, CUSAT, for the timely help and support.

I acknowledge with gratitude the co-operation extended by Dr. I. S Bright Singh, Professor, National Centre for Aquatic Animal Health, Marine Campus, CUSAT, for providing the necessary laboratory facilities, advice and valuable suggestions.

I sincerely thank Dr. N. S. Gopalakrishnan, Chairman, The Inter University Centre for Intellectual Property Rights studies, CUSAT, for his help and co-operation related to the patenting of research results.

I acknowledge with thanks the services rendered by STIC CUSAT, SAIF IIT Madras, SAIF IIT Bombay and NIT Calicut.

I consider it a privilege to thank my colleagues in the DREAM laboratory, Department of Physics, Sreevalsa, Jeeju, Sreekanth, Anand, Anil, Francis, Rajiv Tomy and Manoj, for being with me, extending all sorts of help whenever necessary, during the entire period of my research work. I remember with thanks the encouragement and co-operation shown by senior research students Dr. Ravindranath (late), Dr.Amrithesh, Dr.Vanaja, Dr.Arun and Dr. Dhanya.

I extend my sincere thanks to all the research scholars in the Department of Physics, especially my friends in the OED, Thin Film Photovoltaics and Thin film Microelectronics laborataries, Dr.Sreeja ,Dr.Anish, Arun, Subha, Hasna, Poornima, Namitha and Urmila.

I am extremely thankful to Rev. Sr. Tessa, Manager and Dr. Sr. Teresa, Principal of St. Teresa's college for their support, encouragement and blessings. Words are inadequate to express my gratitude to Rev.Sr.Francis Ann, the former Manager and Rev. Sr. Christabelle, the former Principal, for their constant help, support and prayers.

I express my gratitude to the teaching and non-teaching staff of St. Teresa's college, Ernakulam, and all the members of the Department of Physics, for all the help and encouragement throughout my research career.

I am also grateful to University Grants Commission for providing the teacher fellowship under the FIP programme.

I express my sincere thanks to Alphonsa Vijaya, Roselin Alex and Manzur Ali of the Biotechnology Department, CUSAT, who collaborated with me for pursuing the biological applications of the materials investigated in the research work.

The help extended by Deepa. G. D and Jayesh. P. of National Centre for Aquatic Animal Health, Marine campus, CUSAT is gratefully acknowledged.

I also acknowledge with gratitude the services of Dr. S.K Vaishnavi. and Dr. M. Manjusha, patent attorneys of DePenning & DePenning, Chennai, regarding the patent filing.

I acknowledge with deep affection the love, support, patience and benevolence of my husband, Lazar Thomas Mani and my sons, Ayush and Akshay, without whose care, consideration and prayers, it would not have been possible to bring my efforts to a successful completion.

Above all, I submit everything at the feet of Almighty for the everlasting blessings showered upon me in all my endeavors.

Sajimol Augustine. M

PREFACE

The advancements in science and technology continue to make human life more and more comfortable day by day. Recent developments in nanotechnology has revolutionized all walks of human activity with immense benefits not limited to the arenas of science and technology alone, but to those influencing everyday life as well. The integration of nanotechnology with biotechnology is an attractive trend as nanotechnology can provide the analytical tools and platforms for the investigation of biological systems in the most effective way. This integration has evolved into the development of an exciting field of hybrid nanomaterials with unprecedented potential applications. New technological applications ranging from the design and assembly of electronic and optical devices to biomedical detection and imaging have been realized.

The size and shape dependent properties of the nanostructured materials have opened up, the possibilities for tuning the properties as desired, over wide ranges of the particle size. Polymer based nanocomposites have attracted attention because of their ability to modify the optical, electrical, thermal, magnetic and mechanical properties of the host polymer. Blending the properties of the polymer matrix with those of the inorganic filler often results in the development of high performance materials, in a more economic way. The technique enfolds the advantages of both polymers and filler components, leading to a wide spectrum of applications. In the first phase of the work presented in the thesis, studies on zinc oxide (ZnO) and iron disulphide (FeS_2) based polymer nanocomposite thin films for photonic applications have been addressed.

Fluorescence is a powerful tool in biological research, the relevance of which relies greatly on the availability of sensitive and selective fluorescent probes. Nanometer sized fluorescent semiconductor materials have attracted

considerable attention in recent years due to the high luminescence intensity, low photobleaching, large Stokes' shift and high photochemical stability. The optical and spectroscopic features of nanoparticles make them very convincing alternatives to traditional fluorophores in a range of applications. Efficient surface capping agents make these nanocrystals bio-compatible. They can provide a novel platform on which many biomolecules such as DNA, RNA and proteins can be covalently linked. In the second phase of the present work, bio-compatible, fluorescent, manganese doped ZnS (ZnS:Mn) nanocrystals suitable for bio-imaging applications have been developed and their cytocompatibility has been assessed. Functionalization of ZnS:Mn nanocrystals by safe materials results in considerable reduction of toxicity and allows conjugation with specific biomolecules. The highly fluorescent, bio-compatible and water- dispersible ZnS:Mn nanocrystals are found to be ideal fluorescent probes for biological labeling.

The entire research work included in the thesis is portrayed in different sections as follows:

An overview of nanoscience, nanotechnology and nanobiotechnology is given in **chapter 1**, which includes the fundamental aspects of quantum confinement in nanoscale materials, along with their properties and applications. It deals with the general aspects related to the synthesis and structural properties of semiconductor nanocrystals and its photonic/biological applications.

Chapter 2 gives a detailed description of the various experimental techniques used in the present work. The various synthesis procedures and characterization tools are dealt with in detail. The structural, optical and thermal characterizations of the samples are carried out using different sophisticated instruments and a comprehensive description of the tools utilized is included in this chapter.

The simple and cost effective synthesis of oleic acid modified ZnO nanorods and their structural and optical properties form the essence of the **3rd chapter.** The composite films of oleic acid modified ZnO nanorods in PVA matrix show high optical absorption in the UV region and enhanced photoluminescence emission. The UV filtering applications of ZnO/PVA nanocomposite thin films are also described in this chapter.

Chapter 4 deals with the synthesis of oleic acid modified polyaniline (PANI) and the effect of oleic acid modification on the photoluminescence characteristics of PANI. The enhanced emission intensity in oleic acid modified PANI is the effect of capping of oleic acid on each PANI molecule resulting in the formation of nanostructured PANI.

The solvothermal synthesis of nanocomposites of iron disulphide (FeS_2) using polyvinyl pyrrolidone (PVP) and polyvinyl alcohol (PVA) as templates is discussed in **chapter 5**. A detailed description on the structural and UV shielding properties of thin films of these nanocomposites is also included. The present work aims at developing transparent and flexible UV-shielding films and color filters using cost effective and non toxic, inorganic-polymer nanocomposites.

Chapter 6 is devoted to the systematic investigations on the synthesis of ZnS:Mn nanocrystals capped with chitosan and different aminoacids and their cytotoxicity assessment. The studies on the *in vitro* cellular uptake of these biofunctionalized ZnS:Mn nanocrystals on HEK293T cells are also addressed here.

Chapter 7 gives a detailed description of immobilization of trypsin on bio-compatible, chitosan capped ZnS:Mn nanocrystals, synthesized by chemical capping co-precipitation method, using glutaraldehyde (GA) as cross-linker. Results indicate that the activity of trypsin, immobilized on chitosan modified ZnS:Mn has been improved upon cross-linking, which suggests that the

immobilized trypsin has become more stable and active. This investigation highlights the prospects of potential applications of immobilized trypsin in therapeutic and diagnostic fields.

A novel technique for the rapid detection of a special type of bacteria which can be used for the removal of metal components from industrial effluents is described in **chapter 8.** It illustrates the synthesis of bio-compatible and highly luminescent manganese doped zinc sulphide (ZnS:Mn) nanocrystals by capping with the aminoacid ligand, L-citrulline. The bio-compatible nature of these nanocrystals and their tunable colour properties under different excitation wavelengths, make them ideal for bio-labeling applications.

Chapter 9 gives the summary and the highlights of the work presented in the thesis. The scope for further investigations based on the results of the present work is also emphasized in this chapter.

The **Annexure** section deals with the brief description of the work on " Bio-compatible ZnS:Mn nanocrystals conjugated with L-citrulline, as fluorescent probes for DNA visualization and for finger print analysis in forensic studies", which has been submitted for patent filing.

LIST OF PUBLICATIONS

Papers published in International/National peer reviewed Journals related to the work presented in the thesis.

[1] **M.Sajimol Augustine ,** Roselin Alex, Sreevalsa VG, Deepa GD, Sarita G.Bhat, Jayalekshmi.S, "Highly luminescent and bio-compatible, L-citrulline capped ZnS:Mn nanocrystals for rapid screening of metal accumulating *Lysinibacillusfusiformis* bacteria" *Journal of Biological and Chemical Luminescence* (accepted)

[2] **Sajimol Augustine M**, Anand Puthirath B, Anilkumar Kollery M, Jayalekshmi.S, "Exceptionally good, transparent and flexible FeS_2/PVP and FeS_2/PVA nanocomposite thin films with excellent UV-shielding properties" *Polymer International* (In press)

[3] **M.Sajimol Augustine**, S. J. Varma, Francis Xavier and S. Jayalekshmi, "Enhanced photoluminescence in oleic acid modified Polyaniline" *Transactions of the Indian Institute of Metals***, 64**: 209-212 (2011)

[4] **M. SajimolAugustine ,**P.P. Jeeju, V.G. Sreevalsa, S. Jayalekshmi, "Excellent UV absorption in spin-coatedthin films of oleic acid modified Zinc oxide nanorods embedded in Polyvinyl alcohol" *Journal of Physics and Chemistry of Solids*,**73:** 396-401 (2012)

[5] **M. Sajimol Augustine**, P.P Manzur Ali, K. Sapna, K. K Elyas, S. Jayalekshmi, **"**Size-dependent optical properties of bio-compatible ZnS:Mnnanocrystalsand their application in the immobilization of

trypsin" *Spectrochimica Acta Part A: Molecular and Biomolecular Spectroscopy* (under revision)

[6] **M.Sajimol Augustine**, Abdulaziz Anas, Ani V.Das, S. Sreekanth, S.Jayalekshmi, "Cytotoxicity and Cellular uptake of ZnS:Mn nanocrystals biofunctionalized with Chitosan and Aminoacids" *Journal of Colloid and Interface Science* (communicated)

Other journal publications related to the present work

[7] **M. Sajimol Augustine**, S.J.Varma, P.P Jeeju, P.A Francis Xavier, S. Jayalekshmi, "Enhanced photoluminescence in transparent thin films of PANI/ZnO nanocomposite prepared from oleic acid capped ZnO nanoparticles", *Thin Solid Films* (under revision)

[8] **M. Sajimol Augustine,** P.Indu, V.G Sreevalsa, P.P Jeeju, S.Jayalekshmi, "Solvent dependent optical properties of highly luminescent nanocrystals of ZnS doped with Manganese", *Science and Society,* 9:109-113 (2011)

[9] P.P. Jeeju, P.A. Francis Xavier, **A.M. Sajimol**, V.G. Sreevalsa, Jayalekshmi,"Micelle-assisted synthesis of polypyrrole nanoparticles and their characterization " *Science and Society,* 9:113-121 (2011)

[10] V.G Sreevalsa, P.P Jeeju**, M. Sajimol Augustine,** S. Jayalekshmi, "Studies on L- citrulline Capped Zinc Oxide Nanocrystals" *Science and Society,* 9:183-189 (2011)

[11] Jeeju. P. P, **Sajimol. A.M**, Sreevalsa V.G, S. J.Varma and S.Jayalekshmi, "Size dependent optical properties of transparent,

spin coated Polystyrene- ZnOnanocomposite films" *Polymer International,* **60**: 1263–1268 (2011)

[12] Sreevalsa.V.G, **Sajimol Augustine M**, S.Jayalekshmi, "Characterisation of transparent PVA/aminoacid complex capped ZnOnanocomposite films" *International Journal of Plastics Technology,* 15:10-18 (2011)

[13] V.G. Sreevalsa, P.P. Jeeju,**M.Sajimol Augustine,** K M. Anilkumar, S. Jayalekshmi, "L-Histidine Modified Biocompatible Zinc Oxide Nanocrystals" *Journal of Experimental Nanoscience.* vol.ahead-of-p, 1-10 (2012)

[14] P.P.Jeeju, S. J.Varma, P.A.Francis Xavier, **A. M. Sajimol**, S.Jayalekshmi, "Novel Polypyrrole films with excellent crystallinity and good thermal stability" *Materials chemistry and physics,* **134:**803-808 (2012)

The work on " Bio-compatible ZnS:Mn nanocrystals conjugated with L-citrulline, as fluorescent probes for DNA visualization and for finger print analysis in forensic studies", has been submitted for patent filing with file number **4900/CHE/2012.**

Papers presented in International/National conferences

[1] **M.Sajimol Augustine**, AnasAbdulaziz, AniV.Das, S.Sreekanth and S.Jayalekshmi, "Cytotoxicity Assessment and Uptake Study of Bio-compatible ZnS:Mnnanocrystals" *Proceedings of the International Conference on Nutritional Medicine, Health and Wellness, NUWELL'2012,* at St,Teresa's College, Ernakulam,7- 8 June 2012.

[2] **M. Sajimol Augustine**, P.P Manzur Ali, K.Sapna , K.KElyas, S.Jayalekshmi, "Immobilisation of trypsin with chitosan capped ZnS:Mnnanocrystals for therapeutic applications" *Proceedings of the International Conference on Nanotechnology at the Bio-Medical Interface* at Amrita Centre for Nanosciences& Molecular Medicine, Kochi, during 21 – 23 February, 2012.

[Best Poster Presentation Award (second prize)]

[3] **M. Sajimol Augustine,** P.P Jeeju, S. Jayalekshmi, "Highlyluminescent PANI/ZnO nanocomposite films prepared from oleic acid capped ZnO nanoparticles" *Proceedings of the Third International conference on frontiers in Nano Science and Technology. Cochin Nano – 2011*, Cochin, 14-17 August 2011.

[4] **M**. **Sajimol Augustine,** S. J. Varma, Francis Xavier P.A ,S. Jayalekshmi, "Enhanced photoluminescence in oleic acid modified Polyaniline" *International Symposium for Research Scholars (ISRS-2010) on Metallurgy, Materials Science and Engineering* at IIT Madras, 26-28 December 2010.

[5] **M**. **Sajimol Augustine,** S J. Varma, Francis Xavier, S. Jayalekshmi, "Enhanced photoluminescence behaviour of PANI/ZnOnanocomposite prepared from oleic acid capped ZnO nanoparticles" *Proceedings of the International conference on Recent Trends in Material Science and Technology*, *ICMST 2010*, IIST Trivandrum, 29-31October 2010.

[6] **M. Sajimol Augustine,** S. Jayalekshmi, "Solvent dependent optical properties of spin-coated transparent nanocomposite films of oleic acid capped ZnO quantum dots in PVA matrix" *Proceedings of the*

International conference on Advancements in Polymeric Materials, APT- 2010 , at Rubber Park, Cochin, 26-27 Feb 2010.

[7] **M.Sajimol Augustine**, S. Jayalekshmi, "Optical properties of spin-coated transparent nanocomposite films of oleic acid capped ZnO quantum dots in Polyvinyl alcohol" *Proceedings of the International conference on Advancements in Polymeric Materials,APM-2010*, *Trends and Technology*, at CIPET, Bhuvaneswar, 20-22 Feb 2010.

[8] **M. Sajimol Augustine,** P.Indu, V.G Sreevalsa, P.P Jeeju, S.Jayalekshmi, "Solvent dependent optical properties of highly luminescent nanocrystals of ZnS doped with Manganese" *Proceedings of the National symposium on Nano Science and Technology, Nanostech – 2011*, at Nirmala College Muvattupuzha, Kerala, 1-2September 2011.

[9] **M. Sajimol Augustine,** V.G Sreevalsa, P.P Jeeju, S. Jayalekshmi," Synthesis and Optical Properties of Water-dispersible ZnS:MnNanocrystals Capped by L- aminoacid ligands" *Proceedings of the national seminar onChallenges in Nanoscience and Technology, CNT-2011,*at St,Teresa's College, Ernakulam, 28-29July 2011.

[**Best Paper Award (Oral Presentation)]**

[10] **M.Sajimol Augustine,** S. Jayalekshmi, "Size dependent optical properties of spin-coated nanocomposite films of oleic acid capped ZnO nanoparticles in PVA matrix"*Proceedings of the Ist Kerala Women's Science Congress 2010*, at St.Teresa's college Ernakulam, 10-12 August 2010.

[11] **M.Sajimol Augustine**, S.Jayalekshmi, "Effect of capping on the optical properties of ZnO/PVA nanocomposite thin films*" Proceedings of the national seminar on Nano structured materials and Nano photonics,* at St.Teresa's college,Ernakulam;4-5Jan 2010.

[12] **M**. **Sajimol Augustine,** S.Jayalekshmi, "Influence of synthesis conditions on particle size and optical properties of highly luminescent ZnO nanoparticles doped with Na" *Proceedings of the national seminar on Quantum chemistry and Nano techniques* at SNM College Maliankara, Ernakulum;19-20 Nov 2009.

[13] **M. Sajimol Augustine**, S. Jayalekshmi, "Highly luminescent, transparent and freestanding nanocomposite films of bio-functionalized ZnS:Mn in PS-PMMA matrix" *Proceedings of National Seminar on Recent trends in Photonics, at International school of Photonics, CUSAT, Kerala,* 2-4 November 2012

[14] **M. Sajimol Augustine**, V.G Sreevlasa, P.P Jeeju, S. Jayalekshmi, "Highly luminescent, transparent and flexible nanocomposite films of bio-functionalized ZnS:Mn in PVA-PVP matrix" *Proceedings of National Seminar on Current Trends in the fields of Nanoscience and Nanotechnology,* K.K.T.M Govt.College, Pullut, Kerala, 13-14 December 2012.

[15] Jeeju.P.P,Sreevalsa.V.G, **Sajimol. A. M** and S.Jayalekshmi, "Enhanced UV-shielding properties of ZnO/PS-PMMA nanocomposite films" *Proceedings of the Third International conference on frontiers in Nano Science and Technology. Cochin Nano – 2011*, Cochin, 14-17 August 2011.

[16] Sreevalsa.V.G, Jeeju.P.P, **Sajimol Augustine. M ,**Jayalekshmi.S, "Effect of various capping agents on the optical properties of Zinc oxide nanocrystals" *Proceedingsof the Third International conference on frontiers in Nano Science and Technology. Cochin, Nano – 2011,* 14-17 August 2011.

[17] Sreevalsa.V.G, **Sajimol Augustine M**, S.Jayalekshmi, "Characterisation of transparent PVA/aminoacid complex capped ZnOnano composite films" *Proceedings of the International conference on Advancements in Polymeric Materials.APM-2010, Trends and Technology* at CIPET, Bhuvaneswar, 20-22 Feb 2010.

[18] P.P. Jeeju, P.A. Francis Xavier, **A.M. Sajimol**, V.G. Sreevalsa, .Jayalekshmi,"Micelle-assisted synthesis of polypyrrole nanoparticles and their characterization "*Proceedings of the National symposium on Nano Science and Technology, Nanostech – 2011*, at Nirmala College Muvattupuzha, Kerala, 1-2 September 2011.

[19] V.G Sreevalsa, P.P Jeeju**, M. Sajimol Augustine** and S. Jayalekshmi, "Studies on L- citrulline Capped Zinc Oxide Nanocrystals" *Proceedings of the National symposium on Nano Science and Technology, Nanostech – 2011*, at Nirmala CollegeMuvattupuzha, Kerala, 1-2 September 2011.

[20] P.P Jeeju, **Sajimol A.M,** V.G Sreevlasa, "Linear and Nonlinear optical properties of Transparent, spin-coated ZnO/Polyvinyl alcohol nanocomposite films" *Proceedings of National Seminar on Current Trends in the fields of Nanoscience and Nanotechnology,* K.K.T.M Govt.College, Pullut, Kerala, 13-14 December 2012.

[21] V.G Sreevlasa, **Sajimol Augustine,** P.P Jeeju, "Third order nonlinearity and biocompatibility studies of L-histidine capped ZnO nanoxrystals" *Proceedings of National Seminar on Current Trends in the fields of Nanoscience and Nanotechnology,* K.K.T.M Govt.College, Pullut, Kerala, 13-14 December 2012.

[22] **Sajimol Augustine M**, Lizzy Mathew, Roselin Alex, Deepa G D, Jayalekshmi.S, "L-serine capped ZnS:Mn nanocrystals for plant cell biological studies and as a Growth enhancing agent for Micropropagation of *Bacopa monnieri* Linn. (Brahmi: Scrophulariaceae)" accepted for presentation in *International conference on Optoelectronic Materials and Thin films for Advanced Technology (OMTAT 2013),* Kochi, Kerala, 3-5 January 2013.

[23] **M. Sajimol Augustine,** P.B. Anand, S. Jayalekshmi, "Opto-electronic applications of chitosan capped ZnS:Mn/PVA nanocomposite thin films", accepted for presentation in *Annual International Conference on Optoelectronics, Photonics & Applied Physics (OPAP) 2013,* SINGAPORE, 4-5 February 2013.

CONTENTS

Chapter 1

INTRODUCTION

Contents

A general introduction to the work presented in the thesis is portrayed in this chapter. The basic concepts and relevance of nanoscience and technology, giving emphasis to nanobiotechnology are addressed. The general aspects related to the synthesis and properties of semiconductor nanocrystals and its photonic and biological applications are also considered. The fundamental concepts of nanocomposite materials in bulk and thin film forms, and their important optical characteristics and applications are also dealt with in this chapter.

1.1 Nanoscience

Nanoscience is an emerging research area which is concerned with the study of materials that have very small dimensions, in the nano scale range. Atoms are a few tenths of a nanometer and molecules are typically a few nanometers in size. Nanometer is a magical point on the length scale, for this is the point where the smallest man-made devices meet the atoms and molecules of the natural world. The smallest structures made by humans have

dimensions of a few nanometers and these nanoscale objects represent the most promising field of material science for the next few years.

In 1959, the great physicist Professor Richard Feynman gave the first hint about what is now known as "nanoscience" during his talk, which was entitled as: "There is Plenty of Room at the Bottom ". He consciously explored the possibility of "direct manipulation" of the individual atoms to be effective as a more powerful form of 'synthetic chemistry' [1]. He proposed that by working from the top to down, it should be possible to manipulate things at the atomic scale. Research in materials at the atomic scale is an interdisciplinary approach that involves interaction between researchers in physics, chemistry, mechanics, material science, electronics, computer science, biology and medicine.

1.2 Nanotechnology

Nanotechnology deals with developing materials, devices, or other structures with dimensions on the nanoscale and investigating whether one can directly control and manipulate matter on the atomic scale. Nanotechnology has already influence all walks of human activity. It will definitely revolutionize the future world by introducing devices which are smart and functional. Nanotechnology is an interdisciplinary research field with a host of applications in material technology, manufacturing, instrumentation, energy production and storage, information technology, biotechnology and medicine [2-12]. However there are many issues to be addressed including concerns about the toxicity and environmental impact of nanostructured materials [13] and their potential effects on global economics.

Materials reduced to the nanoscale are endowed with properties quite different from what they exhibit on a macro scale, enabling unique applications.

Opaque substances like copper become transparent, inert materials like platinum attain catalytic properties, stable materials like aluminum become combustible, solids like gold turn into liquids at room temperature and semiconductors like silicon become conductors when deduced to nanoscale dimensions. In nanoscale materials, the surface area to volume ratio becomes quite enhanced which may result in new quantum mechanical effects. Much of the fascination with nanotechnology stems from the unique quantum and surface phenomena that predominate at the nanoscale. Recent developments in nanotechnology and the various quantum size effects in nanostructured materials, imply that most of the novel devices of the future will be based on the characteristics of nanomaterials. Nanotechnology is considered to be the next industrial revolution and is believed to cause enormous impacts on the society, economy and life in general in the near future.

1.3 Nanobiotechnology

The nanobiotechnology deals with the integration of biotechnology with nanotechnology and refers to the ways in which nanotechnology is utilized to realize devices for studying biological systems. It is often used to describe the overlapping multidisciplinary activities associated with biosensors, particularly where photonics, chemistry, biology, biophysics, nanomedicine, and engineering converge. Nanobiotechnology is a rapidly advancing area of profound scientific and technological opportunities that applies the tools and processes of nano/microfabrication to build devices for studying biosystems. This technical approach to biology allows scientists to design and create systems that can be used for biological research to understand better the life processes at the nanoscale.

The most important objectives that are frequently encountered in nanobiology involve applying nanotools to relevant medical/biological problems and refining these applications as required. Developing new tools for the medical and biological fields and the imaging of biomolecules, biological membranes, and tissues using the tools of nanotechnology are some of the prime issues for the nanobiology researchers. Nanobiotechnology is best described as a comrade of modern medicine in its progress from treating symptoms to generating cures and regenerating biological tissues.

1.4 Nanoscale materials

Materials with morphological features on the nanoscale have special properties stemming from their nanoscale dimensions. Nanoscale materials cover various types of nanosturctured materials which posses at least one dimension in the nanometer range. Various nanostructures include zero dimensional nanostructures known as quantum dots, one dimensional nanostructures such as nanowires, nanotubes and nanorods, and two dimensional nanostructures such as quantum well structures. Besides these individual nanostructures, ensembles of these nanostructures form higher dimensional arrays, assemblies, and superlattices. The properties of materials with nanometer dimensions are significantly different from those of atoms and bulk materials. The key characteristics of nanoscale materials that define their potential applications include the following:

- Higher surface area
- Higher chemical reactivity
- Better catalytic properties
- Better adsorbption

- Variety of chemical synthesis routes.
- Natural and synthetic strategies

1.4.1 Zero dimensional nanomaterials (quantum dots)

If the three dimensions of a semiconductor nanostructure are reduced to the size, where quantum confinement effects are possible, then such structures are known as quantum dots. The schematic representation and density of states versus energy diagram of a quantum dot is shown in figure 1.1. In this case the motion of conduction band electrons and excitons are confined in all three spatial directions [14]. The ability to tune the size of quantum dots is advantageous for many applications. For instance, larger quantum dots have a greater spectrum-shift towards red compared to smaller dots, and exhibit less pronounced quantum properties. Conversely, the smaller nanoparticles allow one to take advantage of more subtle quantum effects.

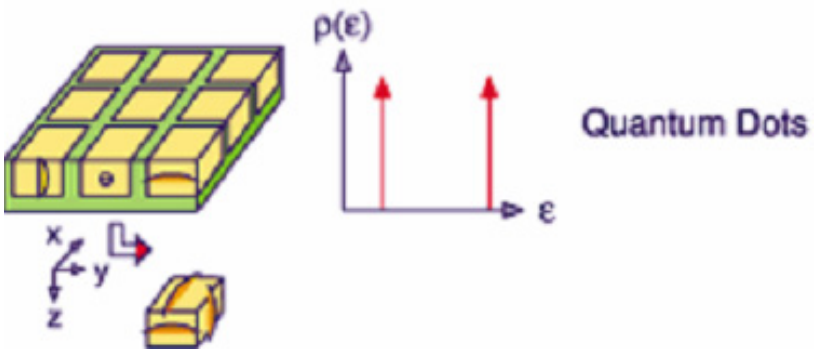

Figure 1.1 Schematic representation and density of states versus energy diagram of a quantum dot.

Being zero dimensional, quantum dots have a sharper density of states than higher-dimensional structures. As a result, they have superior transport and optical properties, and are being researched for use in diode lasers, amplifiers, and biological sensors. High-quality quantum dots are well

suited for optical encoding and multiplexing applications due to their broad excitation profiles and narrow/symmetric emission spectra. The new generation quantum dots have far-reaching potentials for the study of intracellular processes at the single-molecule level, high-resolution cellular imaging, long-term *in vivo* observation of cell trafficking, tumor targeting, and diagnostics.

One dimensional nanomaterials (quantum wires)

Quantum wires are small conducting or semi-conducting nanoparticles with a lateral size comparable to the size capable of producing quantum confinement effects. Schematic representation and density of states versus energy diagram of a quantum wire is shown in figure 1.2. In condensed matter physics, a quantum wire is an electrically conducting wire, in which quantum effects are affecting transport properties. Nanowires are used as interconnections for the transport of electrons in nanoelectronic devices. Various metals such as cobalt, gold, and copper are used to fabricate quantum nanowires. Suspension, deposition and vapour liquid solid (VLS) phase growth are some of the synthesis techniques used for making nanowire structures.

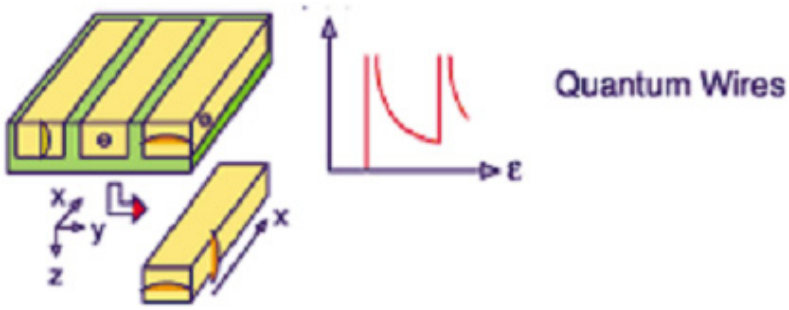

Figure 1.2 Schematic representation and density of states versus energy diagram of a quantum wire.

1.4.2 Two dimensional nanomaterials (quantum wells)

When only one of the dimensions is reduced to nanometer range with the other two dimensions remaining large, the resulting nanostructure is called a quantum well. It is similar to a thin film having thickness in the very low nanometer range or a nano film. The schematic representation and density of states versus energy diagram of a quantum well is shown in figure 1.3. The quantum confinement effects take place when the well thickness becomes comparable to the de-Broglie wavelength of the charge carriers [15, 16]. Thus the carriers can only have discrete energy values. This 'well' is like a cage in which the carriers can be trapped, in much the same way that light can be trapped between the mirrors. By creating 'layers of different semiconductors', it is possible to make particular 'layers' to act as 'traps' for carriers. These 'trapped carriers' can be considered to be in a state of 'quantum confinement'. The quantum well structures have sharper density of states compared to the bulk materials. The thickness of a quantum well is typically 5-20 nm.

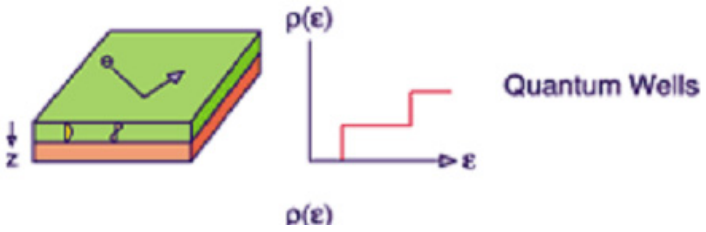

Figure 1.3 Schematic representation and density of states versus energy diagram of a quantumwell.

1.5 Properties of nanoscale materials

Nanoscale materials are of great interest for a wide variety of applications in the fields of information, energy, environmental and medical technologies due to their unique and improved properties determined primarily

by size, composition and structure. A number of physical phenomena become more pronounced as the size of the system decreases. Certain phenomena may not come into play as the system moves from macro to micro level but may be significant at the nano scale. One example is the increase in surface area to volume ratio which alters the mechanical, thermal and catalytic properties of the material. The increase in surface area to volume ratio leads to increasing dominance of the behaviour of atoms on the surface of the particle over that of those in the interior of the particle, thus altering the properties. The electronic and optical properties and the chemical reactivity of small clusters are completely different from the better known properties of each component in the bulk. Some of the size dependent properties of nanomaterials include quantum confinement effects in semiconductors, surface plasmon resonance (SPR) in metallic nanoparticles and para magnetism in magnetic nanoparticles.

The percentage of atoms at the surface of a material becomes significant as the size of the material approaches the nanoscale. Reducing the size of a particle, increases the ratio of surface area to volume. Because the reactive portion of the particle is at its surface, increasing the relative surface area will increase reactivity for a given amount of material. At the nanoscale, both classical physics and quantum physics can govern the behaviour of a particle. The influence of quantum effects can change essential material characteristics with pronounced variations in optical, electrical, physical, chemical and magnetic properties. Such variations extend ample scope for a variety of applications in various fields.

- **Optical**:- Optical properties are modified because of the quantum size effects on the band structure and the band gap is blue shifted for smaller sized nanomaterials. On most smooth metal surfaces, light is

entirely reflected by the very high density of electrons and that is why the surfaces of slabs of metal have mirror-like appearance. In contrast, small particles absorb some of the light, leading to the appearance of colours which depends on size [17] due to quantum confinement, as shown in figure 1.4. For example, bulk gold appears yellow in colour but nanosized gold appears in different colours depending on the size of the gold particles. The particles are so small that electrons are not free to move about as in bulk gold. Because this movement is restricted, the particles react differently to light [18].

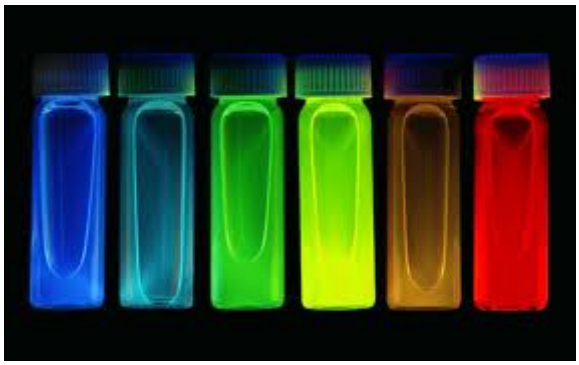

Figure 1.4 Different sized quantum dots emit different colours when irradiated with UV light.

- **Electrical**:- At the nanoscale, electrical properties are not necessarily the same as they are at the macro scale. Materials that are conductors at the macroscale may lose their electrical conductivity at the nanoscale and vice versa. For instance, when an insulator becomes thin enough, it can be rendered conductive through a process called quantum tunnelling, which is a non-classical effect that is generally observed only at the nanoscale [19]. Carbon in the form of graphite (like pencil lead) is soft and malleable. At the nano-scale carbon can be stronger than steel and is six times lighter. Carbon nanotubes are

long, thin cylinders of carbon. They are 100 times stronger than steel, very flexible, and have unique electrical properties. Their electrical properties change with diameter and number of walls. They can be either conducting or semi-conducting in their electrical behaviour [20].

- **Physical**:- One of the unique properties of nanoparticles is that they have lower melting temperatures than their bulk material counterparts. As surface particles have fewer neighbours, less heat is required for their melting. Therefore surface particles have lower melting point as compared to bulk particles which have more neighbours. This melting point depression is used to define the nanoscale region as 1-100 nm. Between the values of 1nm and 100 nm, the change in melting temperature becomes readily noticeable. Above 100 nm, the temperature change remains relatively close to zero. Below 1nm, melting point has no physical meaning as these sizes are governed by subatomic and single atom phenomenon [21].

- **Chemical**:- Chemical reactions involve the atoms that lie at the surface of a material and thus chemical properties are dependent on surface properties. Since surface area at nanoscale is large, nanoparticles have enhanced reaction rates. Nanoparticles can hence be used as reaction catalysts. On the macroscale, gold is considered to be much less catalytically active than other metals. However, nanoscale particles of gold can act as catalysts to enhance the rate of some chemical reactions. One possible application of nanoscale particles is in the catalytic converter, where harmful pollutants produced by automobiles such as carbon monoxide, can

be made to react to form carbon dioxide and water. The use of nanoscale gold particles for this application helps to reduce automobile-related air pollution significantly, since gold particles catalyze the reaction even at sub-zero temperatures.

- **Magnetic**:- Magnetic properties of nanoscale materials are of great scientific and technological interest nowadays. Magnetic nanoparticles are used in a range of applications, including ferrofluids, colour imaging, bioprocessing, refrigeration and high storage density magnetic memory media. The large surface area to volume ratio results in a substantial proportion of atoms to have a different magnetic coupling with neighbouring atoms, leading to different magnetic properties.

1.6 Semiconductor Nanoparticles

Nanostructured metals, semiconductors and metal oxides are of great interest for a wide variety of applications due to their unique and improved properties determined primarily by size, composition and structure along with their self organized film structures. Nanoparticles are broadly classified as organic and inorganic types. Organic nanoparticles include fullerenes, carbon nanotubes (both single and multiwalled) and graphene based nanostructures. Some of the inorganic nanoparticles include magnetic nanoparticles, noble metal nanoparticles and semiconductor nanoparticles. There is a growing interest in inorganic nanoparticles as they provide superior material properties with functional versatility. Inorganic nanoparticles such as metallic and semiconductor nanoparticles exhibit intrinsic optical properties which may enhance the transparency of polymer- particle composites. For such reasons,

inorganic nanoparticles have found special interest in studies devoted to optical properties in composites. Inorganic nanoparticles have been examined as potential tools for medical imaging as well as for treating diseases. Inorganic nanomaterials have been widely used for cellular delivery due to their versatile features like wide availability, rich functionality, good biocompatibility, capability of targeted drug delivery and controlled release of drugs.

Semiconductor nanocrystals are the subjects of a thriving area of physical and synthetic inorganic chemistry (22–29), motivated by both fundamental science and the long-term technological potential of these materials. Semiconductor nanocrystals have already been commercialized for applications as luminescent biolabels (30–32) and have been demonstrated as components in regenerative solar cells (33–35), optical gain devices (36), and electroluminescent devices (37). Two fundamental factors, both related to the size of the individual nanocrystal, are responsible for these unique properties. The first is the large surface area to volume ratio. As the particle becomes smaller, the ratio of the number of surface atoms to those in the interior increases, with greater than a third of all atoms residing on the surface, in very small particles. This leads to the significant influence of the surface properties on the behavior of the material. The second factor is the actual size of the particle. With semiconductor nanoparticles, there are changes in the electronic properties of the material. As the size of the semiconductor nanoparticles becomes comparable to or less than the exciton Bohr radius, the quantum confinement effects become quite dominant. For nanostructured semiconductors, quantum confinement effects lead to considerable blue shift in the band gap and enhancement in the luminescence emission intensity. Out of the wide variety of nanostructured semiconductors, zinc oxide, iron sulphide

and their polymer nanocomposites and manganese doped zinc sulphide, biofunctionalized with various capping ligands have been selected for the present investigations. The effect of oleic acid modification on the luminescence properties of zinc oxide and polyaniline in the form of nanorods, forms a significant part of the present work. The objectives of the present investigations are summarized below.

1.7 Objectives of the present study

- To synthesize oleic acid modified ZnO nanorods using the simple, wet chemical technique and develop nanocomposite thin films of ZnO nanorods embedded in polyvinyl alcohol (PVA) with prospects of UV filtering applications.
- To investigate the effect of oleic acid modification on the photoluminescence characteristics of polyaniline (PANI).
- To develop iron disulphide/polymer (FeS_2/PVP and FeS_2/PVA) nanocomposite thin films with prospects of excellent UV shielding properties.
- To assess the cytocompatibility of manganese doped zinc sulphide (ZnS:Mn) nanocrystals, functionalized with chitosan and aminoacid ligands and to investigate the *in vitro* cellular uptake in HEK293T cells.
- To study the immobilization of trypsin on bio-compatible, chitosan capped ZnS:Mn nanocrystals.
- To investigate the suitability of bio-compatible, L-citrulline capped ZnS:Mn nanocrystals for the detection of metal accumulating *Lysinibacillus fusiformis* bacteria

References

[1] R. P. Feynman. Philosophical Transactions. Reinhold, New York, 1961

[2] T. Numai. Fundamentals of Semiconductor Lasers. Springer, New York, 2004

[3] M. A. Zimmler, J. Bao, F. Capasso, S. Mller, and C. Ronning. *Appl.Phys. Lett*., 93 (2008) 051101

[4] A. Javey, S. Nam, R. S. Friedman, H. Yan, and C. M. Lieber. *NanoLett.*, 7 (2007) 773

[5] L. Tsakalakos, J. Balch, J. Fronheiser, B. A. Korevaar, O. Sulima, and J. Rand. *Appl. Phys. Lett.,* 91 (2007) 233117

[6] S. M. Tanner, J. M. Gray, C. T. Rogers, K. A. Bertness, and N. A. Sanford. *Appl. Phys. Lett.,* 91 (2007) 203117

[7] Z. Y. Fan and J. G. Lu. *Appl. Phys. Lett.,* 86 (2005) 123510

[8] Koyakutty Manzoor, Seby Johny, Deepa Thomas, Sonali Setua,Deepthy Menon and Shantikumar Nair *Nanotechnology* 20 (2009) 065102.

[9] E. C. Garnett, W. Liang, and P. Yang. *Adv. Mater*, 19 (2007) 2946

[10] Lim, E. J.; Park, S. H.; Byun, J. H.; Hwang, C. S. *Bull. Kor. Chem.Soc*. 33 (2012) 1741.

[11] Hauck, T. S., Anderson, R. E., Fischer, H. C., Newbigging, S. & Chan, W. C. W. *Small* 6 (2010) 138–144

[12] Kong, H. Y.; Kim, S. Y.; Byun, J. H.; Hwang, C. S. *Bull. Kor. Chem. Soc.* 32 (2011) 53.

[13] Cristina Buzea, Ivan I. Pacheco and Kevin Robbie *Biointerphases* **2**: MR17-MR71(2007)

[14] A.P. Alivisatos, *Science* 271 **(**1996) 933

[15] Chen, H-Y., Chen, T-Y. & Son, D. H. *J. Phys. Chem. C* 114 (2010) 4418–4423

[16] C.Delure and M.Lanno, "Nanostructures", Springer, New Delhi (2004)

[17] S.V.Gaponenko, "Optical properties of semiconductor nano crystals", Cambridge Studies in Modern Optics; Cambridge University Press (1998).

[18] T. Yao and J. C. Woo; 'Physics and applications of semiconductor quantum structures" IOP publishing Bristol, Philadelphia (2001)

[19] S Ogava, H Nagano and H Petek, *Phys.Rev.Lett*. 88 (2002) 116801

[20] Tran Thi Quynh Hoa, Le Van Vu, Ta Dinh Canh and Nguyen Ngoc Long, *J. Phys.: Conf. Ser.* 187 (2009) 012081

[21] Haiming Zhang, Zhijian Wang, Ligong Zhang, Yuqin Li, Jinshan Yuan and Shenggang Yan. *Journal of Materials Science Letters,* 21 (2002) 1031-1033

[22] A. P. Alivisatos, *J. Phys. Chem*., 100 (1996) 13226

[23] Das, S. K., Sahoo, S. N., Sarangi, S. N. & Sahoo, P. K. *J. Exp. Nanosci.* 8 (2012) 382–388

[24] Holloway, T., Mundle, R., Dondapati, H., Bahoura, M. & Pradhan, A. K. *Chem. Phys. Lett.* 534 (2012) 48–53

[25] A. Eychmu¨ller*, J. Phys. Chem. B,* 104 (2000) 6514

[26] M. Shim, C. Wang, D. J. Norris, and P. Guyot-Sionnest, *MRS Bull.,* 26 (2001) 1005

[27] Kong, H. Y.; Byun, J. H.; Hwang, C. S. *Bull. Kor. Chem. Soc.* 33 (2012) 657

[28] Jingling, G.; Rongjun, Q.; Bo, T. *J. Nanoparticle Res.* 12 (2011) 5289

[29] X. Gao and S. Nie, *Trends Biotechnol.,* 21 (2003) 371

[30] M. Bruchez, Jr., M. Moronne, P. Gin, S. Weiss, and A. P. Alivisatos, *Science,* 281 (1998) 2013

[31] Z. Deng, L. Tong, S. Lin, M. Flores, J. Cheng, H. Yan, Y. Liu* J. Am. Chem. Soc. 133 (2011) 5389–5396

[32] R. Plass, S. Pelet, J. Krueger, M. Graetzel, and U. Bach, *J. Phys. Chem. B,* 106 (2002) 7578

[33] W. U. Huynh, J. J. Dittmer, and A. P. Alivisatos, *Science*, 295 (2002) 2425

[34] Pullarkat P Jeeju, Augustine M Sajimol, Vallath G Sreevalsa, Sreekanth J Varma, S Jayalekshmi, *Polymer International*; 60 (2011) 1263 - 1268

[35] V. L. Colvin, M. C. Schlamp, and A. P. Alivisatos, *Nature* (London), 370 (1994) 354

[36] B. O. Dabbousi, M. G. Bawendi, O. Onitsuka, and M. F. Rubner, *Appl. Phys. Lett*., 66 (1995) 1316

[37] S. Coe, W.-K. Woo, M. G. Bawendi, and V. Bulovic*, Nature* (London), 420 (2002) 800

Chapter 2

EXPERIMENTAL TECHNIQUES

Contents

A brief description of the experimental techniques used for the synthesis of the nanostructured materials investigated in the present study and the various characterization procedures adopted is portrayed in this chapter. The structural, optical and thermal characterizations of the synthesized samples are carried out using different sophisticated instruments and a comprehensive description of the tools utilized is included in this chapter.

2.1 Introduction

Development of synthesis protocols for realizing nanostructured materials over a range of sizes, shapes, and chemical compositions is an inevitable aspect of nanotechnology. The remarkable size dependent properties of nanomaterials have fascinated and inspired research activity in this direction. Though the synthesis and organization of nanoparticles provide complementary tools for nanotechnology, processing of nanomaterials into bulk shapes, retaining the nanometer size is another challenging aspect, as far as structural and engineering applications are concerned.

The past few decades have witnessed tremendous advancements in the synthesis of nanomaterials with strict control over size, shape, crystalline structure and chemical composition. The practical use of nanomaterials requires the development of methods for nanoparticle assembly or dispersion in various media. A majority of studies has been aimed at dispersion in aqueous media for medical applications and studies of environmental effects. However, the principles of synthesis of nanomaterials and their functionalization transcend their eventual applications.

Synthesis methods for nanomaterials are typically grouped into "top-down" and "bottom-up" approaches. The first involves division of a massive solid into smaller portions. This approach may involve milling or attrition, chemical methods, and volatilization of a solid followed by condensation of the volatilized components [1]. The second, "bottom-up", method of nanomaterial synthesis involves condensation of atoms or molecular entities in a gas phase or in solution. The bottom-up approach is more popular compared to the top-down method.

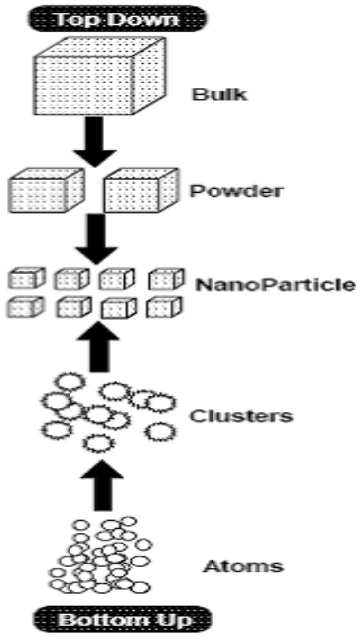

The bottom – up approach refers to the build-up of a material from the bottom, atom-by-atom, molecule-by-molecule, or cluster-by-cluster. In polymer science, polymers are synthesized by connecting individual monomers together. Bottom-up approach also promises better chances to obtain nanostructures with less defects, more homogeneous chemical composition, and better short and long range ordering. The bottom-up approach is driven mainly by the reduction of Gibbs free energy, and hence the resulting nanostructures are in a state closer to a thermodynamic equilibrium.

Oraganometallic chemical route, reverse-micelle route, sol-gel synthesis, colloidal precipitation, hydrothermal synthesis, template assisted sol-gel, electrodeposition etc, are some of the well- known bottom–up techniques for the preparation of luminescent nanomaterials. Among the various "bottom-up" fabrication approaches, wet-chemical routes have been universally distinguished for their ability to provide high-quality nanocrystals with a number of desirable prerequisites, such as controlled composition and crystal phase, tailored geometric parameters, programmed surface functionalities, chemical robustness, and ease of processability.

2.2 Synthesis of nanoscale materials

Several methods are available for the synthesis of nanostructures which are suitable for various applications. Basically there are two broad areas of techniques for the synthesis of nano-structured materials, constituted by the physical methods and chemical methods. Currently used physical methods include the inert-gas evaporation technique [2], pulsed laser ablation (PLA) [3], sputtering technique [4], mechanical deformation technique [5, 6] etc.

Chemical methods of synthesis have several advantages over physical methods. The primary advantage of chemical processes is good chemical homogeneity and tunable surface properties of the synthesized nanoparticles. Some of the chemical methods widely used include, solution chemistry [7], chemical vapour deposition (CVD) [8], hydrothermal method [9], sol-gel method [10-16] and co-precipitation method [17, 18]. Co-precipitation method offers simple and rapid processing, easy control of particle size and composition and the possibilities to modify the particle surface state and overall homogeneity. Chemistry has played a major role in developing new nanostructured materials with novel and technologically important properties.

2.3 Synthesis routes for the present investigations

Nanosized structures with uniform shape and narrow size distribution are shown to possess many interesting properties quite different from their bulk counterparts. They have larger surface area and wider band gap which can effectively modify the optical, electrical, catalytical and magnetic properties. The various methods available for the synthesis of nanostructures can be broadly classified into (a) low temperature and (b) high temperature methods. Among the low temperature techniques, chemical precipitation method has been widely used. The main criteria for selecting the most appropriate method are reproducibility, control over size and shape and reasonable production cost. Chemical precipitation methods include precipitation of solutions from room temperature to 100^0C, hydrothermal synthesis, inverse micelle method and sol-gel synthesis. These methods are ideally suited for precise control of size and shape of the nanomaterials. In addition, they are cost effective because of less energy consumption. The main drawback with precipitation techniques is chemical contamination, in general.

2.3.1 Synthesis of ZnO nanorods with and without oleic acid

The synthesis of nanostructured metal oxides can be effectively carried out using chemical precipitation technique at room temperature. Generally this method comprises three steps. The first step is the preparation of an alcohol based solution. The second step is the addition of the metal oxide precursor to the alcohol based solution to form a reaction mixture. The third step is the reaction of this mixture to form the nanosized metal oxide particles. Synthesis by chemical route has the advantage of being more economical compared to the complex epitaxial methods. In addition, various capping agents can be used to prevent growth and modify the size and shape of the synthesized nanomaterials. In the present work, ZnO nanorods have been synthesized by simple chemical precipitation method with and without oleic acid as the capping agent.

2.3.2 Synthesis of bio-compatible Mn doped ZnS nanocrystals

Fluorescent nanoparticles are receiving a lot of attention for potential applications in biological labeling [19-22] and as phosphor materials in field emission devices.[23] Zinc sulphide doped with manganese ($ZnS:Mn^{2+}$) is an efficient electroluminescent fluorophor exhibiting a wide emission band centered around 590 nm thereby emitting a visible orange luminescence. Although it exhibits much higher photo stability than commercial organic dyes, it has two significant drawbacks when directly applied *in vivo*. Semiconductor nanocrystals containing metal ions are toxic to human health. They are also incompatible with mainly hydrophilic biological systems. To overcome these problems, surface passivation is generally done by biofunctionalizing the nanocrystals using suitable capping agents.

Organic ligands that bind to the surfaces of the nanoparticles during synthesis, naturally provide surface passivation, that protects the nanoparticle surfaces from oxidation and minimizes the electronic trapping capabilities of surface defect. Suitable surface passivation leads to high photoluminescence efficiency in semiconductor quantum dots. In addition, luminescent nanoparticles can be functionalized by proper surface groups for coupling with bio-molecules, and they can be effectively delivered to specific targeting locations of interest. This has led to the development of water soluble and biocompatible, fluorescent nanomaterials, that find applications in bioimaging [24, 25]. In the presentwork, bio-compatible, manganese doped zinc sulphide nanocrystals have been synthesized by chemical capping co-precipitation method, using chitosan and aminoacid ligands as surface capping agents.

2.3.3 Synthesis of ZnO/PVA nanocomposite

Nowadays polymer based nanocomposites are of considerable interest because of their ability to combine the advantages of both polymers and filler components. There are several applications of polymeric nanocomposites based on their optical, electrical, mechanical and magnetic properties. Generally, nanocomposites can be obtained by both in-situ and ex-situ techniques. In in-situ methods, nano particles are generated inside the polymer matrix by decomposition or chemical reduction of a metallic precursor dissolved in the polymer. In the ex-situ approach, nanoparticles are first produced by soft chemistry routes and then dispersed into polymeric matrices. In the present work, zinc oxide/ polymer nanocomposite has been synthesized by direct solution mixing method. Poly Vinyl alcohol (PVA) is used as the polymer matrix for the nanosized zinc oxide in the synthesized ZnO/PVA

nanocomposite. PVA is a water soluble polymer with many technological, pharmaceutical and biomedical applications [26-29].

2.3.2 Synthesis of FeS_2/polymer nanocomposites

The solvothermal technique is becoming one of the most important tools in the processing of nanostructured materials for a wide variety of technological applications. Among various technologies available today in advanced material processing, the solvothermal technique occupies a unique place owing to its advantages over conventional technologies. The solvothermal technique not only helps in processing monodispersed and highly homogeneous nanoparticles, but also acts as one of the most attractive techniques for processing nano-hybrid and nanocomposite materials. Solvothermal processing can be defined as any heterogeneous reaction in the presence of aqueous solvents or mineralizers under high temperature conditions to dissolve and recrystallize materials that are relatively insoluble under ordinary conditions. The temperature, precursor concentration and time of reaction are the principal parameters in solvothermal processing. The solvothermal processing can be used to achieve high product purity and homogeneity, crystal symmetry, narrow particle size distribution, and a wide range of chemical compositions. It has the additional advantage of lower energy requirements and fast reaction times.

In the present investigation, FeS_2/polymer nanocomposites have been synthesized by solvothermal method. Synthesis under solvothermal conditions requires a vessel suitable for taking highly corrosive solvents at high temperature and pressure conditions. Ideal solvothermal apparatus popularly known as the autoclave should be inert towards acids, bases and oxidizing

agents, be of sufficient length to attain the desired temperature gradient and be leak-proof to the required temperature and pressure conditions. It should also be possible to assemble and dismantle the apparatus easily. The autoclave used in the present study for the synthesis of the $FeS2_2$/polymer nanocomposites is shown in figure 2.1.

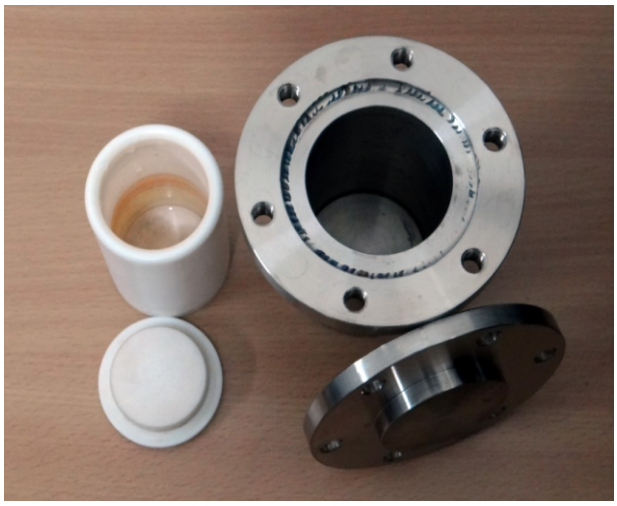

Figure 2.1 Autoclave and container used for the synthesis of FeS_2/polymer nanocomposites

In the solvothermal synthesis, the precursor materials are taken in a container. The closed container is then placed into the sealed stainless steel autoclave and put into the furnace after setting the desired temperature. Temperature fluctuations of the furnace have negative consequences because, rise in the temperature leads to a higher dissolution rate disturbing the dynamic equilibrium of dissolution-crystallization, and lowering of temperature leads to higher supersaturation.

2.3.4 Synthesis of polyaniline (PANI) and oleic acid modified PANI

Conducting polymers are generally synthesized by chemical or electrochemical oxidation of a monomer. Chemical method has the advantage of being simple with high production possibilities of bulk quantities. Chemical oxidative polymerization is typically carried out using relatively strong oxidants like ammonium peroxydisulphate. Peroxydisulphate is the most commonly used oxidant, and its ammonium salt is preferred to the potassium counterpart because of its better solubility in water. The oxidant is able to oxidize the monomer in solution, leading to the formation of cation radicals. These cation radicals further react with other monomers yielding the insoluble polymer. The oxidation of aniline is exothermic and the temperature of the reaction mixture can be used to monitor the progress of reaction. The efficient polymerization of aniline is achieved only in an acidic medium, where aniline exists as an anilinium cation. A variety of inorganic and organic acids of different concentration has been used in the syntheses of PANI. The synthesized PANI, protonated with various acids, differs in solubility, electrical conductivity, and stability. In the present study, chemical oxidative polymerization method has been used to synthesize PANI and oleic acid modified PANI.

2.3.5 Nanocomposite film coating techniques

Any solid material with one of its dimensions much less than that of the other two may be called a 'thin solid film' [30]. If the film growth is atom by atom or molecule by molecule, it is called a thin film and if the growth is grain by grain it is a thick film. The thickness is not as important in defining a film as the way it is created with the consequential effects on its nanostructure and

properties. The advances in thin film deposition techniques have revolutionized the device technology because of the possibility of device fabrication on large areas and flexible substrates at comparatively lower production costs.

Thin film properties are strongly dependent on the methods of deposition, the substrate materials, the substrate temperature, the rate of deposition and the background pressure. The properties of nanocomposite films can be easily adjusted by varying the composition of the filler materials. A wide variety of nanostructured films can be obtained by simply varying the deposition conditions during the growth of the films. Solution casting and spin-coating techniques have been used for the deposition of thin film samples investigated in the present work. Solution casting approach has been employed for the deposition of FeS_2/polymer nanocomposite films, and spin-coating technique, for the deposition of PANI and ZnO/PVA nanocomposite films. The spin coating unit (Spin 150) used in the present work is depicted in figure 2.2.

Figure 2.2 Spin-coating unit (Spin 150)

2.4 Characterization Techniques

The various tools used for the structural characterization of the samples investigated in the present work include, X-ray powder diffraction (XRD), transmission electron microscopy (TEM), field emission scanning electron microscopy (FESEM) and Fourier transform infrared (FT-IR) spectroscopy. Compositional analysis has been carried out by energy dispersive X-ray (EDX) technique. The thickness of the film samples has been estimated using stylus profiler. The optical characterization of the various nanostructures investigated in the present work has been carried out using the UV-Vis-NIR spectroscopic techniques. Thermogravimetric analysis (TGA) has been used for the thermal characterization of the samples. The photoluminescence (PL) studies have been conducted using the spectroflourimeter and fluorescence images obtained with fluorescence microscope.

2.4.1 X- Ray Diffraction (XRD)

X-ray diffraction is a versatile, non-destructive analytical method for identification and quantitative determination of various crystalline forms. The analysis can be made for a variety of crystalline solids including ceramics, metals, insulators, polymers, and semiconductors. Diffraction occurs as X-rays interact with a regular structure whose repeat distance is approximately the same as the X-ray wavelength.

X-ray diffraction can be used to study the crystallographic properties of polycrystalline, powder and thin film samples and also for the compositional analysis of nanocomposites. It can provide information about lattice parameters, orientation of the crystallites, phase composition and grain size. X-ray diffraction studies in the present work are done using Rigaku automated

X-ray diffractometer. The filtered Cu-K_α radiation (λ=1.5414A˚) is used for recording the diffraction pattern. A given crystalline substance always produces a characteristic diffraction pattern. Compared with conventional chemical analysis, X-ray diffraction has the advantage that it is usually much faster, requires only very small quantities of sample and is non-destructive [31, 32].

From the peak positions (diffraction angles) of the X-ray diffraction patterns together with their relative intensities, the crystalline phase of the sample can be identified. The average grain size 'd' of the sample can be calculated using the Debye Scherrer's formula,

$$d = \frac{0.9\lambda}{\beta \cos\theta}$$

where, λ is the wavelength of the X-rays, β is the full width at half maximum intensity [31] of the diffraction peaks in radians and θ is the glancing angle [33].

2.4.2 Field Emission Scanning Electron Microscope (FESEM)

Field Emission Scanning Electron Microscope (FESEM) is a type of electron microscope with a wide range of applications in material science and engineering. It works with electrons instead of light [34]. The electrons are liberated by a field emission source. These electrons interact with the atoms that make up the sample, producing signals that contain information about the sample's surface topography, composition, and surface roughness. Schematic representation of a field emission scanning electron microscope is shown in figure 2.3.

The electrons liberated from the field emission source are accelerated in a high electrical field gradient. Within the high vacuum column, these primary electrons are focused and deflected by electronic lenses to produce a narrow scan beam that bombards the specimen under study. As a result, secondary electrons are dislocated from each spot on the specimen. Detection of the secondary electrons results in a kind of three-dimensional shadow-cased surface representation of the sample and an image of the sample surface is constructed by comparing the intensity of these secondary electrons with that of the scanning primary electron beam. Finally the image is displayed on a monitor.

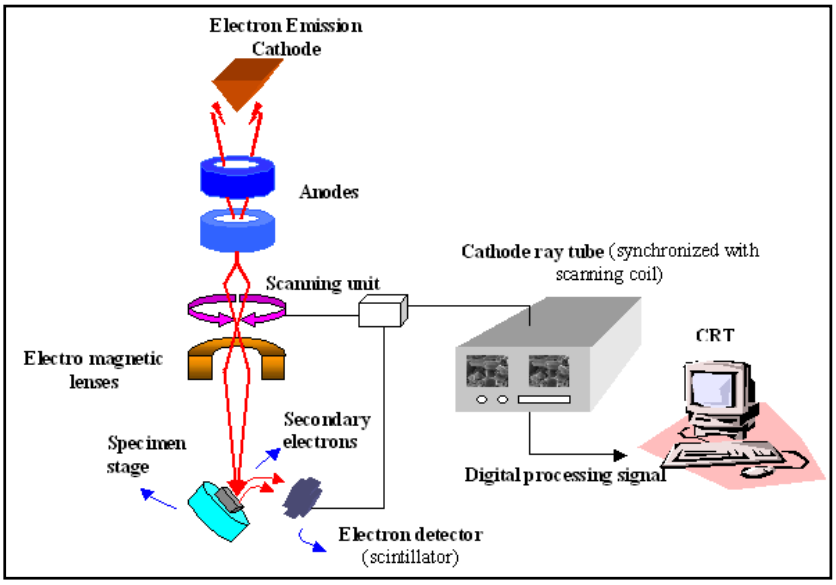

Figure 2.3 Schematic representation of a Field Emission Scanning Electron Microscope

FESEM produces a clean image of the sample with less electrostatic distortions and good spatial resolution giving specific information about topography, crystallography, surface characterization and specimen composition.

2.4.3 Transmission electron microscopy (TEM)

The transmission electron microscope (TEM) has become the premier tool for the microstructural characterization of materials. It is an imaging technique whereby a beam of electrons is focused onto a specimen, causing an enlarged version to appear on a fluorescent screen or layer of photographic film or to be detected by a CCD camera. The first practical transmission electron microscope was built by Albert Prebus and James Hillier at the University of Torondo in 1938 using concepts developed earlier by Max Knoll and Ernst Ruska.

The basic principle of TEM is quite similar to their optical counterpart, the optical microscope. The major difference is that in TEM, a focused beam of electrons instead of light is used to "image" and achieve information about the structure and composition of the specimen. An electron source usually named as the “Gun” produces a stream of electrons which is accelerated towards the specimen using a positive electrical potential. This stream is then focused using metal apertures and magnetic lenses called “condenser lenses” into a thin, focused, monochromatic beam. The focused beam strikes the specimen and a part of it gets transmitted through it. This portion of the beam is again focused using a set of lenses called “objective lenses” into an image. This image is then fed down the column through the “intermediate and projector lenses”, which enlarges the image, depending upon the set magnification. A phosphor image screen is used to produce the image. The image strikes screen and light is engendered, which enables the user to see the image [35]. The schematic diagram of a transmission electron microscope is shown in figure 2.4.

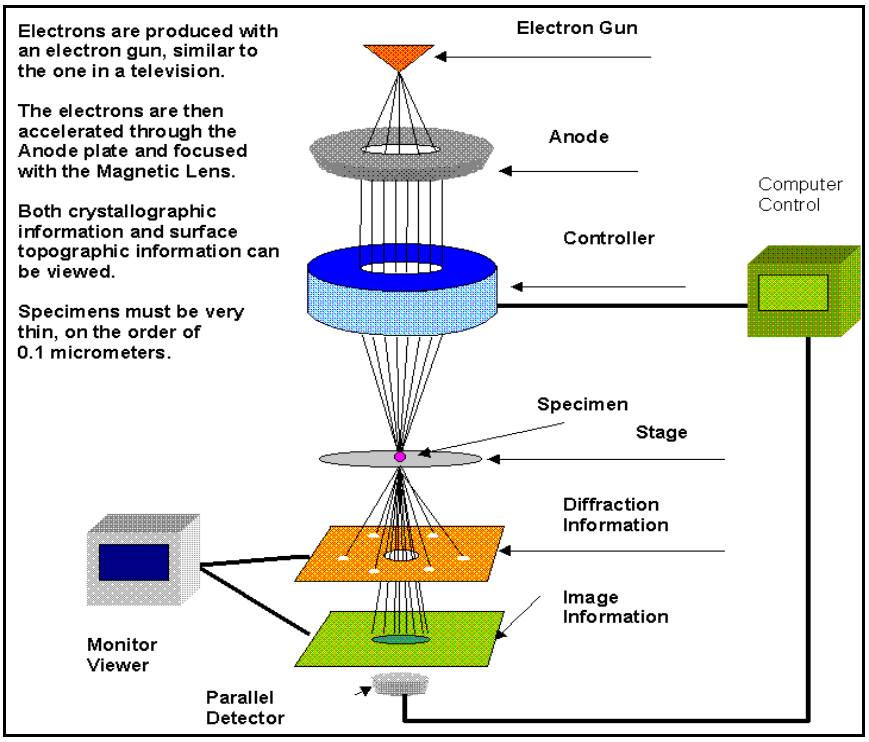

Figure 2.4 Schematic diagram of transmission electron microscope

From TEM images, size of the nanoparticles can be determined. Parallel lines in the high resolution transmission electron micrograph (HRTEM) represent planes in the crystal lattice and distance between them corresponds to d spacing. By comparing these d spacing values with the JCPDS data, one can identify the orientation of the planes in the synthesized material. The TEM images of the synthesized nanocrystals in the present work have been obtained using TEM, JEOL 3010 operating at an accelerating voltage of 200 kV.

2.4.4 Fourier Transform Infrared Spectroscopy (FT-IR)

Fourier Transform Infra-Red (FTIR) Spectroscopy is well proven as a sensitive, rapid technique for characterization of a broad range of materials. It

is the study of interaction of infrared radiation with matter as a function of photon frequency, which provides specific information about the vibration and rotation of the chemical bonding and molecular structures, making it useful for analyzing organic materials and certain inorganic materials. An infrared spectrum represents a fingerprint of a sample with absorption peaks which correspond to the frequencies of vibrations between the bonds of the atoms making up the material. Since each different material is a unique combination of atoms, no two compounds produce exactly the same infrared spectrum. Infrared spectroscopy can hence result in a qualitative analysis of every different kind of material. In addition, the intensity of the peaks in the spectrum is a direct indication of the quantity of material present. IR spectra originate in transitions between two vibrational levels of a molecule in the electronic ground state and are usually observed as absorption spectra in the infrared region. The advantages of infrared spectroscopy include wide applicability, nondestructiveness, measurement under ambient atmosphere and the capability of providing detailed structural information. Infrared spectroscopy by Fourier transform (FTIR) has additional merits such as: higher sensitivity, higher precision, quickness of measurement and extensive data processing capability [36-40].

An FT-IR spectrometer is based on a Michelson Interferometer. The interferometer consists of a beam splitter, a fixed mirror, and a mirror that translates back and forth. The beam splitter transmits half of the radiation striking it and reflects the other half as shown in figure 2.5. Radiation from the source strikes the beam splitter and gets separated into two beams. One of the beams is transmitted through the beam splitter to the fixed mirror and the second is reflected off the beam splitter to the moving mirror. The fixed and

moving mirrors reflect the radiation back to the beam splitter. Half of this reflected radiation is transmitted and half is reflected at the beam splitter, resulting in one beam passing to the detector and the second back to the source. In FTIR spectrometer the sample is placed between the output of the interferometer and the detector. The sample absorbs the radiation of a particular wavelength. After the collection of data, a computer performs a fast Fourier transform, which results in a frequency domain trace (i.e. intensity vs. wave number).

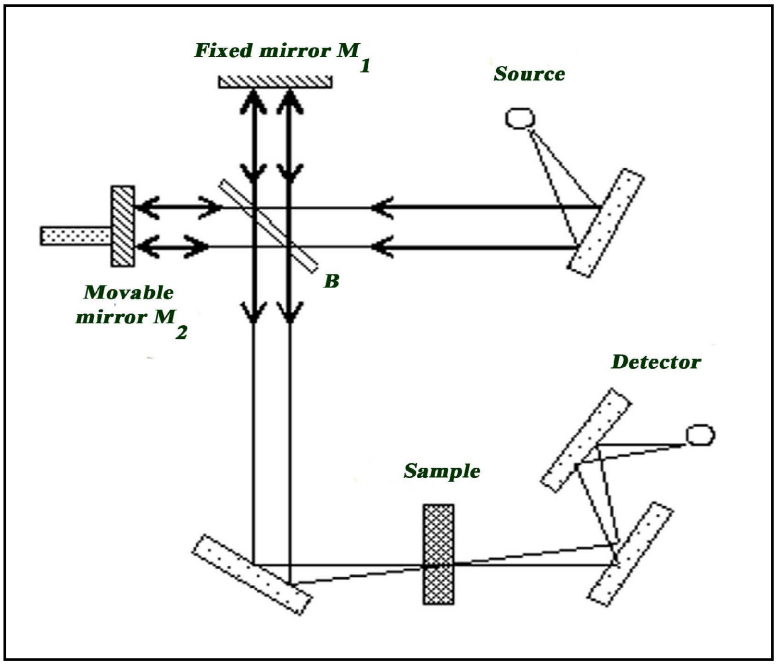

Figure 2.5 Schematic diagram of a Fourier transform infrared spectrometer

The frequency domain can be divided into two regions. the functional group region and the finger print region. The region ranging from 1500cm^{-1} to 4000 cm^{-1} is called the functional group region and the region below 1500cm^{-1} corresponds to the fingerprint region. The functional group region includes

generally stretching vibrations which are localized and gives information about the nature of the components that make up the molecule. The finger print region includes molecular bending vibrations characteristic of the entire molecule [41]. Fourier transform infrared spectra of the samples synthesized in the present investigation are taken using AVTAR 370 system with a resolution of $4cm^{-1}$ in the range $400\text{-}4000cm^{-1}$.

2.4.5 Energy dispersive X-ray (EDX) spectroscopy

Energy dispersive X-ray spectroscopy (EDS or EDX) is an analytical technique used for the elemental analysis or chemical characterization of a sample. As a spectroscopic technique, it relies on the investigation of a sample through interactions between electromagnetic radiation and matter, analyzing X-rays emitted by the matter in response to being hit by charged particles. Its characterization capabilities are due in large part to the fundamental principle that each element has a unique atomic structure allowing X-rays that are characteristic of an element's atomic structure to be identified uniquely from each other. The EDX analysis system works as an integrated feature of a scanning electron microscope (SEM), and cannot operate on its own without the latter [42, 43].

To stimulate the emission of characteristic X-rays from a specimen, a high energy beam of charged particles such as electrons or protons, or a beam of X-rays, is focused into the sample being studied. At rest, an atom within the sample contains ground state (or unexcited) electrons in discrete energy levels or electron shells bound to the nucleus. The incident beam may excite an electron in an inner shell, ejecting it from the shell while creating an electron hole where the electron was. An electron from an outer, higher-energy shell

then fills the hole, and the difference in energy between the higher-energy shell and the lower energy shell may be released in the form of an X-ray. The number and energy of the X-rays emitted from a specimen can be measured by an energy dispersive spectrometer. As the energy of the X-rays are characteristic of the difference in energy between the two shells, and of the atomic structure of the element from which they were emitted, this allows the elemental composition of the specimen to be accurately determined.

2.4.6 Thermo Gravimetric Analysis (TGA)

Thermo gravimetric analysis (TGA) is an experimental technique in which the weight of a sample is measured as a function of sample temperature or time. It is commonly employed to determine degradation temperatures, absorbed moisture content of materials, the level of inorganic and organic components in materials, decomposition points of explosives, and the presence of solvent residues. The analyzer usually consists of a high-precision balance with a pan (generally platinum) loaded with the sample. The pan is placed in a small electrically heated oven with a thermocouple to accurately measure the temperature. Analysis is carried out by heating the sample at a constant heating rate and plotting weight against temperature. The results of the measurement are usually displayed as a TGA curve in which percent weight is plotted against temperature. The atmosphere may be purged with an inert gas to prevent oxidation or other undesired reactions. A computer is used to control the instrument.

2.4.7 Stylus profiler for film thickness measurement

Thickness is one of the most important thin film parameters to be accurately determined, since it plays an important role in the film properties

unlike a bulk material. Reproducible properties are achieved only when the film thickness and the deposition parameters are kept constant. Film thickness may be measured either by in-situ monitoring of the rate of deposition or after the film deposition. The thickness of the film samples investigated in the present work has been measured by Veeco Dektak 6M stylus profiler.

The stylus profiler takes measurements electromechanically by moving the sample beneath a diamond tipped stylus. The high precision stage moves the sample according to a user defined scan length, speed and stylus force. The stylus is mechanically coupled to the core of a linear variable differential transformer (LVDT). The stylus moves over the sample surface. Surface variations cause the stylus to be translated vertically. Electrical signals corresponding to the stylus movement are produced as the core position of the LVDT changes. The LVDT scales an ac reference signal proportional to the position change, which in turn is conditioned and converted to a digital format through a high precision, integrating, analog-to-digital converter. The film whose thickness has to be measured is deposited with a region masked. This creates a step on the sample surface. The thickness of the sample can be determined accurately by measuring the vertical motion of the stylus over the step.

2.4.8 UV-VIS-NIR absorption spectroscopy

Absorption spectroscopy refers to spectroscopic techniques that measure the absorption of radiation, as a function of frequency or wavelength, due to its interaction with a sample. The sample absorbs energy, i.e., photons, from the radiating field. The intensity of the absorption varies as a function of frequency, and this variation is the absorption spectrum. Absorption

spectroscopy uses light radiation in the visible, ultraviolet (UV) and near infrared (NIR) ranges. The UV-VIS-NIR spectrophotometer used for optical characterization is shown schematically in figure 2.6.

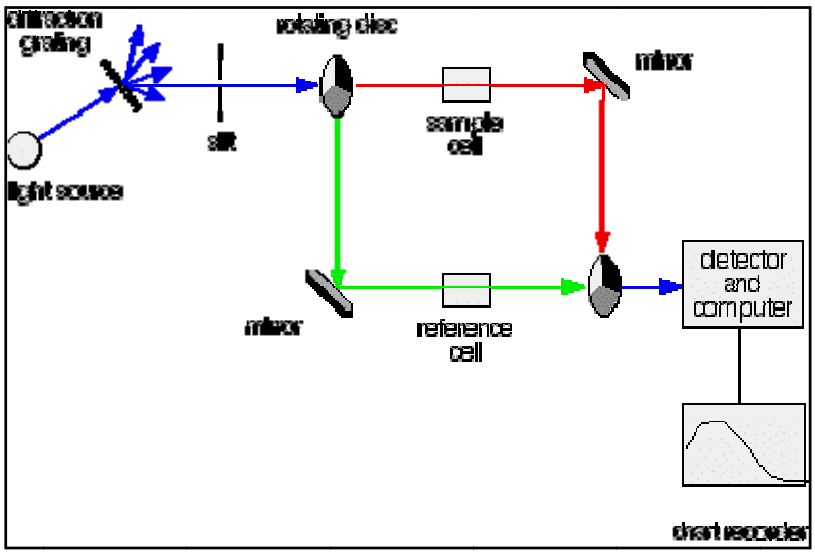

Figure 2.6 UV-VIS-NIR spectrophotometer

An optical absorption spectrum provides information on the wavelength of electromagnetic radiation that can be absorbed by the samples under study. This is determined by varying the wavelength and recording the intensity of the transmitted beam. When light is absorbed, the energy of absorbed photons is used to excite a transition between electronic levels, usually starting from the electronic ground state. The position of higher energies can be derived from the absorption spectrum [44]. Also it can be used to determine the band gap of the material [45]. When an incident light beam reaches a medium, part of the beam will be reflected by the medium, part of it will be transmitted through the medium and the rest of the beam will be absorbed. Absorption of photons results in the transition of electrons from the

lower energy level to the higher energy levels. The absorption ability of a material is measured by its absorption coefficient.

If assuming a parabolic band structure for the material, the absorption coefficient α and band gap E_g can be related by the expression

$$\alpha = \frac{A}{h\nu} (h\nu - E_g)^r$$

where hν is the photon energy and A is the parameter which depends upon the transition probability. The constant r depends upon the nature of electronic transition. For direct allowed transitions r=1/2, for indirect allowed transitions r=2, for forbidden indirect transitions r=3 and for forbidden direct transitions r=3/2. The absorption coefficient can be deduced from the absorption or transmission spectra using the relation

$$I=I_0 \exp(-\alpha t)$$

where I is the transmitted intensity and I_0 is the intensity of the incident light and t is the thickness of the sample. The band gap energy can be determined by extrapolating the linear portion in the $(\alpha h\nu)^2$ versus hν plot to the abscissa. The absorption coefficient is a function of frequency. In the present studies, the optical absorption of the samples has been recorded using JASCO V570 spectrophotometer**.**

2.4.9 Diffuse Reflectance Spectroscopy (DRS)

The optical band gap E_g of powder samples is estimated from the UV-VIS diffuse reflectance spectroscopic (UV-VIS DRS) studies in the wavelength range from 190nm to 1200nm. The samples for this study are used in the form of powder and pure $BaSO_4$ is used as the reference. Diffuse

Reflectance Spectroscopy (DRS), also sometimes known as Elastic Scattering Spectroscopy, is a non-invasive technique that uses the interaction of light with the medium. Reflection and scattering produce a characteristic reflectance spectrum, providing information about the structure and composition of the medium. The light from a broadband source is launched into a fiber-optic bundle, the end of which constitutes a reflectance probe. Light leaves the probe and enters the medium under investigation. After the processes of scattering and absorption, light that leaves the medium is collected by another fiber, and directed into a spectrometer. This is interfaced to a computer, which controls the data acquisition and displays the collected spectrum.

Based on the optical properties of the sample, several models have been proposed to describe the diffuse reflectance phenomena. The Kubelka - Munk (KM) model put forward in 1931 [46, 47] is widely used and accepted in DRS studies. The KM theory is based on a continuum model where reflectance properties are described by differential equations for infinitesimally small layers. When the depth of the sample is infinite, the theory is solved to arrive at the Kubelka - Munk function $f(r_\alpha)$,

$$f(r_\alpha) = (1-r_\alpha)^2 / 2r_\alpha = k / s$$

Where $r_\alpha = R_\alpha$ (sample) $/ R_\alpha$ (standard)

R_α denotes the diffuse reflectance of the sample and the standard used is BaSO4. R_α (standard) is taken as unity. The intensity of the diffusely reflected light therefore depends on the scattering coefficient s and the absorption coefficient k. The band gap is estimated from the plot of $[(k/s).h\nu]^2$ versus $h\nu$.

2.4.10 Photoluminescence (PL)

Photoluminescence (PL) is the spontaneous emission of light from a material under optical excitation. Photoluminescence spectroscopy is a contact-less, nondestructive method of probing the electronic structure of materials. Light is directed onto a sample, where it is absorbed and imparts excess energy to the material in a process called photo-excitation. One of the ways through which this excess energy can be dissipated by the sample is through the emission of light, or luminescence. In the case of photo-excitation, this luminescence is called photoluminescence. Photo-excitation causes electrons within the material to move into permissible excited states. When these electrons return to their equilibrium states, the excess energy is released either through the emission of light, which is a radiative process or through non-radiative processes. The energy of the emitted light (photoluminescence) is related to the difference in energy levels between the two electron states involved in the transition between the excited state and the equilibrium state. The intensity and spectral content of the photoluminescence give a direct measure of various important material properties. The excitation energy and intensity are chosen to probe different regions and excitation concentrations in the sample [48].

Photoluminescence (PL) investigations can be used to characterize a variety of material parameters. The intensity of the PL signal provides information on the quality of surfaces and interfaces. Luminescence is a process which involves at least two steps: the excitation of the electronic system of the material and the subsequent emission of photons. When light of sufficient energy is incident on a material, photons are absorbed and electronic excitations are created. Eventually, these excitations relax and the electrons

return to the ground state. If radiative relaxation occurs, the emitted light is called PL. This light can be collected and analyzed to yield a wealth of information about the photo excited material. The PL intensity gives a measure of the relative rates of radiative and non-radiative recombination. The schematic block diagram showing the components of photoluminescence set up is shown in figure 2.7.

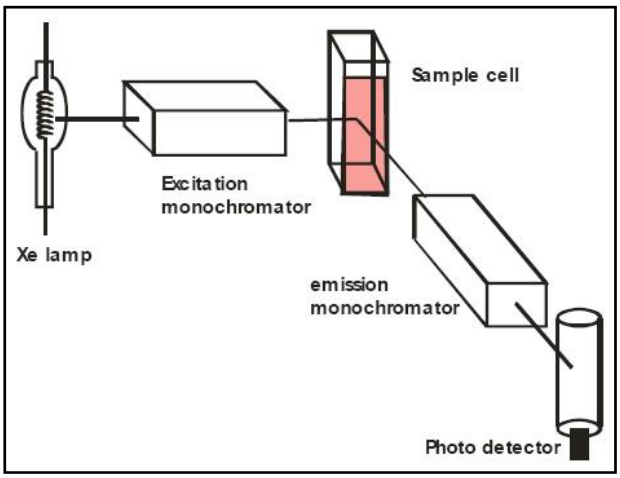

Figure 2.7 Schematic diagram of a photoluminescence set up

In the present work, the excitation and emission spectra of the samples are recorded using Fluoromax -3 spectroflurometer consisting of 150W Xenon arc lamp, monochromator and a detector. A continuous source of light shines on to an excitation monochromator, which selects a band of wavelengths. This monochromatic light is directed onto the sample, which shows luminescence emission. The emitted light is directed to a second emission monochromator which selects a band of wavelengths and shines them onto a photon counting detector. The signal from the detector is directed to a system controller and a host computer, where the data can be manipulated and presented using spécial software.

2.4.11 Fluorescence microscope

British scientist Sir George G. Stokes was the first to described fluorescence in 1852 and was responsible for coining the term when he observed that the mineral fluorspar emitted red light when it was illuminated by ultraviolet excitation. Stokes noted that fluorescence emission always occurred at a longer wavelength than that of the excitation light. Early investigations in the 19th century showed that many specimens (including minerals, crystals, resins, crude drugs, butter, chlorophyll, vitamins, and inorganic compounds) fluoresce when irradiated with ultraviolet light. However, it was not until the 1930s that the use of fluorochromes was initiated in biological investigations to stain tissue components, bacteria, and other pathogens. Several of these stains were highly specific and stimulated the development of the fluorescence microscope. The technique of fluorescence microscopy has become an essential tool in biology and the biomedical sciences, as well as in material science due to attributes that are not readily available in other contrast modes with traditional optical microscopy.

The Principle of Fluorescence

In photoluminescence there is always a certain time lapse between the absorption and emission of light. If the time lag is greater than 1/10,000 of a second, it is generally called phosphorescence. On the other hand, if the time lapse is less than 1/10,000 of a second, it is known as fluorescence**.** Fluorescence is initiated when a molecule absorbs energy from a passing wave of light. The excited molecule, after a brief period of time, will return to its fundamental energy state after emitting fluorescent light. Thus, fluorescence is a physical phenomenon in which a compound absorbs light and re-emits this

as light of a usually higher wavelength. Since the excitation light source and the emitted fluorescence can be separated very well, one can detect fluorescence with very high sensitivity, making it even possible to visualize single molecules. The Jablonski diagram, which illustrates the electronic states of a molecule and the transitions between them is shown in figure 2.8.

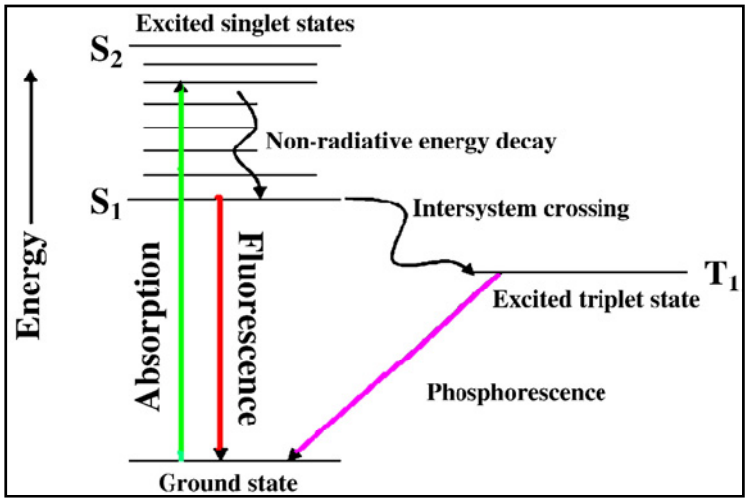

Figure 2.8 Jablonski diagram illustrating the electronic states of a molecule and the transitions between them

The basic function of a fluorescence microscope is to irradiate the specimen with a desired and specific band of wavelengths, and then to separate the much weaker emitted fluorescence from the excitation light. In a properly configured microscope, only the emission light should reach the eye or detector so that the resulting fluorescent structures are superimposed with high contrast against a very dark (or black) background. The limits of detection are generally governed by the darkness of the background, and the excitation light is typically several hundred thousand to a million times brighter than the emitted fluorescence.

The fluorescence microscope is an instrument that is indispensible in certain diagnostic and research endeavors. It differs from an ordinary brightfield microscope in several respects. First of all, it utilizes a powerful mercury vapor arc lamp for its light source. Secondly, a darkfield condenser is usually used in place of the conventional Abbé brightfield condenser. The third difference is that it employs three sets of filters to alter the light that passes up through the instrument to the eye.

The design of a fluorescence microscope consists of a basic reflected light microscope in which the wavelength of the reflected light is longer than that of the excitation. The universal reflected light vertical illuminator is interposed between the observation viewing tubes and the nosepiece carrying the objectives. Johan S. Ploem is credited with the development of the vertical illuminator for reflected light fluorescence microscopy. In a fluorescence vertical illuminator, light of a specific wavelength (or defined band of wavelengths), often in the ultraviolet, blue or green regions of the visible spectrum, is produced by passing multispectral light from an arc-discharge lamp or other sources through a wavelength selective **excitation** filter. Wavelengths passed by the excitation filter get reflected from the surface of a **dichromatic** mirror or beam splitter, through the microscope objective to bath the specimen with intense light. If the specimen fluoresces, the emission light gathered by the objective passes back through the dichromatic mirror and is subsequently filtered by a **barrier** (or **emission**) filter, which blocks the unwanted excitation wavelengths. An upright fluorescence microscope (Olympus BX51) with the fluorescent filter cube turret above the objective lenses, coupled with a digital camera used for the present investigations is shown below in figure 2.9

Figure 2.9 The Olympus BX51 Fluorescence Microscope

It is important to note that fluorescence is the only mode in optical microscopy where the specimen, subsequent to excitation, produces its own light. The emitted light re-radiates spherically in all directions, regardless of the excitation light source direction.

References

[1] M. S. Hussain , Salah Al- Swailem and Ahmed Hala, *International J of Nanoparticles* 2 (2009) 282

[2] K. E. Gonsalves, S. P. Rangarajan and J. Wang edited by H. S. Nalwa, Nanostructured Materials and Nanotechnology, Academic Press, Newyork (2002).

[3] A. Rahm, M. Lorenz, T. Nobis, G. Zimmermann, M. Grundmann, B. Fuhrmann and F. Syrowatka, *Appl. Phys. A* 88 (2007) 31

[4] C. Johnson, R. Gemmen and N. Orlovskaya, *Composites Part B: Eng*. 35 (2004) 167

[5] C. C. Koch, *Nanostructured Mater*. 9 (1997) 13

[6] T. L. Brown, S. Swaminathan, S. Chandrasekar, W. D. Compton, A. H. King and K. P. Trumble, *J.Mater. Res*. 17 (2002) 2484

[7] Li,Yuntao,Sue,Hung-jue, Nishimura, Riichi, Miyatake, Nubuo," Process for preparing nanosized metal oxide particles-patent 7482382 (2009)

[8] M. Ohring. Materials Science of Thin Films: Deposition and Structure. Academic Press, New York, 2001.

[9] K. Byrappa, I. Yoshimura, and M. Yoshimura. Handbook of Hydrothermal Technology. William Andrew Publishing, New York, 2001.

[10] P. Layrolle, A. Ito, and T. Tateishi, *J. Am. Ceram. Soc*. 81(1998) 1421

[11] G. Kordas and CC. Trapalis, *J. Sol-gel Sci. Tech*. 9 (1997) 17

[12] A. Jillavenkatesa and Sr RA. Condrate, *J. Mater. Sci*. 33 (1998) 4111

[13] A. Jillavenkatesa, D.T. Hoelzer, and RA. Condrate, *J. Mater.Sci.* 34 (1999) 4821

[14] M.F. Hsieh, L.H Perng., T.S. Chin, and H.G. Perng, *Biomaterials* 22 (2001) 2601

[15] M.F. Hsieh, L.H. Perng, and T.S. Chin, *J. Sol-gel Sci. Tech*. 23 (2002) 205

[16] K.A. Gross, C.S. Cahi, G.S.K. Kannangara, and B. Ben Nissan. *J. Mater. Sci. Mater. Med.* 9 (1998) 839

[17] Tas A. Cuney, F. Korkusuz, M. Timicin, and N. Akkas, *J. Mater.Sci. Mater. Med*. 8 (1997) 91

[18] S.H. Rhee and J. Tanaka, *J. Am. Ceram. Soc*. 81 (1998) 3029

[19] M. Bruchez, M. Moronne, P. Gin, S. Weiss and A. P. Alivisatos, *Science*, 281 (1998) 2013

[20] W. C. W. Chan and S. Nie, *Science*, 281 (1998) 2016

[21] R. Elghanian, J. J. Storhoff, R. C. Mucic, R. L. Letsinger and C.A. Mirkin, *Science,* 277 (1997) 1078

[22] F. V. D. Rijke, H. Zijlmans, S. Li, T. Vail, A. K. Raap, R. S. Niedbala and H. J. Tanke, *Nat. Biotechnol.,* 19 (2001) 273

[23] A.C Wright, I.V.F Viney: *Philosophical Magazine B*. Vol. 81(3) (2001), p.279.

[24] D. Gerion, F. Pinaud, S. C. Williams, W. J. Parak, D. Zanchet, S. Weiss, Alivisatos, A. P. *J. Phys. Chem. B* 195 (2001) 8861

[25] Y. W. Jun, J. T. Jang, J. W. Cheon, *Bull. Kor. Chem. Soc.* 27 (2006) 961

[26] C.M. Hassan and N.A. Peppas, *Adv. Polym. Sci.* 153 (2000) 37-65

[27] M. Kokabi, M. Sirousazar, and Z. Hassan, *Eur. Polym. J*. 43 (2007) 773-781

[28] M. Nagura, T. Hamano, H. Ishikawa, *Polym*. 30 (1989) 762-765

[29] C.A. Scotchford, M.G. Cascone, S.Downes, and P.Giusti, *Biomaterials*. 19 (1998) 1-11

[30] K.L Chopra, S. Major, and D. K. Pandya, *Thin solid films* 102 (1983) 1

[31] B.D.Cullity and S.R. Stock," Elements of X-Ray Diffraction", Third edition, New Jersey, Prentice Hall (2001)

[32] M.J. Buerger, "X-Ray Crystallography", John Wiley and sons, NewYork (1962)

[33] C. Kittel, Introduction to Solid State Physics, Seventh edn, Wiley Eastern Limited, USA (1996)

[34] D. K. Schroder, Materials and Device Characterization, Wiley-Interscience, N .Y, 1998.

[35] P. E. J. Flewitt and R. K. Wild, Physical methods for materials characterisation, IOP Publishing Ltd, London (2003)

[36] Fately,W.G., Mc Devit,N., Bentely,F.F.: *Appl.Spectrosc*., 25 (1971) 155

[37] Halberstadt, E.S., Henish, H.K.: *J.Crystal Growth*, 3 (1968) 363

[38] Hobden, M.V.: *J.Appl.Phys.,* 38 (1967) 4365

[39] Kaneko, N., Kaneko, M., Takanashi, H. : *Spectrochim. Acta Part A*, 40 (1984) 33

[40] Lippincott, E.R., Schroeder, R .: *J.Chem.Phys*., 23 (1955) 1099

[41] Stuart.A.V, Sutherland,G.B. M.J. *Chem.Phys*. 24 (1956) 559

[42] D. K. Schroder Semiconductor material and device characterization, second edition, A Wiley-interscience publication, New York, 1998.69

[43] P. E .J. Flewit and R. K. Wild, Physical methods for material characterization, second edition, IOP publishing, London, 2003.

[44] D.R.Viji, "Luminescence of solids", Plenum Press, NewYork (1998)

[45] A.L. Fahrenbruch and R.H.Bube," Fundamentals of solar cells", Academic Press, NewYork (1983)

[46] P. Kubelka and F. Munk, Zh. Tekh. Fiz. 12 (1931) 593

[47] P. Kubelka, *J. Opt. Soc. Am*. 38 (1948) 448

[48] T.H.Gfroerer," Photoluminescence in Analysis of Surfaces and Interfaces", JohnWiley & Sons Ltd, Chichester (2000)

Chapter 3

OPTICAL PROPERTIES OF ZINC OXIDE/POLYVINYL ALCOHOL NANOCOMPOSITE FILMS

Contents

This chapter deals with the synthesis of oleic acid modified ZnO nanorods and ZnO/PVA nanocomposite films and the detailed structural and optical characterization of the synthesized samples. It has been observed that the optical absorption of ZnO/PVA nanocomposite films prepared from OA modified ZnO nanorods in the UV region is quite high. Oleic acid modification is also found to enhance the photoluminescence emission intensity in ZnO/PVA nanocomposite films, significantly. The excellent UV absorption around 300 nm, observed in these nanocomposite films offers prospects of applications as efficient UV filters in this wavelength region.

M. Sajimol Augustine et al.

Journal of Physics and Chemistry of Solids,73 (2012) 396-401
"Excellent UV absorption in spin-coatedthin films of oleic acid modified Zinc oxide nanorods embedded in Polyvinyl alcohol"

3.1 Introduction

Design and synthesis of new polymer nanocomposites have gained increasing attention in many technologically important fields. There are several applications of polymeric nanocomposites based on their optical, electrical and mechanical properties [1, 2]. Combining the properties of the polymer matrix and the inorganic filler creates an economic way to obtain desired high performance materials [3]. Significant progress has been made in this area during the past decades. A variety of polymer/inorganic filler nanocomposites that offer attractive mechanical, thermal, optical and electrical properties has been investigated extensively [4-7]. In particular, ZnO/ polymer nanocomposite materials have attracted global interest. The introduction of ZnO filler into polymer matrices can suitably modify the optical, electrical and mechanical properties of the polymers, with the possibilities of designing materials with desired characteristics [8-10].

Zinc oxide is a well known transparent conducting oxide (TCO) with a wide and direct band gap of about 3.37 eV and high room temperature exciton binding energy of 60 meV. These factors make it a highly pursued material for optical and optoelectronic applications [11]. Simple and cost effective chemical techniques can be used to synthesize ZnO, which offer the possibilities of achieving uniform dispersion in polymer matrices. Semiconductor nanocrystals generally have mechanical, optical, electrical and thermal properties quite different from their bulk analogue [12]. One-dimensional (1D) nanostructured materials, such as nanorods, nanowires, nanotubes, and nanobelts, have recently attracted much attention because of their wide potential applications in optoelectronics and photonics [13,14].

Polyvinyl alcohol (PVA) is a water-soluble, transparent and biodegradable polymer with many technological, pharmaceutical and biomedical applications [15–18]. Usually inorganic semiconductors including ZnO are much more expensive than organic polymers. The cost, therefore, becomes a prohibiting factor for mass production of ZnO/polymer nanocomposites. An ideal strategy is to incorporate only a small amount of ZnO to significantly improve the properties of the polymers.

The significance of the present work is that it was possible to synthesize good quality, well separated ZnO nanorods by the simple wet chemical method at room temperature in the presence of oleic acid. This technique is quite cost effective compared to the techniques already reported for synthesizing ZnO nanorods [19, 20]. Highly transparent ZnO/PVA nanocomposite thin films could also be prepared successfully using spin-coating technique using pristine and oleic acid modified ZnO nanorods. The surface modification of ZnO nanorods with oleic acid capping has found to be quite effective in enhancing the PL emission intensity and UV absorption of the ZnO/PVA nanocomposite films.

3.2 Experimental Details

3.2.1 Synthesis of ZnO nanorods

The synthesis of ZnO nanorods by wet chemical method with zinc acetate and sodium hydroxide in ethanol at room temperature has already been reported [19]. In the present work, this technique has been modified by carrying out the synthesis in the presence of oleic acid. Synthesis by chemical

route has the advantage of being more economical compared to the complex epitaxial methods**.** In addition, the presence of oleic acid can suitably modify the size and shape of ZnO nanorods by controlling the growth conditions.

In the present work, ZnO nanorods were obtained by the reaction of zinc acetate with sodium hydroxide in a 1:2 molar ratio with ethanol as solvent at room temperature. Zinc acetate dihydrate (0.1 mol L^{-1}) was dissolved in 50ml ethanol and then sodium hydroxide (0.2 mol L^{-1}) was added and stirred well. The colloidal solution obtained was filtered and dried to get the white ZnO powder which was used for structural analysis and also for making nanocomposite thin films. The experiment was repeated under the same conditions at room temperature in the presence of oleic acid (wt% = 0.05), to get oleic acid modified ZnO nanorods.

3.2.2 Synthesis of ZnO/PVA nanocomposite in bulk and thin film forms

The ZnO/PVA nanocomposite was synthesized by adding ZnO powder into aqueous solution of PVA (Molecular Weight-1,25,000; Purchased from Central Drug House, Private Limited, Delhi, India) and then stirring the mixture for two hours and sonicating for five minutes. From this solution, highly transparent and homogeneous thin films of the nanocomposite were deposited on ultrasonically cleaned and optically flat glass substrates using spin-coating technique (Spin 150). ZnO/PVA nanocomposite thin films were obtained with both pristine and oleic acid modified ZnO, using 1, 2 and 3 weight % of ZnO powder. The thickness of these films was fixed to be around 1μm (measured using Veeco Dektak 6M stylus profiler) by controlling the coating time and spinning speed of the spin-coating unit.

3.3 Sample Characterization

The XRD analysis of the samples was carried out using Rigaku X-ray Diffractometer with Cu-Kα (1.5418 A^o) radiation, operating at 30 kV and 20 mA. Scanning was carried out in the 2θ range from 10^o–70^o at a scan speed of 2^o per minute. The high resolution transmission electron microscope (HRTEM) images of the synthesized nanocrystals were obtained using JEOL 3010 instrument with a UHR polepiece. Field emission scanning electron microscopy (FESEM) images were obtained using a HITACHI SU 6600 Microscope with an accelerating voltage of 20 kV. The energy dispersive X-ray spectrum (EDXS) of the nanoparticles and composites were obtained with JEOL Model JSM - 6390LV scanning microscope. Fourier transform infrared (FT-IR) spectra of the samples were obtained with AVTAR 370 DTGS FTIR spectrophotometer in the wave number range 400–4000cm^{-1}. UV-Visible absorption spectra were recorded on a Jasco-V 500 spectrophotometer in the wavelength range 190–700 nm. The PL emission spectra of the samples were obtained with Fluoromax-3 Spectrofluorimeter using Xe lamp as excitation source under an excitation at 325 nm.

3.4 Results and Discussion

3.4.1 X-Ray Diffraction (XRD) analysis

The XRD patterns of pristine and OA modified ZnO nanorods are shown in figure 3.1. The XRD patterns show sharp and intense diffraction peaks of ZnO for both pristine and OA modified samples. The diffraction peaks corresponding to (100), (002), (101), (102), (110), (103), and (112) planes confirm the hexagonal wurtzite structure of zinc oxide [21]. The broadening of the XRD peaks indicates the formation of nano sized particles

in the prepared samples. The grain size is estimated using Scherrer formula given by

$$d = 0.9\lambda/\beta \cos\theta \qquad (1)$$

where d, λ, β and θ are the average particle size, the wavelength of the X-ray, full width at half maximum(FWHM) intensity expressed in radians and diffraction angle respectively.

The size of the nanorods in pristine and OA modified ZnO is calculated as 7 nm and 22 nm, respectively. This shows that the particle size has increased slightly in OA modified ZnO, though the synthesis conditions are kept the same [22]

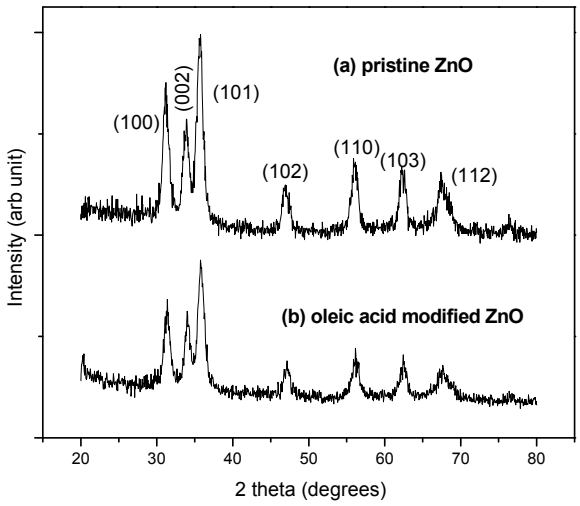

Figure 3.1 XRD patterns of pristine and OA modified ZnOnanorods

The XRD patterns of OA capped ZnO nanorods, pure PVA film and ZnO/PVA nanocomposite film are shown in figure 3.2. The XRD pattern of OA capped ZnO shows all the characteristic peaks of ZnO. The PVA film has a broad noncrystalline peak at 20^{o} and the ZnO/PVA film shows the peaks of

both ZnO and PVA. This confirms the formation of the ZnO/PVA nanocomposite in the prepared sample. The presence of ZnO produces neither new peaks nor peak shifts with respect to PVA showing that nanosized ZnO filled PVA composites consist of two phase structures.

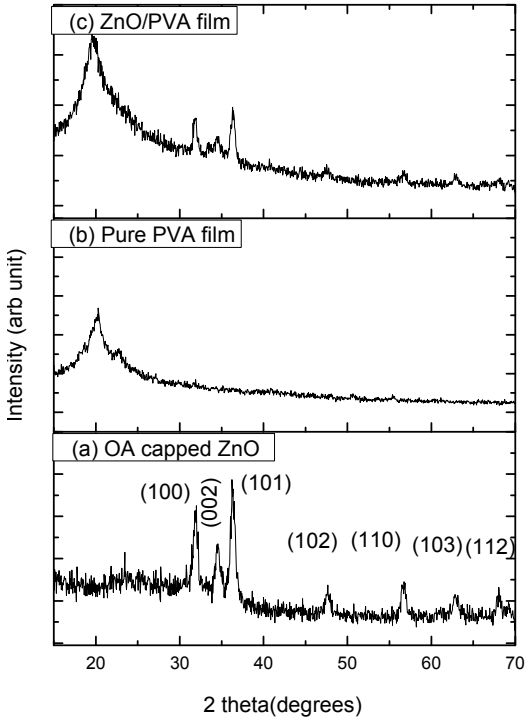

Figure 3.2 XRD patterns of (a) OA modified ZnO, (b) PVA film and (c) ZnO/PVA film

3.4.2 Energy Dispersive X-ray (EDX) spectral analysis

The Energy Dispersive X-ray (EDX) spectrum of OA capped ZnO nanorods is shown in figure 3.3, which provides the elemental composition of the sample. The diagram shows the peaks of zinc, oxygen and carbon, which confirms the presence of zinc oxide and oleic acid in the prepared sample of oleic acid modified ZnO nanorods.

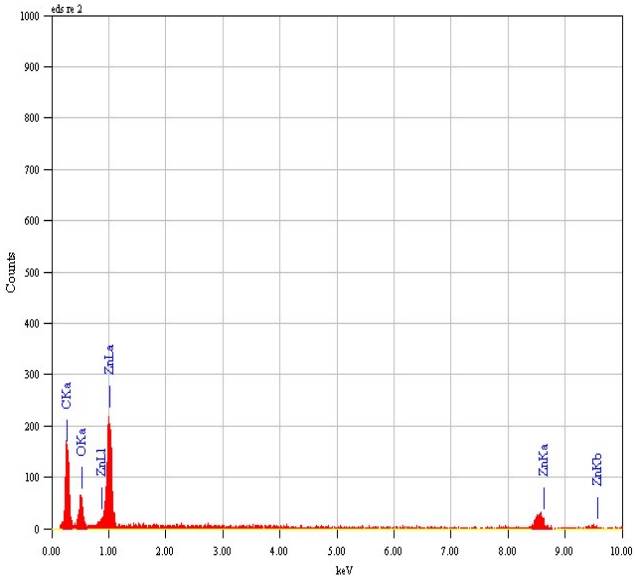

Figure 3.3 EDXS pattern of OA modified ZnO nanorods.

3.4.3 Transmission Electron Microscopy (TEM) studies

The Transmission Electron Microscope (TEM) images of pristine and oleic acid modified ZnO nanorods are shown in figures 3.4 (a) and (b). From the TEM images it is seen that well separated ZnO nanorods of average diameter 25nm can be obtained with the addition of oleic acid at room temperature. Atomic scale image (HRTEM) of the OA modified ZnO nanorods is depicted in figure 3.4 (c), which shows that these nanorods of average size 25 nm are polycrystalline in nature and they are aggregations of nanocrystals.

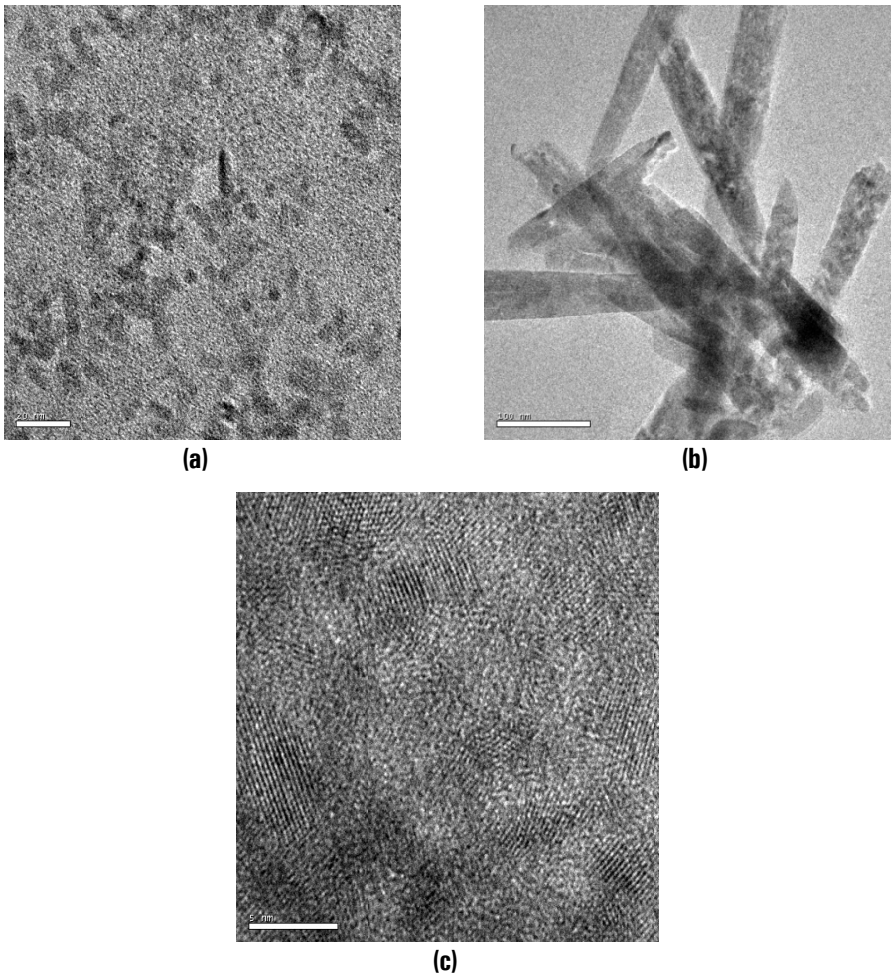

Figure 3.4 TEM images of (a) pristine ZnO nanorods (scale bar:20 nm), (b) OA modified ZnO nanorods (scale bar:100 nm) and (c) HRTEM image of OA modified ZnO nanorods (scale bar:5 nm).

3.4.4 Field emission scanning electron microscopy (FESEM) Analysis

Field emission scanning electron microscope (FESEM) images of ZnO (both pristine and OA modified) /PVA nanocomposite films are shown in figures 3.5 (a) and (b). The images confirm homogeneous dispersion of pristine and OA modified ZnO nanorods in the PVA matrix . It is observed

that OA modified ZnO nanorods are more homogeneously dispersed in the PVA matrix compared to the unmodified ones. The efficiency of nanoparticles in improving the properties of the polymer matrix is determined by the degree of dispersion in the matrix.

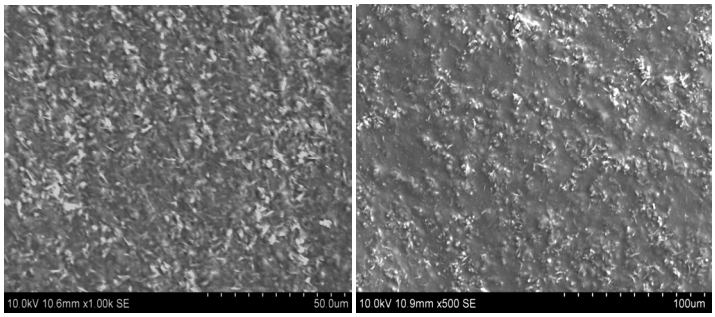

Figure 3.5 FESEM images of ZnO/PVA nanocomposite film using (a) pristine ZnO nanorods and (b) OA modified ZnO nanorods

3.4.5 Fourier transform infrared (FT-IR) spectral studies

Fourier transform infrared (FT-IR) spectrum of pure PVA is shown in figure 3.6. The bands seen in the spectrum at 3380 cm^{-1}, 1423 cm^{-1} and 1096 cm^{-1} are assigned to the characteristic vibrations of –OH, $–CH_2$, and C–O groups of PVA respectively.

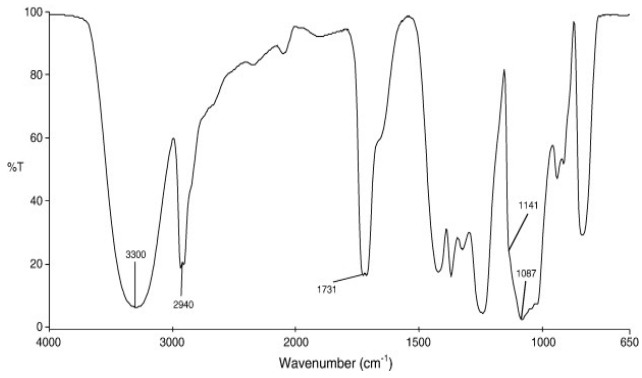

Figure 3.6 FT-IR spectrum of pure PVA

The FT-IR spectra of pristine ZnO, OA modified ZnO and OA modified ZnO/PVA nanocompositeare shown in figure 3.7. In the spectrum of ZnO, the band observed at 420 cm^{-1} is assigned to Zn-O vibrations**.** The absorption band near 3400 cm^{-1} represents O-H stretching mode and the three bands centered at 1339 , 1408 and 1576 cm^{-1} observed in the ZnO spectrum are attributed to the stretching vibrations of C=O, C=C and C-H groups in the acetate species, used to synthesize ZnO. The strong symmetric carboxylate stretching band of oleate at 1407cm^{-1} , the asymmetric carboxylate stretching band of oleate at 1594 cm^{-1} and the strong (C-H) bands observed at 2853 and 2925 cm^{-1} in the FT-IR spectrum of oleic acid modified ZnO, confirm the presence of oleic acid. The Zn-O stretching vibration is observed at 444 cm^{-1} in the spectrum of oleic acid modified ZnO.

On comparing the FTIR spectrum of pure PVA with that of oleic acid capped ZnO/PVA nanocomposite, it is seen that the characteristic vibrational peaks of PVA corresponding to –OH vibrations at 3380 cm^{-1}, $-CH_2$ vibrations at 1423 cm^{-1}, and C–O vibrations at 1096 $cm^{-1}$are shifted to 3300, 1432 and 1087 cm^{-1} respectively. This shift in the vibrational frequencies indicates that the possible interaction between PVA and OA capped ZnO could be weak van der Waals type of interaction. Besides the vibrational bands of PVA, the broad band observed between 650 and 700 cm^{-1} can be assigned to the Zn–O vibration, which confirms that the composite is composed of PVA and ZnO.

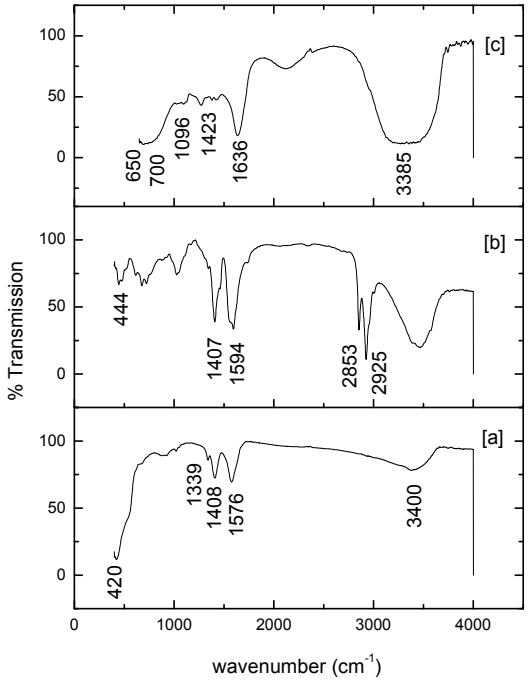

Figure 3.7 FT-IR spectra of (a) pristine ZnO, (b) OA modified ZnO and (c) OA modified ZnO/PVA nanocomposite.

3.4.6 Optical Characterization

(a) UV-Visible transmission spectra

UV–Visible transmission spectra of PVA film and ZnO/PVA nanocomposite films, grown with pristine and OA modified ZnO nanorods, recorded in the wavelength range 200-700 nm are shown in figure 3.8. The nanocomposite films containing OA modified ZnO nanorods, absorb UV light starting at around 362 nm down to 300 nm and maximum absorption is found to be at 300 nm with around 95% absorption. There is substantial increase in the absorption intensity of the nanocomposite films compared to PVA film. Moreover, the intensity of absorption is more in films prepared from OA modified ZnO nanorods compared to pristine ZnO nanorods.

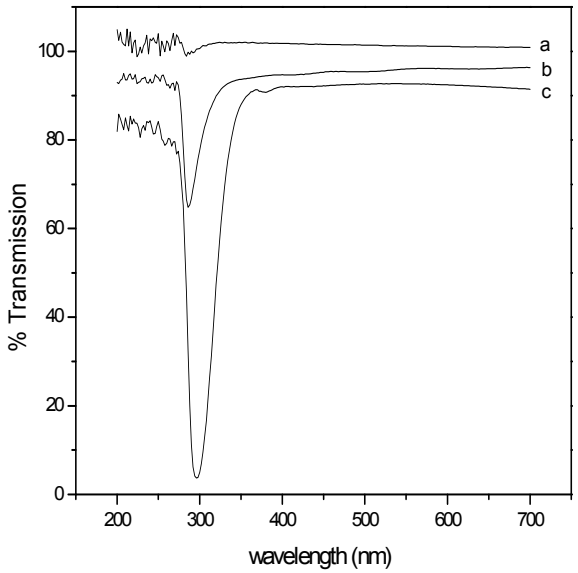

Figure 3.8 UV–Visible transmission spectra of (a) PVA film and ZnO/PVA films with (b) pristine ZnO and (c) OA modified ZnO

The UV-visible transmission spectra of PVA and ZnO/PVA nanocomposite films for 1, 2 and 3 weight % of OA modified ZnO nanorods are shown in figure 3.9. The PVA film does not absorb UV light as seen earlier, while the PVA nanocomposite films containing ZnO nanorods absorb UV light starting at around 362 nm, down to 300 nm. All signals come to minimum transmission (corresponding to maximum absorption) in the UV region irrespective of the ZnO content, which shows that absorption is independent of the ZnO content. This means that even small amounts of the filler nanomaterial (OA modified ZnO nanorods) can bring about the required modifications in the optical characteristics of the polymer nanocomposite, which is significant in the view point of the production cost of such nanocomposites.

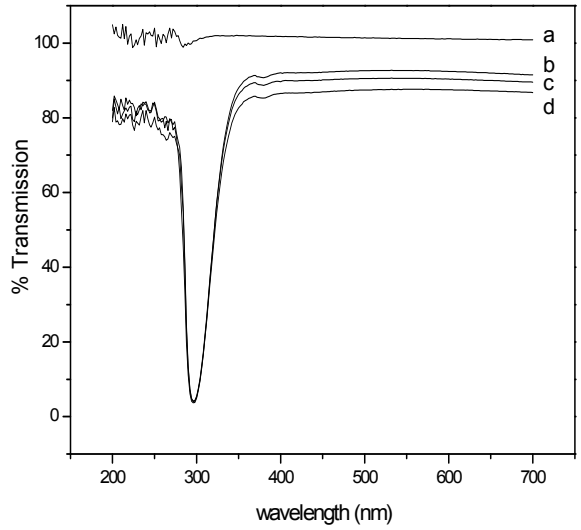

Figure 3.9 UV–Visible transmission spectra of (a) PVA film and ZnO/PVA films with different ZnO [OA modified] concentrations (b) 1wt%, (c) 2 wt% and (d) 3wt%

The photographs of the ZnO/PVA films containing pristine ZnO and oleic acid capped ZnO, coated on glass plates are taken and are shown in figures 3.10 (a) and (b) respectively. The photographs establish the excellent transparency of these films in the visible region.

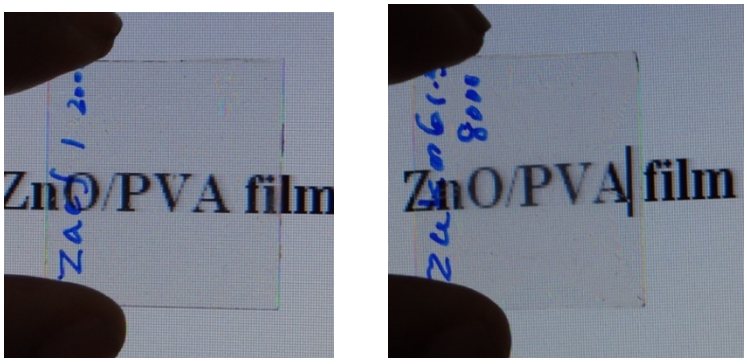

(a) (b)

Figure 3.10 Photographs of transparent ZnO/PVA film prepared from (a) pristine ZnO and (b) OA modified ZnO

(b) Photoluminescence Studies

The photoluminescence emission spectra of pristine and OA modified ZnO nanorods obtained under excitation at 325 nm are shown in figure 3.11. These

nanorods show photoluminescence emission across the visible region of the electromagnetic spectrum which is due to the intrinsic and extrinsic defects of ZnO. The PL emission peaks at 412 and 438 nm are due to the interstitial defects of oxygen [23, 24]. The PL emission at 468 nm corresponds to the transition between oxygen vacancies and oxygen interstitial defects and the emission at 563 nm is due to the oxygen vacancies [25]. In the case of OA modified ZnO, the PL emission spectrum is found to be more intense, though similar in shape to that of the unmodified one. Band-edge emission in ZnO (UV peak) is not prominent in these curves due to the higher emission intensity in the region 400-500 nm. For clarification, the PL spectrum in the 350-380 nm range showing UV peak at 361 nm is given in the inset.

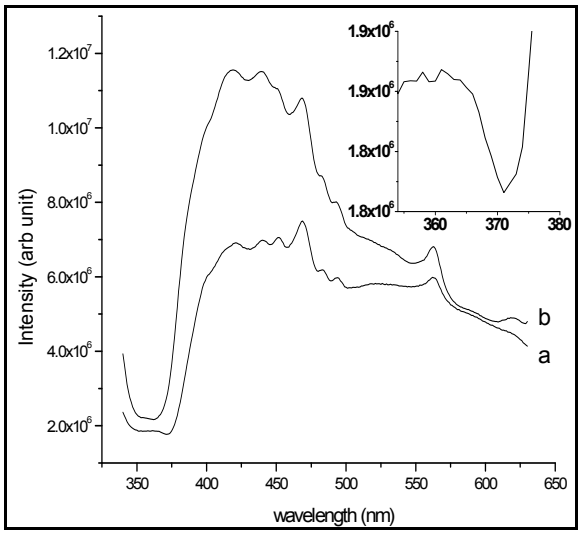

Figure 3.11 PL spectra of (a) pristine ZnO and (b) OA modified ZnO (Inset shows the PL spectrum in the 350–380 nm range showing the UV peak at 361 nm)

Photoluminescence emission spectra of PVA and ZnO/PVA nanocomposite films prepared with pristine and OA modified ZnO nanorods (1weight%) under excitation at 325 nm at room temperature are shown in figure 3.12. It is observed that PVA film alone does not give any appreciable

PL emission, where as the composite films show intense PL emission centered around 364 nm, along with a weaker and broad emission around 397 nm. The intensity of these emission peaks is found to be more for ZnO/PVA nanocomposite films prepared with OA modified ZnO nanorods, compared to the films prepared with pristine ZnO. It has been observed that oleic acid can be absorbed on to the surfaces of ZnO nanorods via electrovalent bonds, resulting in the homogeneous dispersion of ZnO nanorods in the PVA matrix. The better dispersion of OA modified ZnO nanorods in the PVA matrix can be attributed to the observed higher PL intensity in the ZnO/PVA nanocomposite films prepared from OA modified ZnO. The PL emissions observed in ZnO nanorods at 468 and 563 nm have decreased considerably in intensity and are almost quenched in the composite films. The green emission in ZnO originates mainly from the deep surface traps, which can almost be eliminated via surface passivation by the polymer matrix, in the composite.

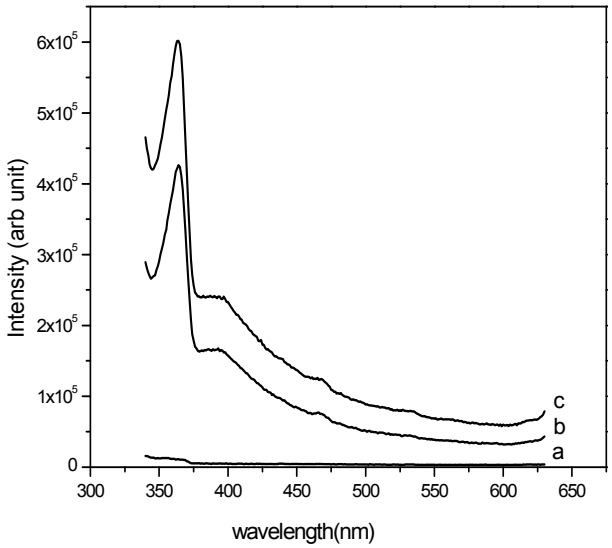

Figure 3.12 PL spectra of (a) PVA film and ZnO /PVA films for (b) pristine ZnO and (c) OA modified ZnO

The PL spectra of PVA and ZnO/PVA nanocomposite films for 1, 2 and 3 weight % of OA modified ZnO are shown in figure 3.13. The composite films show intense luminescence emission centered around 364 nm in the UV region and the intensity of this emission is found to increase with the increase of ZnO content in the composite. The PL emission at 397 nm also shows a similar trend. The absence of the emission peaks in the visible region is an indication of surface modification of ZnO nanorods by the polymer matrix. The surface modification results in the removal of defect states within ZnO and facilitates sharp near band edge PL emission at 364 nm.

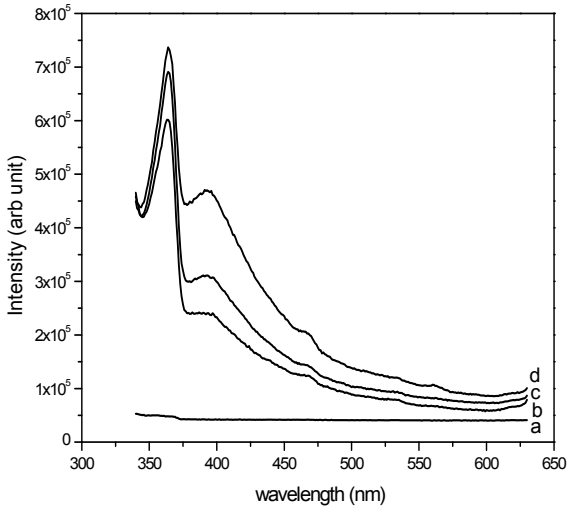

Figure 3.13 PL spectra of (a) PVA film and ZnO/PVA films for different ZnO [OA modified] concentrations (b)1wt%, (c) 2 wt% and (d) 3 wt%

3.5 Conclusions

In the present study, ZnO nanorods have been synthesized by wet chemical method at room temperature with and without oleic acid. Modification with oleic acid is found to result in the growth of long and well separated ZnO nanorods of approximately 25 nm in diameter. Highly

transparent ZnO/PVA films could be prepared using spin-coating technique from pristine and OA modified ZnO nanorods.

UV-visible transmission spectra of PVA and ZnO/PVA nanocomposite films prepared with pristine and OA modified ZnO nanorods are studied and compared. It is observed that the intensity of UV absorption is much higher for films prepared from OA modified ZnO nanorods, compared to the films from pristine ZnO. One of the highlights of the present work is that, small amounts of oleic acid modified ZnO nanorods (1wt%) are sufficient as filler material to suitably modify the optical absorption characteristics of the ZnO/PVA nanocomposite . This is quite significant from the view point of the production cost of such nanocomposites. The excellent UV absorption around 300 nm of OA modified ZnO/PVA nanocomposite films offers prospects of making efficient UV filters, or UV protectors for the UV shielding in plastics, textiles, paints, cosmetics, and packaging in a cost effective way.

The intensity of PL emission observed at 364 nm is higher in films prepared from OA modified ZnO nanorods. Oleic acid can be absorbed on to the surfaces of ZnO nanorods via electrovalent bonds which can affect the homogeneous dispersion of nanorods in the PVA matrix. The better dispersion of OA modified ZnO nanorods in the PVA matrix can be the prime factor contributing towards the higher PL intensity in the ZnO/PVA nanocomposite films prepared from OA modified ZnO. Another interesting aspect is the significant extent of surface modification of ZnO nanorods, brought about by the PVA matrix. The surface modification results in the removal of defect states within ZnO and the quenching of the PL emission in the visible region. The PL emission in the ZnO/PVA nanocomposite films is hence confined mainly to the UV region.

References:

[1] L. Beecroft, C. K. Ober, *Chem. Mater*. 9 (1997) 1302-1317

[2] R. V. Kumar, R. Elgamiel, Y. Diamant, and A. Gedanken, *Langmuir* 17 (2001) 1406-1410

[3] Kickelbick G, *Prog. Polym. Sci.* 28 **(**2003)83–114

[4] Kojima Y, Usuki A, Kawasumi M, Okada A, Fukushima Y,Kurauchi T and Kamigaito O *J. Mater. Res*. 8 (1993) 1185–9

[5] Zhu J, Uhl F M, Morgan A B and Wilkie C A, *Chem.Mater.* 13 (2001) 4649–54

[6] Huynh W U, Dittmer J J and Alivisatos A P, S*cience.* 295 (2002) 2425–7

[7] Brosseau C, Queffelec P and Talbot P, *J. Appl. Phys.* 89 (2001)4532–40

[8] J. Lee, D. Bhattacharyya, A. J. Easteal, and J. B. Metson, *Curr. Appl. Phys*. 8 (2008) 42-47

[9] X. M. Sui, C. L. Shao, and Y. C. Liu, *Appl. Phys. Lett*. 87 (2005) 113115

[10] M. Xiong, G. Gu, B. You, and L. Wu, *J. Appl. Polym. Sci*..90 (2003) 1923 -1931

[11] LittyIrimpan,V.P.N.Nampoori, and P. Radhakrishnan, *Journal of Applied Physics.*103 (2008) 094914

[12] Alivisatos A P, *Science* 271 (1996)933–7

[13] Wang J F, Gudiksen M S, Duan X F, Cui Y and Lieber C M 2001 *Science* 293 (2001) 1455-1457

[14] Kind H, Yan H Q, Messer B, Law M and Yang P D 2002 *Adv. Mater.* 14 (2002) 158

[15] C. M. Hassan and N. A. Peppas, *Adv. Polym. Sci.* 153 (2000) 37-65

[16] M. Kokabi, M. Sirousazar, and Z. Hassan, *Eur. Polym. J*. 43 (2007) 773-781

[17] M. Nagura, T. Hamano, H. Ishikawa, *Polym*. 30(1989) 762-765

[18] C. A. Scotchford, M. G. Cascone, S. Downes, and P. Giusti, *Biomaterials*. 19 (1998) 1-11

[19] H L Cao, X F Qian, Q Gong, W M Du, X D Ma and Z K Zhu, *Nanotechnology*.17(2006)3632-3636.

[20] M. Yin, Y. Gu, I.L. Kuskovsky, T. Andelman, Y. Zhu, G.F. Neumark and S. O'Brien, J. Am. Chem. Soc. 126 (2004) 6206-6207

[21] Pullarkat P Jeeju, Augustine M Sajimol, Vallath G Sreevalsa, Sreekanth J Varma and S Jayalekshmi, *Polymer International,* 60 (2011) 8

[22] T.M.Hammad, Jamil K. Salem and Roger G. Harrison *Rev.Adv.Mater.Sci*. 22(2009) 74-80

[23] Ahmad, C. Pan, J. Zhao, J. Iqbal, and J. Zhu. *Materials Chemistry and Physics*, 120(2010) 319

[24] J. Liu, S. Lee, Y. H. Ahn, J. Y. Park, and K. H. Koh. *J. Phys. D:Appl. Phys.*, 42 (2009) 095401

[25] R. S. Ajimsha, G. Anoop, Arun Aravind, and M. K. Jayaraj. *Electrochem. and Solid-State Lett.*, 11(2008) K14

Chapter 4

ENHANCED PHOTOLUMINESCENCE IN OLEIC ACID MODIFIED POLYANILINE

Contents

The studies on the effect of oleic acid modification on the photoluminescence characteristics of orthophosphoric acid doped polyaniline (PANI) form the essence of this chapter. The capping of oleic acid on each PANI molecule is found to result in the formation of nanostructured PANI. The band gap of oleic acid modified PANI is found to be blue shifted considerably from that of PANI which is another signature of the formation of nanostructured PANI samples upon modification with oleic acid.The enhanced photoluminescence emission observed in oleic acid modified PANI is due to the effect of capping and the homogeneous distribution of PANI molecules of reduced particle size.

M.Sajimol Augustine et al.

*Transactions of the Indian Institute of Metals***,** 64(2011) 209-212
"Enhanced photoluminescence in oleic acid modified Polyaniline"

4.1 Introduction

Polyaniline (PANI) is endowed with a host of advantageous characteristics which make it a highly sought after material. It can be synthesized using cheap and easily available precursor materials and the yield of polymerization is generally high. It has excellent thermal and environmental stability and its tunable electrical and optical properties are quite desirable for a variety of potential applications [1-4]. It has been extensively investigated as hole-injecting electrodes in polymer LEDs [5-8]. It exhibits good solution processability and has prospective applications in electrochromic displays [9], organic storage batteries [10], microelectronic devices [11], liquid crystal devices [12], and as anti-corrosion coatings [13] and adsorbent materials [14]. It has been reported that PANI doped with orthophosphoric acid exhibits quite intense photoluminescence emission and is a promising material with prospects of applications in optoelectronics devices [15].

Recently, various nanoscale applications have motivated research on one dimensional (I D) nanostructures such as nanorods, nanofibers and nanotubes [16-18]. Nanostructured PANI has caught much attention due to its interesting electrical transport properties and the colour changing characteristics corresponding to diverse redox states [19-24]. The present work is mainly focused on a comparative study of the structural, morphological, electrical and photoluminescence (PL) characteristics of PANI and oleic acid modified PANI in the form of nanorods.

4.2 Experimental Details

4.2.1 Synthesis of PANI and oleic acid modifiedPANI

Orthophosphoric acid doped PANI and oleic acid modified PANI doped with orthophosphoric acid, were synthesized using chemical oxidative polymerization. Distilled aniline (AR grade, Spectrochem Pvt Ltd, Mumbai, India) was dissolved in orthophosphoric acid (AR grade, Sd fine Chem Limited Mumbai, India) solution. The oxidizing agent ammonium persulfate (Laboratory Rasayan, extra pure, India) was added drop-wise under constant stirring at 0^{o}C. The monomer to oxidizing agent ratio was kept at 1:1. After complete addition of the oxidizing agent, the reaction mixture was kept under constant stirring for 4 hours. Precipitated polymer was filtered and washed with distilled water until the filtrate was colourless. Finally, thefiltrate was dried in an oven at 80 ^{o}C for 12 hours to get the green powder of the conducting form of PANI. To synthesize the oleic acid modified PANI, 1ml oleic acid (AR grade, Merck Specialities, Mumbai, India) was added after adding the oxidising agent and the procedure was repeated as before.

4.2.2 Deposition of thin films of PANI and oleic acid modified PANI

Solutions of PANI and oleic acid modified modified PANI were prepared by dissolving 0.2 g of powder samples in 2 ml of m-cresol (LR, Laboratory rasayan, Sd fine Chem. Limited, Mumbai) by stirring continuously for about 12 hours. The obtained solutions were used to deposit thin film of PANI and oleic acid modified PANI by spin-coating technique (Spin 150). Transparent films of light green colour were coated on ultrasonically cleaned and optically flat glass slides by spin-coating process. The thickness of these film samples was recorded using Veeco Dektak 6M stylus profiler. The

thickness of PANI and oleic acid modified PANI thin films was measured as 150 nm and 100 nm respectively.

4.3Sample Characterization

The X-ray diffraction analysis of the samples was done using Rigaku X-ray Diffractometer with Cu-Kα (1.5418 A^o) radiation operating at 30 kV and 20 mA. Scanning was carried out in the 2θ range from 5^o–60^o at a scan speed of 2^o per minute. Field emission scanning electron microscopy (FESEM) images of the samples were obtained using a HITACHI SU 6600 Microscope with an accelerating voltage of 20 kV. The surface morphology of PANI and oleic acid modified PANI film samples was studied using FESEM. Fourier transform infrared (FT-IR) spectra of the samples were obtained with AVTAR 370 DTGS FTIR spectrophotometer in the wave number range 400 - 4000 cm^{-1}. UV-VIS-NIR absorption spectra of the thin film samples were recorded using Jasco-V 500 spectrophotometer in the wavelength range 190-800 nm. The photoluminescence emission spectra of the samples were obtained with Fluoromax-3 Spectrofluorimeter using Xe lamp as the source under an excitation at 350 nm.

4.4 Results and Discussion

4.4.1 X-Ray Diffraction (XRD) analysis

The structural analysis of the PANI samples was carried out using X-ray diffractometer. The XRD pattern of orthophosphoric acid doped PANI shows amorphous peaks at 11^0 as shown in figure 4.1. It also shows sharp crystalline peaks at 14^o and 17^o with higher intensity. However in the XRD pattern of oleic acid modified PANI, shown in figure 4.2, the peaks have

broadened considerably. This could be due to the capping effect of oleic acid on each PANI molecule which reduces the particle size and makes the polyaniline sample nanostructured.

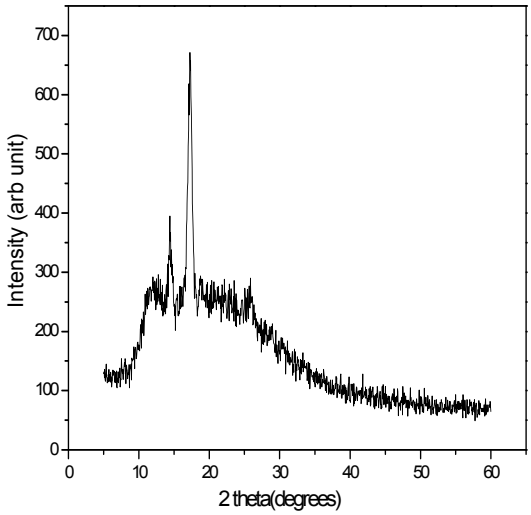

Figure 4.1 XRD pattern of orthophosphoric acid doped PANI

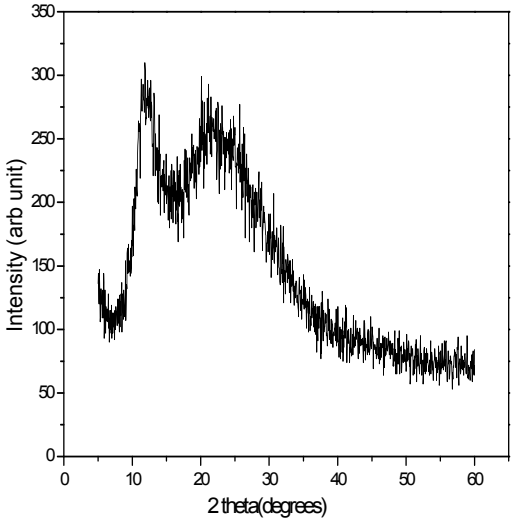

Figure 4.2XRD pattern of orthophosphoric acid doped PANI modified with oleic acid

4.4.2 Fourier transform infrared (FT-IR) spectral studies

The Fourier Transform Infrared spectra of orthophosphoric acid doped PANI and orthophosphoric acid doped PANI modified with oleic acid are shown in figure 4.3 and figure 4.4 respectively.The major peaks observed in both spectra, at around 3429 cm^{-1} (NH stretching vibration), 2923 cm^{-1} (CH stretch), 1594 cm^{-1}(C =N stretch of the quinonoid unit of PANI), 1457 cm^{-1} (C=C stretch of the benzenoid unit of PANI) and 1110 cm^{-1} (quinonoid unit vibration of doped PANI), agree quite well with the already reported values [15]. The major peak around 3429 cm^{-1} is found to be more stronger in oleic acid modified PANI.

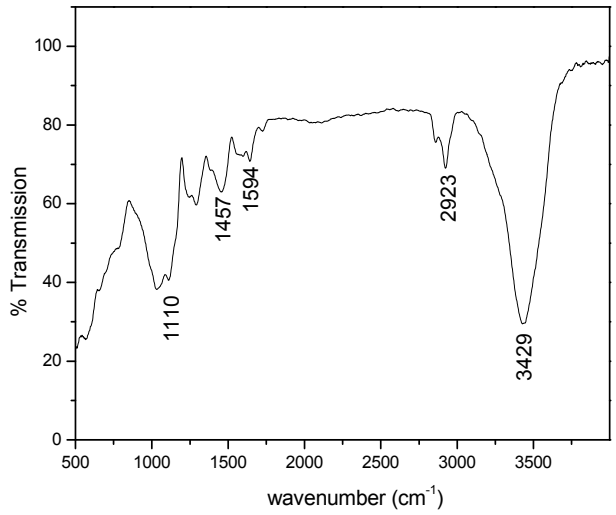

Figure 4.3 FTIR spectrum of orthophosphoric acid doped PANI

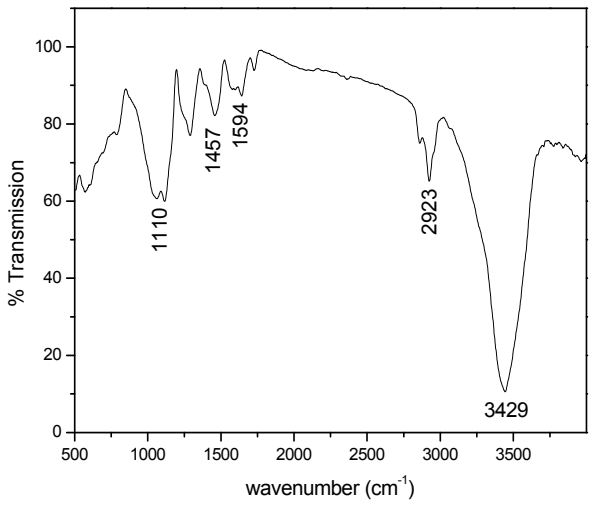

Figure 4.4 FTIR spectrum of orthophosphoric acid doped PANI modified with oleic acid

4.4.3 Field emission scanning electron microscopy (FESEM) studies

The surface morphology of orthophosphoric acid doped PANI and oleic acid modified, orthophosphoric acid doped PANI was analysed using FESEM and the images are shown in figure 4.5 and figure 4.6 respectively. It is clear from figure 4.6 that the surface of oleic acid modified PANI is smoother compared to that of PANI without oleic acid. The incorporation of oleic acid to PANI results in the formation of rod like structures with diameter less than 100 nm as observed in figure 4.6. PANI molecules without oleic acid modification (figure 4.5) show the tendency for agglomeration, resulting in the formation of bigger sized clusters of size about 1μm. The particle size distribution is also not uniform without oleic acid modification. The FESEM images indicate more homogeneous particle distribution in oleic acid modified PANI.

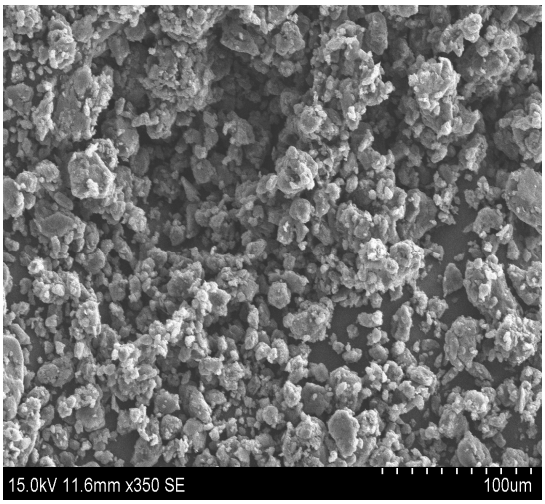

Figure 4.5 FESEM image of orthophosphoric acid doped PANI (scale bar:100 μm)

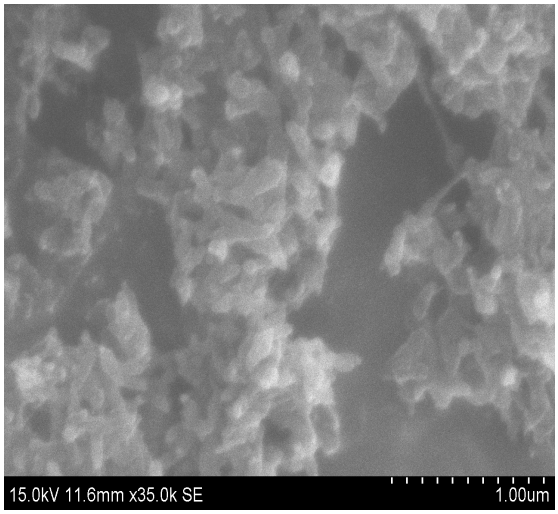

Figure 4.6 FESEM image of orthophosphoric acid doped PANI modified with oleic acid (scale bar:1μm)

4.4.4 Optical Characterization

(a) UV-VIS-NIR absorption spectral studies

In the present work, a comparative study of the optical transitions of orthophosphoric acid doped PANI and oleic acid modified orthophosphoric acid doped PANI samples in thin film form is attempted. The UV-VIS-NIR absorption spectra of these films were recorded in the range 190 nm to 800 nm and are shown below in figure 4.7 and figure 4.8. The absorption peak corresponding to π- π* transition in m-cresol film of orthophosphoric acid doped PANI can be seen at 472 nm and that of oleic acid modified PANI at 460 nm. The absorption spectrum of oleic acid modified PANI shows blue shift as a consequence of the nanostructure formation in oleic acid modified PANI.

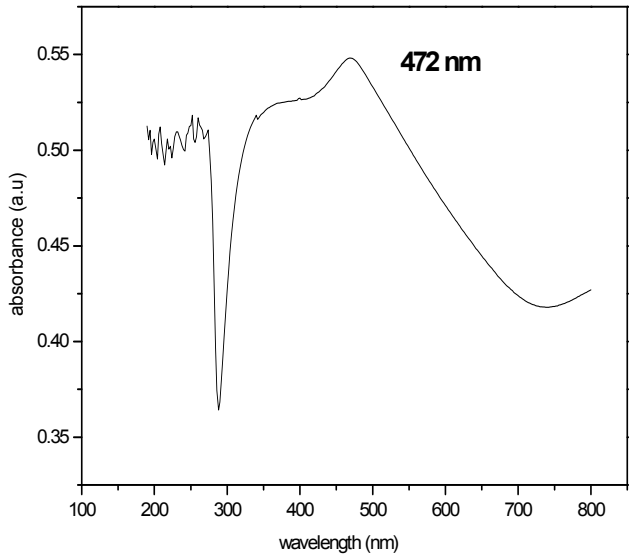

Figure 4.7 Absorption spectrum of m-cresol film of orthophosphoric acid doped PANI

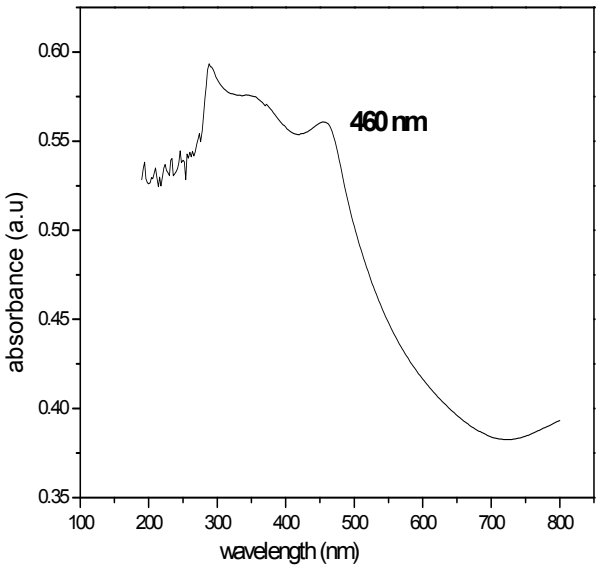

Figure 4.8 Absorption spectrum of m-cresol film of oleic acid modified PANI

The optical band gap of these films was determined from the plot of $(\alpha h\upsilon)^2$ vs $h\upsilon$ for the absorption coefficient α which is related to the band gap E_g by Tauc's expression as

$$(\alpha h\upsilon) = k\,(h\upsilon - E_g)^{1/2}$$

where $h\upsilon$ is the incident light energy and k is a constant. Extrapolation of the linear part to the $h\upsilon$ axis gives E_g. The optical band gap of orthophosphoric acid doped PANI film is found to be 1.62 eV and that of oleic acid modified PANI, 2 eV as shown in figures 4.9 and 4.10 respectively.

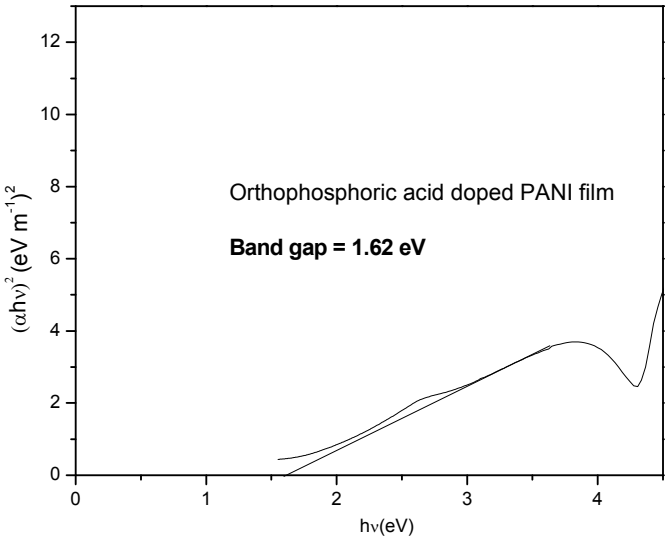

Figure 4.9 The plot of $(\alpha h\upsilon)^2$ vs $h\upsilon$ of m-cresol film of orthophosphoric acid doped PANI

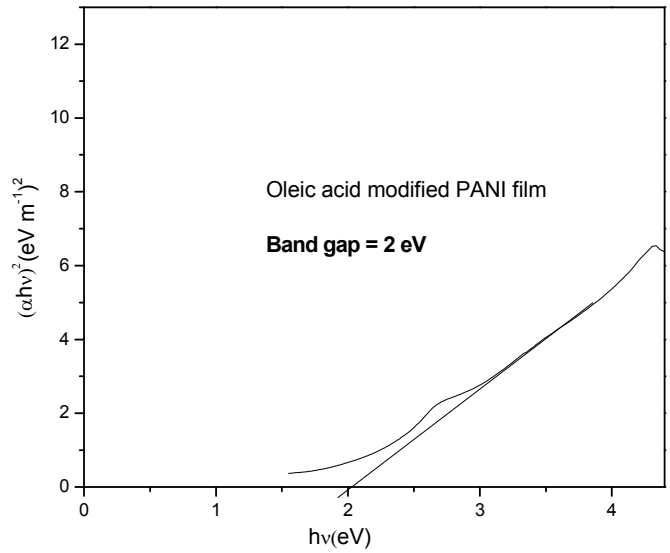

Figure 4.10 The plot of $(\alpha h\upsilon)^2$ vs $h\upsilon$ of m-cresol film of orthophosphoric acid doped PANI modified with oleic acid

(b) Photoluminescence Studies

Photoluminescence (PL) spectra of orthophosphoric acid doped PANI and oleic acid modified PANI were recorded for an excitation wavelength 350 nm. The PL emission spectrum of orthophosphoric doped polyaniline shows a broad spectrum in the blue region with good photoluminescence intensity. Oleic acid modified PANI shows blue emission with much higher PL intensity as compared to orthophosphoric acid doped PANI, as shown in figure 4.11. The photograph of the intense blue emission obtained from oleic acid modified PANI is also depicted in figure 4.11.

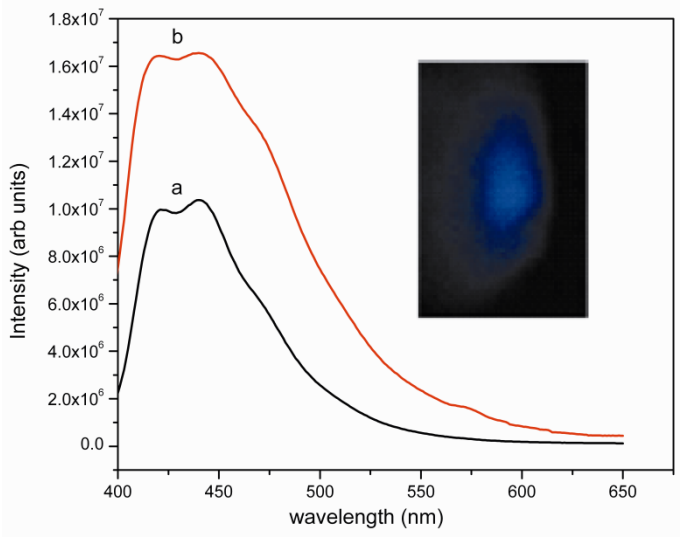

Figure 4.11 PL emission spectra of (a) orthophosphoric acid doped PANI and (b) oleic acid modified PANI doped with orthophosphoric acid

The enhanced photoluminescence intensity is due to the nanostructure of oleic acid modified PANI where the capping effect of oleic acid on each PANI molecule has to be expected. For the nanostructured sample, the oscillator strength increases thereby increasing the quantum efficiency

followed by increased intensity in PL emission. The presence of oleic acid inhibits agglomeration of PANI particles and brings about better homogeneity in particle size distribution. The reduction in the particle size and homogeneous distribution of the particles in oleic acid modified PANI are the factors responsible for the observed enhancement in the photoluminescence intensity.

4.4 Conclusions

The present work highlights the enhanced photoluminescence emission observed in oleic acid modified PANI doped with orthophosphoric acid, compared to orthophosphoric acid doped PANI. The enhanced emission intensity in oleic acid modified PANI is the effect of capping of oleic acid on each PANI molecule resulting in the formation of nanostructured PANI. The band gap of oleic acid modified, orthophosphoric acid doped PANI is found to be blue shifted considerably from that of orthophosphoric acid doped PANI which is another signature of the formation of nanostructured PANI samples upon modification with oleic acid. From FESEM studies, the oleic acid modified PANI is found to have rod like structure of diameter less than 100 nm, compared to the PANI sample without oleic acid where the PANI molecules are found to have agglomerated, resulting in the formation of micrometer sized bigger aggregates. The more homogeneous particle size distribution and reduced particle size in oleic acid modified PANI can be the factors responsible for the observed enhancement in the photoluminescence intensity.

References

[1] A. Pud, N. Ogurtsov, A. Korzhenko, G. Shapoval, *Prog. Polym. Sci*. 28 (2003) 1701–1753

[2] H. Zengin, W. Zhou, J. Jin, R. Czrew, D.W. Smith Jr., L. Echegoyen, D.L. Carroll, S.H. Foulger, *J. Ballato, Adv. Mater*. 14 (2002) 1480–1483

[3] R. Sainz, A.M. Benito, M.T. Martinez, J.F. Galindo, J. Sotres, A.M. Baro,O. Chauvet, A.B. Dalton, R.H. Baughman, W.K. Maser, *Nanotechnology* 16 (2005) 150–154

[4] Y. Cao, P. Smith, A.J. Heeger, *Synth. Met*. 48 (1992) 91–97

[5] Y. Yang, A.J. Heeger, *Appl. Phys. Lett*. 64 (1994) 1245–1247

[6] T. Nakajima, T. Kawaqoe, Synth. Met. 28 (1989) 629–638

[7] Z.M. Tahir, E.C. Alocilia, D.L. Grooms, *Biosens. Bioelectr*. 20 (2005) 1690–1695

[8] C.H. Yang, Y.K. Chih,W.C.Wu, C.H. Chen, Electrochem. *Solid-State Lett*. 9 (2006) C5–C8

[9] E. Harlev, T. Gulakhmedova, I. Rubinovich, G. Aizenshtein, *Adv. Mater.* 8 (1996)994–997

[10] J.I.I. Laco, F.C. Villota, F.L. Mestres, *Prog. Org. Coat*. 52 (2005) 151–160

[11] M.V.B. Krishna, D. Karunasagar, S.V. Rao, J. Arunachalam, *Talanta* 68 (2005) 329–335

[12] Y. Yang, E Westerweele, C. Zhang, P. Smith, A.J. Heeger, *J. Appl. Phys.* 77 (1995) 694–698

[13] G. Gustafsson, Y. Cao, G.M. Treacy, F.K. Lavetter, N. Colaneri, A.J.Heeger, *Nature* 357 (1992) 477–479

[14] S.A. Carter, M. Angelopoulos, S. Karg, P.J. Brock, J.C. Scott, *Appl. Phys.Lett.* 70 (1997) 2067–2069

[15] M. Amrithesh, S. Aravind, S. Jayalekshmi, R.S. Jayasree, *J.of Alloys and Compounds*. 458 (2008) 532-535

[16] J Jang, J Bae, K Lee, *Polymer* 46 (2005) 3677

[17] S J Tans, A R M Verschueren, C Dekker, *Nature,* 393 (I 998) 49

[18] R Q Long, R T Yang, *J.Am. Chem.Soc*.123 (2001) 2058

[19] Z Wang, MChen, H L Li, *Mater. Sci. Eng. A* 328 (2002) 33

[20] Z Wei, Z Zhang, M Wan,*Langmuir* 18 (2002) 917

[21] J Stejskal, M Spirkova, A Riede, M Helmstedt,PMokreva, J Prokes, *Polymer* 40 (1999) 248

[22] Pullarkat P. Jeeju, Sreekanth J. Varma, Puthampadath A. Francis Xavier, Augustine M. Sajimol, Sankaran Jayalekshmi, *Materials Chemistry and Physics* 134 (2012) 803-808

[23] Sreekanth J. Varma, Jerin George, P.P. Jeeju, S. Jayalekshmi, *Journal of Luminescence* 132 (2012) 801-805

[24] Sreekanth J Varma, Francis Xavier, Soney Varghese, Sankaran Jayalekshmi, *Polymer International* 61(2012)743-748

Chapter 5

TRANSPARENT AND FLEXIBLE IRON DISULPHIDE/POLYMER NANOCOMPOSITE FILMS WITH EXCELLENT UV-SHIELDING PROPERTIES

Contents

In this chapter, the details of solvothermal synthesis of nanocomposites of iron disulphide (FeS_2) with polyvinylpyrrolidone (PVP) and polyvinyl alcohol (PVA) and their various characterizations are addressed. The growth of transparent and flexible thin films of these nanocomposites from homogeneous solution by solution casting approach is also discussed. The transmission studies in the UV-Visible spectral range reveal the UV-shielding efficiency of these nanocomposite films and the films are found to be exceptionally good for UV shielding applications in the wavelength range 200 to 400 nm. The present work aims at developing transparent and flexible UV-shielding films and color filters using cost effective and non toxic, inorganic-polymer nanocomposites.

M. Sajimol Augustine et al.
Polymer International (in press)
"Exceptionally good, transparent and flexible FeS_2/PVP and FeS_2/PVA nanocomposite thin films with excellent UV-shielding properties"

5.1 Introduction

Semiconducting nanomaterials have attracted extensive interest because of their fundamental physical, chemical, optical, electrical and magnetic properties, which are distinct from their bulk counterparts, and also due to their potential applications in nano-scale devices [1–8]. Iron disulphide pyrite is an interesting material for solar energy conversion in photo-electrochemical and photovoltaic solar cells [9-11] due to its favourable solid state properties [12-14]. It is currently recognized as an important inorganic material with potential applications, and several methods have been developed to synthesize nanocrystals of iron sulphide [15]. Among them, solvothermal synthesis offers an attractive method due to its simplicity and productivity.

Nanostructured organic–inorganic composites are quite different from the conventional composites owing to the inherent nanostructure of these composites [16]. These nanocomposites with strong chemical bonds can have potential applications in the fields of optoelectronics, photonics and mechatronics [17-20]. In particular, metal-polymer nanocomposites are considered to be interesting functional materials with many applications due to their size and shape dependent properties. Furthermore, the flexibility and processability of water-soluble polymer matrices such as PVA and PVP can provide good mechanical properties along with good transparency and compatibility.

In the present work, FeS_2/PVP and FeS_2/PVA nanocomposites have been prepared by a facile solvothermal technique, in which ferric chloride ($FeCl_3$) has been used as the metal-ion source and thiourea (CH_4N_2S) as the sulphur source. One prominent feature of the reaction, in contrast to the use of

Na_2S or K_2S as the sulphur source, is that, no by-products such as NaCl or KCl are formed in the as-prepared nanocomposites, which is an important advantage. Polyvinyl pyrrolidone (PVP) and polyvinyl alcohol (PVA) are chosen as the host polymer matrices because of their excellent solubility and chemical stability. These polymers are transparent, water-soluble and biodegradable with many technological, pharmaceutical and biomedical applications [21–24]. They are not at all toxic and can be cast in the form of thin films quite easily.

The objectives of the present work include the realization of transparent and flexible, FeS_2/PVP and FeS_2/PVA thin films using homogeneous solutions of their respective nanocomposites, synthesized by solvothermal process. As the particle size is reduced down to the nanometer scale with corresponding significant increase of the surface-to-volume ratio, the surface features gain significant effects on the optical properties. The present studies have been confined mainly to the structural and optical properties of the thin films of these nanocomposites. There are only a few reports available on the preparation of FeS_2/PVP and FeS_2/PVA nanocomposites [25, 26]. There are no earlier reports on the synthesis of FeS_2/PVP nanocomposite films and the previous studies on FeS_2/PVA nanocomposite films present a different synthesis approach [26]. The present work is mainly focused on the prospective applications of the FeS_2/PVP and FeS_2/PVA nanocomposite films on developing flexible and free standing films with excellent UV-shielding properties and flexible colour filters [27, 28].

5.2 Experimental Details

5.2.1 Synthesis of FeS_2/PVP and FeS_2/PVA nanocomposites

The nanocomposites, FeS_2/PVP and FeS_2/PVA were synthesized by solvothermal synthesis method. All reagents used were commercial products with analytical grade and were used without further purification. To synthesize the FeS_2/PVP composite, 1 mmol of ferric chloride ($FeCl_3$) (Merck Specialities Private Limited, Mumbai, India), 3 mmol of thiourea (CH_4N_2S) (Spectrochem, Private Limited, Mumbai, India) and 3 mmol of PVP (Loba Chemie, Private Limited, Mumbai, India) were first dissolved in 20 ml of dimethylformamide (DMF) (Sd fine Chem Limited Mumbai, India) under magnetic stirring at room temperature. The mixed solution was then subjected to ultrasonication for 30 minutes to obtain a red transparent solution. Subsequently, the solution was transferred into a teflon-lined stainless steel autoclave of 80-ml capacity. The autoclave was sealed and maintained at 150^{o}C for 10 hrs and then cooled to room temperature naturally. In order to study the influence of reaction time on the optical behavior of the samples, time-dependent experiments were also conducted for two other time intervals of 20 hrs and 30 hrs, keeping the reaction temperature constant at 150^{o}C. The synthesized red, nanocomposite solution was used to cast thin films of the nanocomposite.

The FeS_2/PVA nanocomposite was also synthesized in a similar manner as described above. In this experiment, an appropriate amount of ferric chloride ($FeCl_3$), (about 10% based on PVA weight) was dissolved in a 10% (by weight) homogeneous, aqueous solution of PVA (Central Drug House, Private Limited, Delhi, India). To this solution, thiourea (50% excess based

on $FeCl_3$) was added and the mixture was transferred into the teflon-lined stainless steel autoclave of 80-ml capacity. The autoclave was maintained at 150°C for 10 hrs and then cooled to room temperature. The obtained brown, viscous solution was used to cast thin films of the nanocomposite.

5.2.2 Casting of films of FeS_2/PVP and FeS_2/PVA nanocomposites

The solutions of FeS_2/PVP and FeS_2/PVA nanocomposites thus obtained were used for casting thin films on optically flat and ultrasonically cleaned transparent glass plates and flexible substrates such as PET (polyethylene terephthalate). The films were dried at 60°C for 4 hrs for the complete removal of the solvents. The films so obtained were homogeneous and transparent. The thickness of these films was measured using Veeco Dektak 6M stylus profiler and found to be around 1μm and 5 μm for FeS_2/PVP and FeS_2/PVA films respectively. It was also observed that, films of FeS_2/PVA with thickness around 5μm could be peeled off from the glass substrates to get free standing films. Such free standing films offer many potential application prospects. Due to the limitations on thickness, it was not possible to make free standing films of FeS_2/PVP nanocomposite. However, good quality films of this nanocomposite could be cast on both glass and flexible substrates.

5.3 Sample Characterization

X-ray diffraction analysis of the samples was done using Rigaku X-ray Diffractometer with Cu-Kα (1.5418 A^o) radiation operating at 30 kV and 20 mA. Scanning was carried out in the 2θ range from 10^o–80^o at a scan speed of

2^o per minute. Fourier transform infrared (FT-IR) spectra of the samples were obtained with AVTAR 370 DTGS FTIR spectrophotometer in the wave number range 400–4000 cm^{-1}. Thermo gravimetric analysis (TGA) of FeS_2/PVP and FeS_2/PVA nanocomposite samples was carried out on a Diamond TG/DTA instrument. Samples were heated to 800^0C at a scan rate of 10^oC per minute in nitrogen atmosphere. UV-VIS- NIR absorption spectra of the samples were recorded on a Jasco-V 500 spectrophotometer in the wavelength range 200–800 nm.

5.4 Results and Discussion

5.4.1 X-Ray Diffraction (XRD) analysis

The XRD patterns of the FeS_2/PVP and FeS_2/PVA nanocomposite films are shown in figure 5.1 All the diffraction peaks of FeS_2 can be clearly seen in the XRD patterns of FeS_2/PVP and FeS_2/PVA films, in which, peaks at $2\theta = 28.12^o$, 32.5^o, 37.41^o, 40.34^o, 46.4^o and 57^o correspond to the reflections from (111), (200), (210), (211), (220) and (220) planes of the pyrite FeS_2 respectively. This confirms the presence of FeS_2 in the nanocomposite samples. The crystallite size of FeS_2 calculated from the width of the diffraction peaks is about 20 nm, using the Debye-Scherrer equation, $\beta = k\lambda/d\cos\theta$, where β is the full width at half maximum (fwhm) in radians of the diffraction peak, λ is the X-ray wavelength, k is a constant (0.89), θ is the Bragg angle of the peak and d is the average particle size. The particle size, thus determined confirms the nano structure of FeS_2 in the composite.

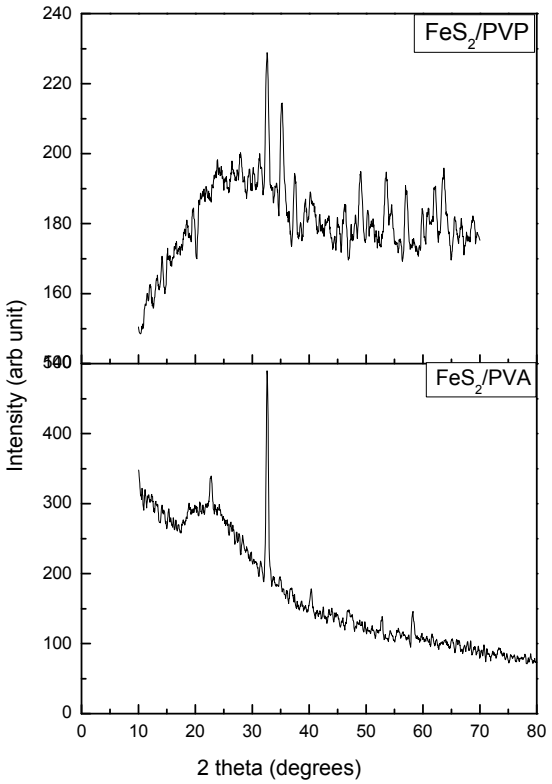

Figure 5.1 XRD patterns of FeS_2/PVP and FeS_2/PVA nanocomposite films

5.4.2 Energy Dispersive X-ray (EDX) spectral analysis

The Energy Dispersive X-ray (EDX) spectra of FeS_2/PVP and FeS_2/PVA nanocomposites are shown in figures 5.2 (a) and (b) respectively, which provide the elemental composition of the samples. The diagrams show the peaks of iron and sulphur elements, revealing the expected composition of FeS_2. The presence of polymer matrix is confirmed by the presence of carbon and oxygen in the EDX spectra. Thus the formation of the nanocomposites in the synthesized samples is established.

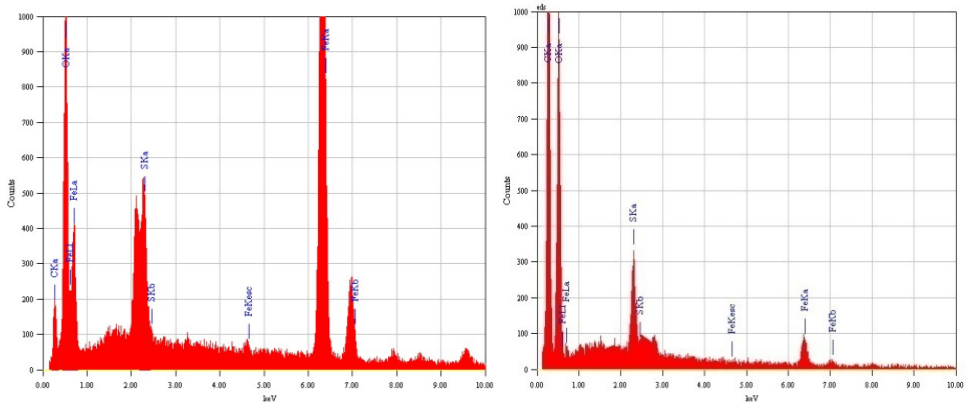

(a) (b)

Figure 5.2 EDX spectra of (a) FeS_2/PVA and (b) FeS_2/PVP nanocomposite samples

5.4.3 Fourier transform infrared (FT-IR) spectral studies

The FT-IR spectra of the FeS_2/PVP and FeS_2/PVA nanocomposites are depicted in figure 5.3 The spectra of both the nanocomposites exhibit the characteristic absorption bands corresponding to FeS_2 and polymeric groups. In the spectrum of FeS_2/PVP nanocomposite, the band at 1070cm^{-1}corresponds to the asymmetric S-O stretching of the sulphate species and the peak at 640 cm^{-1} is related to the disulphide stretch (S-S) [29]. Besides the vibration bands of FeS_2, the bands seen in the composite at 2914 $cm^{-1}$and 1440 cm^{-1} are indicative of the C-H stretching and symmetrical deformation of CH_2 group respectively, confirming that the composite is composed of FeS_2 and PVP. The presence of a small peak at about 790 $cm^{-1}$is attributed to the out-of-plane OH bending mode [30]. The spectrum of FeS_2/PVA nanocomposite shows a band at 1107 cm^{-1} corresponding to the asymmetric S-O stretching of the sulphate species and a peak at 472 cm^{-1} corresponding to the disulphide stretch (S-S). The absorption band at 1387 cm^{-1}can be assigned to the vibration of the C–O group of PVA. The broad peak observed in both of the spectra at 3440 cm^{-1}

and the peak around 1630 cm^{-1} are assigned to the O-H stretching and bending mode of water respectively. The absorption near 2060 cm^{-1} may be due to N-H-O vibration [31], suggesting organic contamination from the source materials.

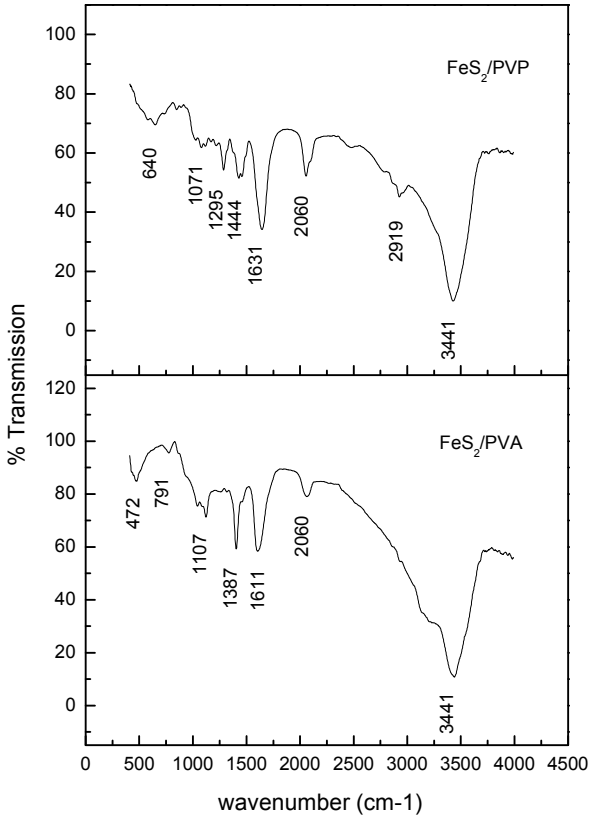

Figure 5.3 FTIR spectra of FeS_2/PVP and FeS_2/PVA nanocomposites

5.4.4 Thermal analysis using TGA

Thermo gravimetric analysis (TGA) of the nanocomposite samples was carried out on a Diamond TG/DTA instrument. Samples were heated to 900^oC at a scan rate of 10^oC per minute in nitrogen atmosphere. The TGA curves of

FeS_2/PVA and FeS_2/PVP nanocomposites are shown in Figure 5.4. Compared to FeS_2/PVA nanocomposite, the degradation temperature of the FeS_2/PVP nanocomposite sample is higher, which shows that the nanocomposite of FeS_2 with PVP is more thermally stable than the nanocomposite with PVA.

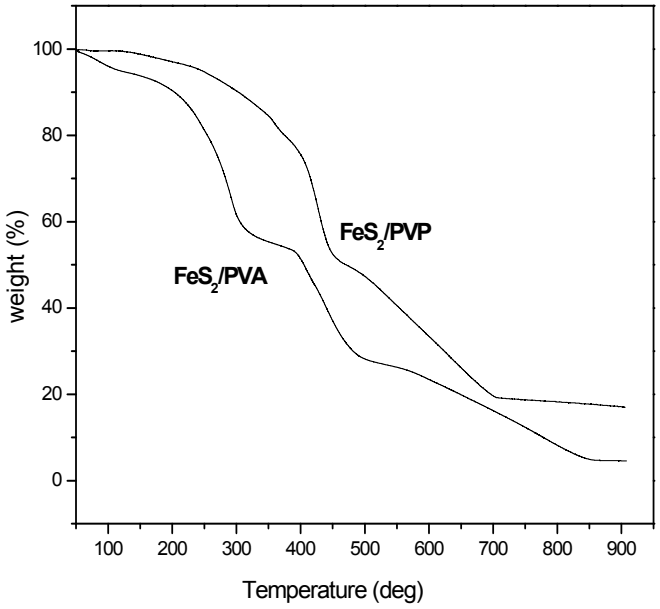

Figure 5.4 TGA curves of FeS_2/PVP and FeS_2/PVA nanocomposites.

5.4.5 Optical Characterization

The UV-Visible spectra were recorded in transmission mode and the spectra obtained for films of FeS_2/PVA and FeS_2/PVP nanocomposites, prepared at 150^oC for 10 hrs are shown in figures 5.5 (a) and (b) respectively. In both of the films, the % transmission is found to be reduced to zero (100% absorption) at a wavelength of 550 nm which extends up to 300 nm, except for a small kink observed at 395 nm in the case of FeS_2/PVP film. In the wavelength range from 300 nm to 200 nm, a slight increase in transmission is

observed. The films grown from FeS_2/PVP nanocomposite seem to be more transparent in the visible region compared to FeS_2/PVA nanocomposite films.

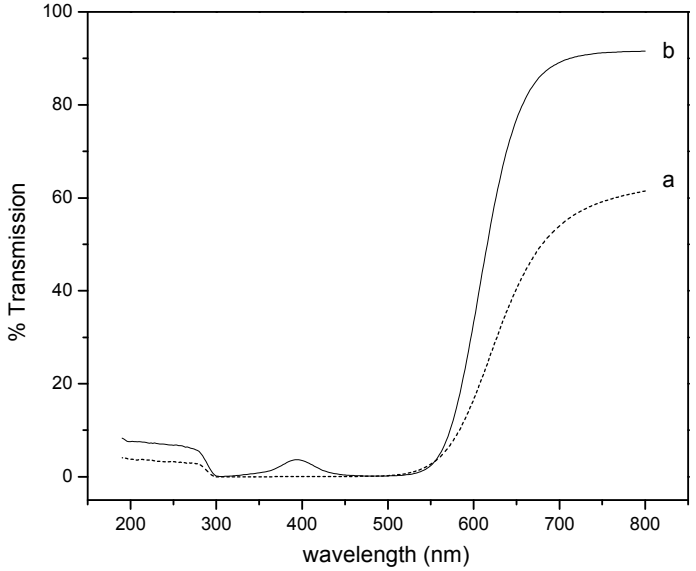

Figure 5.5 UV–Visible transmission spectra of (a) FeS_2/PVA film and (b) FeS_2/PVP film of the nanocomposites synthesized at 150°C for 10 hrs

In an attempt to eliminate the kink observed at 395 nm in the transmission spectrum of FeS_2/PVP film, the influence of reaction time on the optical properties of this film was studied. The transmission spectra of films of FeS_2/PVP nanocomposite, synthesized at 150°C for three different time intervals of 10, 20 and 30 hrs were recorded, and are depicted in figures 5.6 (a), (b) and (c) respectively. From the analysis of these transmission spectra, it is found that for the FeS_2/PVP nanocomposite film, synthesized at 150°C for a time interval of 20 hrs, the kink at 395 nm is almost reduced to zero. Further increase in reaction time was found to increase the kink intensity at 395 nm.

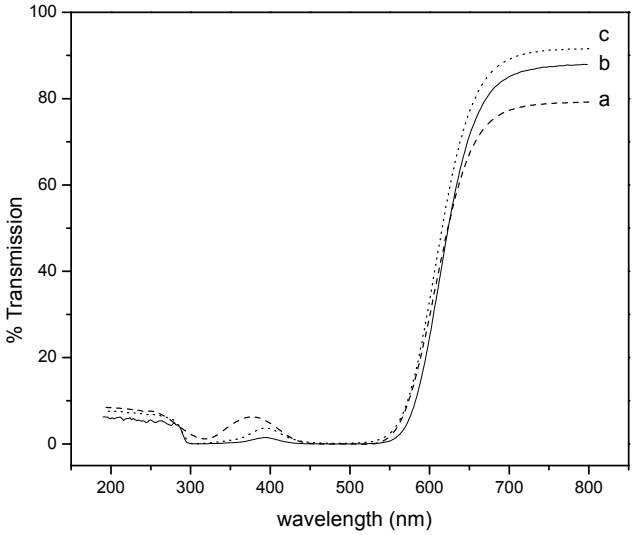

Figure 5.6 UV–Visible transmission spectra of films of FeS_2/PVP nanocomposite synthesized at 150°C for three different time intervals (a)10, (b) 20 and (c) 30 hrs

In order to assess the transparency of the films, photographs of the FeS_2/PVP films coated on glass plate and PET sheet were taken and are shown in figures 5.7 (a) and (b) respectively. In figure 5.7 (c), the photograph of FeS_2/PVA film, peeled off from the substrate is shown.

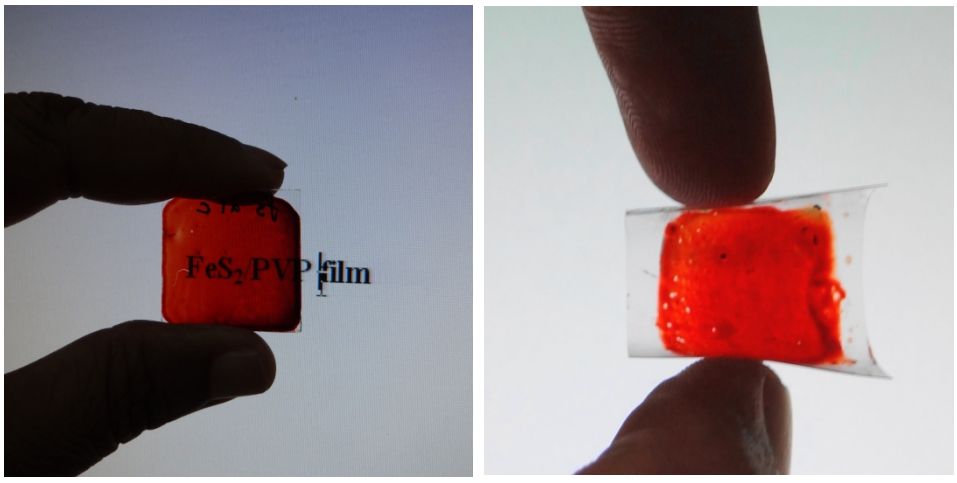

(a) (b)

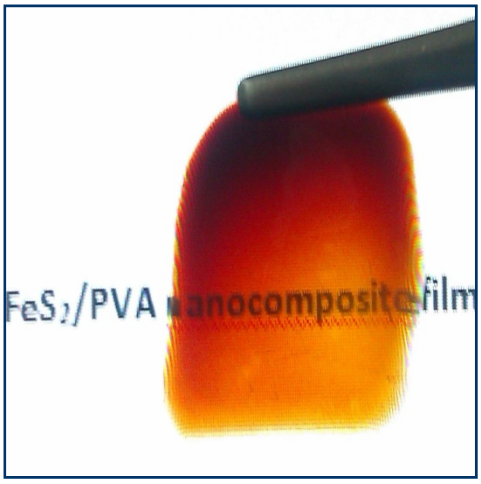

(c)

Figure 5.7 Photographs of transparent films of FeS_2/PVP nanocomposite on (a) glass substrate, (b) PET sheet and (c) freestanding film of FeS_2/PVA

The optical band gap of the nanocomposite films is estimated from the plot of $(\alpha h\upsilon)^2$ vs $h\upsilon$ for the absorption coefficient α which is related to the band gap E_g by Tauc's expression as

$$(\alpha h\upsilon) = k\,(h\upsilon - E_g)^{1/2}$$

where $h\upsilon$ is the incident light energy and k is a constant. The band gap can be estimated by the extrapolation of the linear portion of the graph to the $h\upsilon$ axis. The optical band gap determination of the films of FeS_2/PVA and FeS_2/PVP nanocomposites, synthesized at 150^oC for 10 hrs are shown in figures 5.8 (a) and (b) respectively. The band gap is found to be exactly the same (2.21eV) for both the composite films synthesized under the same conditions. The observed increase in band gap of the composite films with respect to that of the pyrite FeS_2 (0.95eV) establishes the blue shift of the absorption edge of the nanocomposite films. This is due to the fact that surface functionalization of FeS_2 by the polymer facilitates the incorporation of these particles into the polymer matrix.

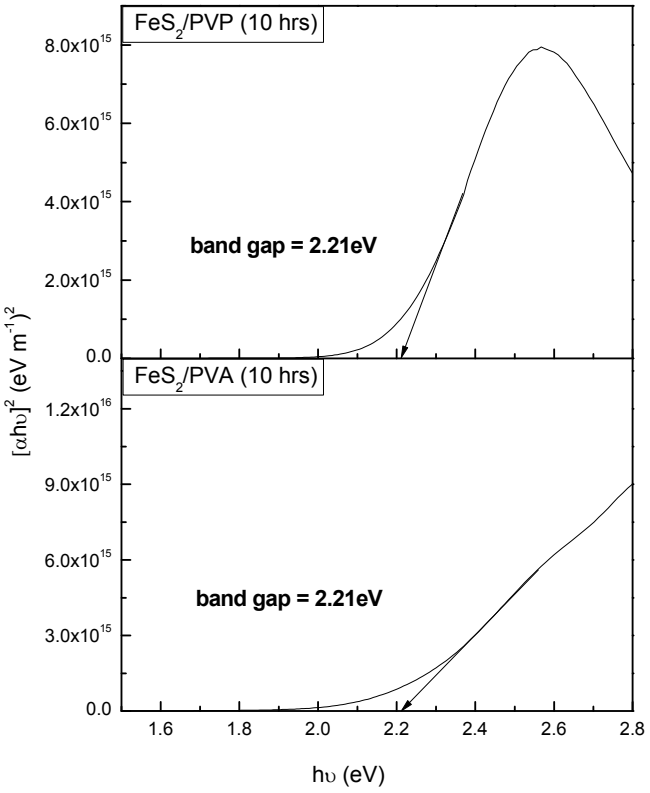

Figure 5.8 Band gap determination of films of (a) FeS_2/PVA and (b) FeS_2/PVP nanocomposites synthesized at 150°C for 10 hrs

The band gap determination of the respective films of FeS_2/PVP nanocomposites synthesized at 150°C for three different time intervals of 10, 20 and 30 hrs is illustrated in figures 5.9 (a), (b) and (c). The optical band gap of these films, grown from the nanocomposites synthesized at various reaction times, seems to be slightly time-dependent and is found to be 2.21, 2.17 and 2.18 eV for time intervals of 10, 20 and 30 hrs respectively. The band gap comes to a minimum value of 2.17 eV for a reaction time of 20 hrs, the time for which the kink seen in the transmission spectra of FeS_2/PVP nanocomposite film disappears.

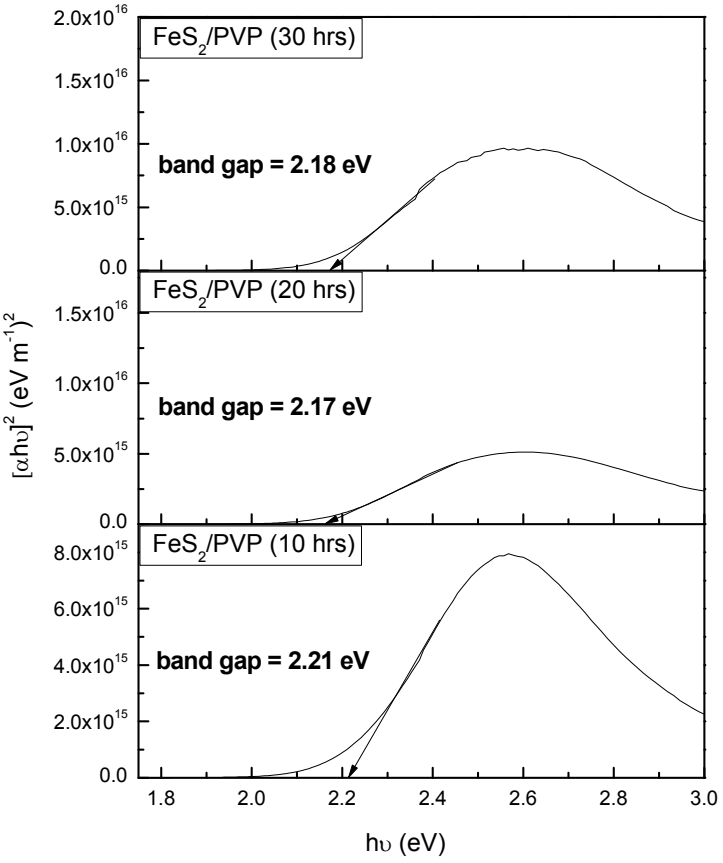

Figure 5.9 Band gap determination of films of FeS_2/PVP nanocomposites synthesized at 150°C for reaction time intervals (a)10, (b)20 and (c)30 hrs

5.5 Conclusions

Nanocomposites of pyrite FeS_2 with PVP and PVA as templates were successfully synthesized using thiourea-mediated solvothermal process at 150°C. The XRD analysis confirms the formation of nanostructured FeS_2 particles of size around 20 nm. A simple and effective solution casting approach was used to grow films of these nanocomposites on glass and flexible substrates.

The UV-Visible transmission spectra of both FeS_2/PVP and FeS_2/PVA nanocomposite films exhibit 100% absorption (zero transmission) from 200 to 550 nm. In general, the nanocomposite films show excellent UV shielding properties in the wavelength range from 200 to 400 nm. Such a combination of excellent UV shielding efficiency and visible transparency offer prospects of applications of these films as UV protectors and colour filters. The films of FeS_2/PVA nanocomposite can be peeled off from the substrates to form free standing films with the additional advantage that these transparent and flexible films can be directly attached as UV protective layers. This work opens new opportunities for developing good quality, transparent and flexible films for UV shielding applications by controlling the reaction time, temperature and also by employing other soft templates.

References

[1] S. Iijima, *Nature*, 354 (1991) 56

[2] W.Q. Han, S.S. Fan, Q.Q. Li, Y.D. Hu, *Science*, 277 (1997) 1287

[3] A.P. Alvisatos, *Science*, 271 (1996) 933

[4] S.S. Wang, E. Joselevich, A.T. Woolley, C.L. Cheung, C.M.Lieber, *Nature*, 394 (1998) 52

[5] Y. Huang, X. Duan, Y. Cui, L.J. Lauhon, K. Kim, C.M. Lieber, *Science*, 294 (2001) 1313

[6] C.J. Lee, T.J. Lee, S.C. Lyu, Y. Zhang, H. Ruh, H.J. Lee, *Appl.Phys. Lett*., 81 (2002) 3648

[7] S. Frank, P. Poncharal, Z.L. Wang, W.A. Heer, *Science*, 280 (1998) 1744

[8] J. Hu, M. Quyang, P. Yang, C.M. Lieber, *Nature*, 399 (1999) 48

[9] H. Tributsch, *Struct. Bonding*, 49 (1982) 128

[10] H. Tributsch, in: J.O.Bockris (Ed.), *Modern Aspects of Electrochemistry*, Pergamon, Oxford, 1986, vol. 14, Chap. 4

[11] E. Bucher, *Appl. Phys*., 17 (1978) 1

[12] T.A. Bither, R.J. Bouchard, W.H. Cloud, P.C.Donohue, W.J. Siemons, *Inorg. Chem*., 7 (1968) 2208

[13] A. Ennaoui, S. Fiechter, H.Goslowsky, H.Tributsch, *J. Electrochem. Soc.,*132 (1985) 1579

[14] A. Ennaoui, S. Fiechter, W. Jaegermann, H.Tributsch, *J. Electrochem. Soc*., 133 (1986) 7

[15] Lira-Cantu´, M.; Go´mez-Romero, *P. Chem Mater.,*10 (1998) 698

[16] Wang, Y.; Herron, N. *Chem Phys Lett* ., 200 (1992) 71

[17] Carotenuto, G. C.; Her, Y. S.; Matijevic, *E. Ind EngChem Res*., 35 (1996) 2929

[18] Lira-Cantu´, M.; Go´mez-Romero, *P. Chem Mater*.,10 (1998) 698

[19] Tunney, J. J.; Detellier, *C. Chem Mater*., 8 (1996) 927

[20] Wang, Z.; Pinnavaia, T. *J. Chem Mater*., 10 (1998) 1820

[21] C. M. Hassan and N. A. Peppas, *Adv. Polym. Sci.,* 153 (2000) 37-65

[22] M. Kokabi, M. Sirousazar, and Z. Hassan, *Eur. Polym. J*., 43 (2007) 773-781

[23] M. Nagura, T. Hamano, H. Ishikawa, *Polym*., 30 (1989) 762-765

[24] C. A. Scotchford, M. G. Cascone, S. Downes, and P. Giusti, *Biomaterials*., 19 (1998) 1-11

[25] Yanbao Zhao, Li Yao, Yuanchun Qi, Lei Sun, Zhishen Wu, *J Sol-Gel Sci Technol*. 50 (2009) 3–7

[26] X. F. Qian, J. Yin, Y. F. Yang, Q. H. Lu, Z. K. Zhu, J. Lu, *Journal of Applied Polymer Science*, 82 (2001) 2744–2749

[27] Zheng M, Gu M, Jin Y, JinY. *Mater. Res. Bull.* 36 (2001) 853-859

[28] Carotenuto G. *Appl. Organomet. Chem*. 15 (2001) 344-351

[29] Philias, J.M, Marsan, B., *Electrochimica Acta ,* 44 (1999) 2351-2363

[30] Philip, D., Eapen, A, Aruldhas, G., *Journal of Solid State Chemistry,* 116 (1995) 217-223

[31] Kabil, M.A., Ghazy, S.E., El-Asmy A.A, Sherif, Y.E., *Analytical Sciences,* 12 (1996) 431- 437

Chapter 6

CYTOTOXICITY AND CELLULAR UPTAKE STUDIES OF BIOFUNCTIONALIZED ZnS:Mn NANOCRYSTALS

Contents

Semiconductor quantum dots have received much attention as novel types of fluorescent probes for biomedical applications, especially cellular imaging. It is mandatory to have a careful assessment of unexpected toxicities and biological interactions associated with these quantum dots. This chapter deals with the investigations carried out on the cytotoxicity assessment and uptake studies of highly luminescent, manganese doped zinc sulphide (ZnS:Mn) nanocrystals bio-functionalized with chitosan and amino acid ligands, which are commercially available and cost effective. The toxicity of these nanocrystals has been assessed in mouse fibroblast L929 cells using the colorimetric MTTS in vitroassay. The results show that L- citrulline capped ZnS:Mn nanocrystals are 100% non toxic and hence highly bio-compatible. In vitro cellular uptake studies of these bio-compatible ZnS:Mn nanocrystals in human embryonic kidney (HEK293T) cells reveal that ZnS:Mn nanoparticles capped with L-arginine show the maximum uptake. The cytotoxicity assessment and uptake studies offer prospects of applications of these bio-functionalized ZnS:Mn nanocrystals in biomedical and imaging fields.

6.1 Introduction

Semiconductor nanomaterials have received much attention in the last two decades as efficient fluorescent probes for live cell imaging of cellular and sub-cellular processes [1-6]. A major requirement for expanding their biological application demands the synthesis of monodispersed, water soluble and biofunctionalized nanoparticles, non toxic to animal cells. Several strategies have been adapted previously for biofunctionalization [7–13] of nanoparticles for diverse applications such as cell labelling, [14–19] cell tracking, *in vivo* imaging [20–22] and multiplexing [23–25]. Biofunctionalization involves attachment of biorecognition molecules such as proteins, peptides, antibodies, carbohydrates, nucleic acids, aminoacids and polymer materials. These bio-compatible capping agents bind to the surfaces of the nanoparticles during synthesis and provide surface passivation, that protects the nanoparticle surfaces from oxidation. Such surface passivation effects often lead to higher luminescence intensity and quantum efficiency in semiconductor nanocrystals. These surface modified nanocrystals can be attached to the target bio-molecules via covalent bonding or self assembly in the same phase. The conjugation of surface modified nanoparticles with specific biomolecules allows researchers to target the desired location with reduced overall toxicity and enhanced efficiency of the imaging probes [26].

The synthesis and optical characterization of water dispersible, ZnS:Mn nanocrystals capped with L-valine, cysteine, histidine, arginine, methionine and chitosan have already been reported earlier [27-30]. The present work is aimed at synthesizing fluorescent ZnS:Mn nanocrystals suitable for bio-imaging applications, using chitosan and amino acid ligands as capping materials, which is an effective technique for the synthesis of bio-compatible

semiconductor nanocrystals. Chitosan is well-known as a capping agent due to its significant chemical and biological properties such as hydrophilicity, biocompatibility, biodegradability, and antibacterial properties [31]. The passivation layer of chitosan on the surface of nanocrystals makes them bio-compatible so that they can be attached to biomolecules such as DNA [32], RNA, proteins [33, 34], peptides [35] etc. More recently, amino acid ligands have been developed as effective surface capping agents in the synthesis of semiconductor nanocrystals with controllable size distribution. Surface modification of these nanocrystals by suitable aminoacid ligands makes these nanocrystals bio-compatible. Organic ligands that bind to the surfaces of the nanoparticles during synthesis provide the required surface passivation that protects the nanoparticle surfaces from oxidation and minimizes the electronic trapping capabilities of surface defects, both of which lead to a high photoluminescence efficiency in semiconductor nanocrystals. The presence of reactive amine and –OH groups in aminoacids makes them good candidates for biomedical and pharmaceutical applications.

Manganese doped zinc sulphide (ZnS:Mn) is a highly pursued phosphor material which exhibits excellent luminescence characteristics including high luminescence intensity, narrow emission bands, low photobleaching, large Stokes' shift and high photochemical stability [36–40]. Its high luminescence efficiency and stability at ambient temperatures are critical properties required for biological applications**.** Detailed studies on the toxicity of these nanoparticles at cellular and subcellular levels are mandatory for approving their biological applications. Several groups have investigated the toxicity of nanoparticles based on various factors including shape, size, surface chemistry, chemical composition, surface activity and solubility

[41–45]. Recommendations for the use of nanoparticles in various fields have emerged as a result of these initial toxicity studies. A few reports have appeared recently on toxicity studies of quantum dots (QDs) in cells and animals [46, 47]. Cell culture experiments have shown that QDs undergo design-dependent intracellular localization which can cause cytotoxicity by releasing free toxic materials into solution and by generating free radical species. In animal experiments, QDs preferentially enter the liver and spleen following intravascular injection which undergo minimal excretion if larger than 6 nm, and appear to be safe to the animal. The present work is focused on the cytotoxicity and cellular uptake studies of ZnS:Mn nanoparticles biofunctionalized with chitosan and various aminoacids. The cytotoxicity of these biofunctionalized nanoparticles was evaluated in mouse fibroblast cells and cellular uptake in human embryonic kidney cells employing MTT assay and fluorescent microscopic techniques.

6.2 Experimental Details

6.2.1 Synthesis of bio-compatible ZnS:Mn nanocrystals

Introduction of different methods for the synthesis of nanoparticles and optimization of various conditions involved in the synthesis have significantly improved the quality of the nanoparticles. Out of the various techniques available, in the present work, the simple and cost effective wet chemical co-precipitation method was used for the synthesis of bio-compatible ZnS:Mn nanocrystals. The reactants used were zinc acetate [Zn $(CH_3COO)_2.2H_2O$] (Merck Specialities Private Limited, Mumbai,>98%), manganese acetate [$Mn(CH_3COO)_2.4H_2O$] (Merck Specialities Private Limited, Mumbai, >99.5%), and sodium sulphide [$Na_2S.9H_2O$] (Merck Specialities Private Limited, Mumbai, 98%). In a typical

experiment, 0.1mol L^{-1} zinc acetate, 0.01mol L^{-1} manganese acetate and 0.025mol L^{-1}capping agent were mixed in 50 ml of water to which 0.1mol L^{-1} aqueous solution of sodium sulphide was added dropwise to form the capped ZnS:Mn nanoparticles. The mixture was kept under constant stirring for one and a half hour and then filtered and dried in an oven at 40^0C. The powder sample thus obtained has been found to be readily dispersible in water.

6.2.2 *In vitro* toxicological study of bio-compatible ZnS:Mn nanocrystalsin mouse fibroblast L929 cells

Cytotoxicity of ZnS:Mn nanoparticles coated with chitosan and different aminoacids was evaluated using, 3-(4,5-dimethylthiazole-2-yl)-2,5-diphenyltetrazolium chloride (MTT) assay. Here, ~$1x10^6$ mouse fibroblast L929 cells were inoculated into 96 well tissue culture plates containing Dulbecco's modified eagle's medium [DMEM] supplemented with 10% fetal bovine serum [FBS] and incubated for 48 hrs at 37^0C. The cells were copiously washed with phosphate-buffered saline [PBS], and the medium was exchanged with DMEM containing different concentrations of capped ZnS:Mn nanoparticles ranging from 0.1 to 1000 nM. The cells were incubated for 24 hrs at 37 ^{O}C and subjected for MTT assay following standard protocol. Briefly, nanoparticle treated cells were supplemented with 50µl of MTT solution (5mg mL^{-1}) prepared in PBS and kept for incubation under dark at 37^OC for 3 hrs. Subsequently, the viability of the cells was measured as a function of reduction of MTT to insoluble formazan by mitochondrial dehydrogenase enzyme of healthy cells. Formazan crystals were dissolved in dimethyl sulphoxide and the absorbance was recorded at 570 nm using a microplate reader (Biotech, USA).

6.2.3 *In vitro* cellular uptake study of bio-compatible ZnS:Mn nanocrystals in human embryonic kidney (HEK293T) cells

HEK293T cells were used for the uptake studies. The cells were grown in DMEM with 10% FBS under the standard condition of 37^0C and 5% CO_2. For uptake studies, cells were seeded on cover slips in 24-well plate at a density of 10,000 cells/0.3 cm^2 and were incubated at 37^0C, 5% CO_2. After reaching ~60% confluency, cells were incubated with 2 μL of each type of capped ZnS:Mn nanoparticles and incubated for another 2 hrs. Controls were also kept without adding any nanoparticles. The medium was completely removed and 20% drug diluted in DMEM with 10% FBS was added to the corresponding wells excluding control well. The cells were kept in CO_2 incubator for 2 hrs. After incubation the medium was removed and cells were very gently washed with PBS for three times. After PBS wash, cells were fixed with 4% paraformaldehyde for 15 minutes at 4^0C. The cells were washed with PBS thrice. Nuclear staining of cells was done by adding 200 μL of DAPI to each well and incubating at room temperature for 20-30 minutes. DAPI was removed and washed with PBS thrice. The cover slips were very carefully lifted from the wells and mounted on glass slides with fluoromount. The cells were then visualized under UV microscope for the presence of nanoparticles and photographs were taken using Andor 885 camera. In order to check whether the concentration of the nanoparticles used for the uptake study affects the viability of the cells, the MTT assay as previously described was also performed.

6.3 Sample Characterization

The X-ray powder diffraction (XRD) patterns of the synthesized ZnS:Mn nanoparticles were recorded on a Rigaku X-ray diffractometer with

Cu-Kα radiation (1.5418 Å) operating at 30 kV and 20 mA. Scanning was carried out in the 2θ range from 20^o - 60^o at a scan speed of 2^o per minute. Transmission electron microscope (TEM) image of the synthesized ZnS:Mn sample was obtained using JEOL 3010 instrument. The energy dispersive X-ray spectrum (EDXS) was obtained with JEOL Model JSM - 6390LV scanning microscope. Fourier transform infrared (FT-IR) spectra of the samples were obtained with AVTAR 370 DTGS FTIR spectrophotometer in the wave number range 400–4000 cm^{-1}. The PL emission spectra of the samples were recorded with Fluoromax-3 Spectrofluorimeter using Xe lamp as the excitation source.

6.4 Results and discussion

6.4.1 X-Ray Diffraction (XRD) analysis

The structural analysis of the capped ZnS:Mn powder samples is carried using XRD technique and figure 6.1 shows the XRD patterns of the Mn doped ZnS nanoparticles capped with chitosan and the aminoacids, L-citrulline, L-lysine, L-arginine, L-serine, L-histidine and glycine. The samples are having cubic crystal structure and the diffraction data are in agreement with the JCPDS data for ZnS (JCPDS card No.050566). The XRD patterns are quite broad with three main peaks corresponding to reflections from the (111), (220) and (311) planes which suggest zinc blende crystal structure. The particle size is determined from the full width at half maximum (FWHM) of the diffraction peaks, using Debye - Scherrer formula

$$d = 0.9\lambda/\beta \cos\theta \qquad (1)$$

where d, λ, β and θ are the average particle size, the wavelength of the X-ray, full width at half maximum intensity expressed in radians and diffraction angle

respectively. The ZnS:Mn nanoparticles capped with chitosan, L-citrulline, L-lysine, L-arginine, L-serine, L-histidine and glycine are found to have particle size around 10.4 nm, 10 nm, 12.9 nm, 8.4 nm, 8.8 nm, 8.2 nm and 10.7 nm respectively.

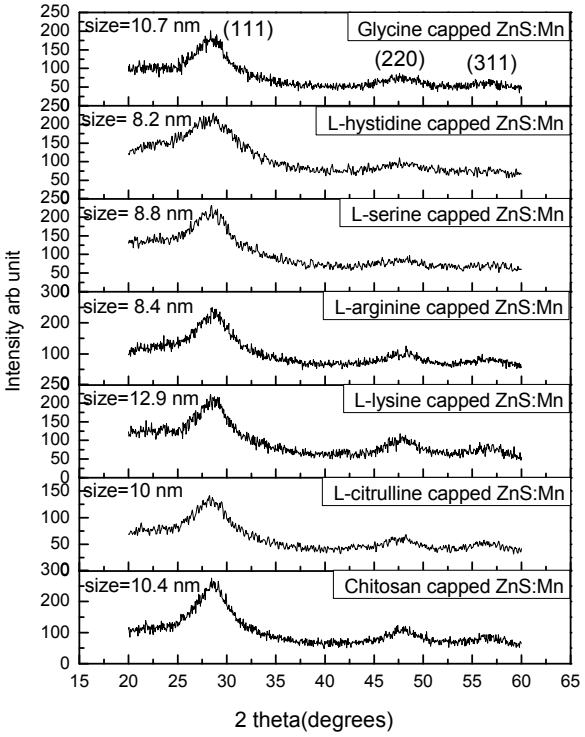

Figure 6.1 XRD patterns of ZnS:Mn nanoparticles capped with chitosan, L-citrulline, L-lysine, L-arginine, L-serine, L-histidine and glycine.

6.4.2 Transmission electron microscopy (TEM) studies

The TEM image of a typical capped ZnS:Mn sample (L-citrulline capped ZnS:Mn) was recorded to estimate the crystallite size and the image is shown in figure 6.2(a). The average crystallite size is approximately 10 nm. The average particle size obtained from TEM analysis is found to be approximately equal to that determined from the XRD peaks using the Debye-

Scherrer formula. The energy dispersive X-ray spectrum (EDXS) of this typical sample is shown in figure 6.2 (b), which provides the elemental composition of the sample. The presence of zinc, sulphur, manganese, carbon and oxygen in the powder sample can be confirmed from the spectrum. The presence of carbon and oxygen in the EDX spectrum is an indication of the effective capping of ZnS:Mn by the aminoacid, L-citrulline.

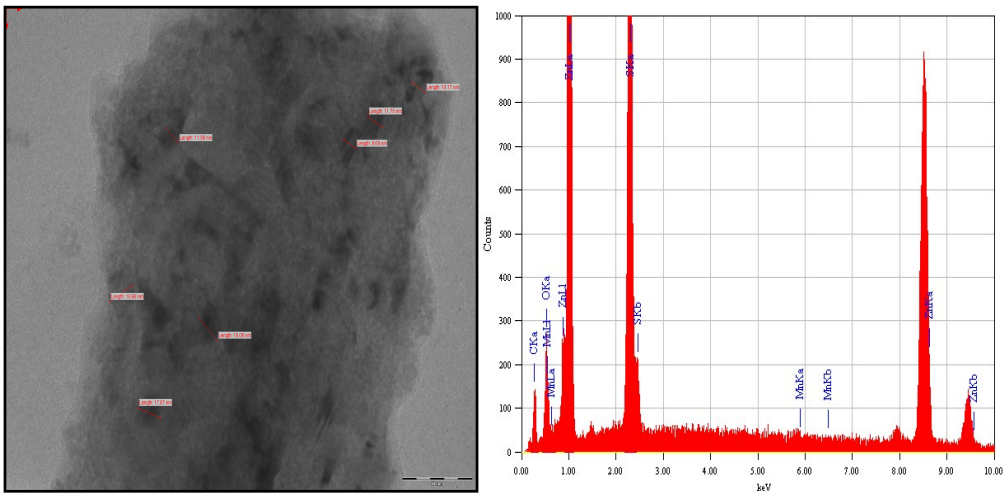

(a) (b)

Figure 6.2 (a) TEM image (scale bar:50 nm) and (b) EDX Spectrum of ZnS:Mn nanoparticles capped with L- citrulline.

6.4.3 Fourier transform infrared (FT-IR) spectral studies

The FTIR spectra of the capped ZnS:Mn nanocrystals are shown in figure 6.3. The major peaks appearing at 662 cm^{-1}, 1014 cm^{-1} and 1400 cm^{-1} in figure 6.3 are attributed to the characteristic vibrations of the ZnS:Mn. The strong peaks appearing around 3400 cm^{-1} and 1550 cm^{-1} are assigned to the vibrational modes of zinc coordinated $–NH_2$ and –COO groups for the corresponding aminoacids and chitosan. The IR spectra provide ample

confirmation for the attachment of the aminoacid ligands and chitosan onto the surfaces of the ZnS:Mn nanoparticles.

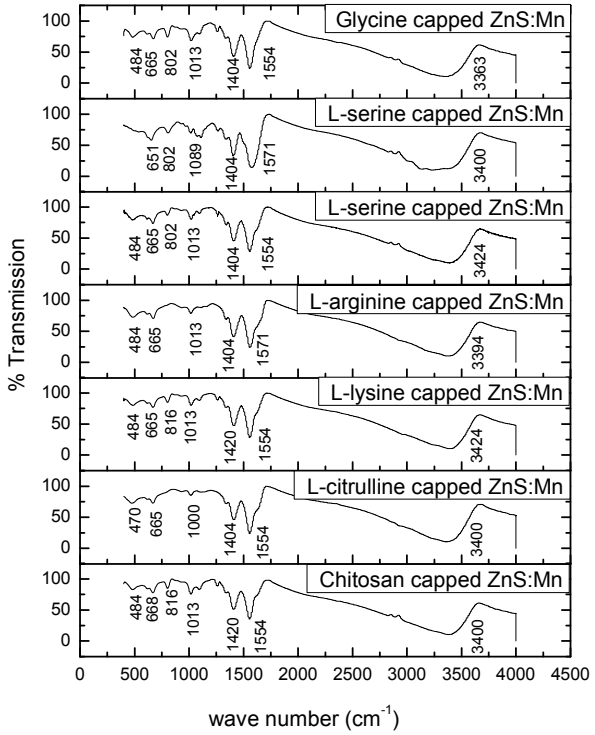

Figure 6.3 FT-IR spectra of ZnS:Mn nanoparticles capped with chitosan, L-citrulline, L-lysine, L-arginine, L-serine, L-histidine and glycine.

6.4.4 Photoluminescence studies

The energy transfer mechanism in ZnS:Mn nanophosphor under UV radiation is described schematically in figure 6.4. These fluorescent nanocrystals display two PL emission peaks when excited at 330 nm. The weak emission at around 420 nm arises due to the transition of electrons from shallow electron traps near the conduction band to sulphur vacancies present near the valence band, which is characteristic of the blue photoluminescence observed in bulk ZnS. The strong orange emission at about 600 nm can be

attributed to the $^4T_1$-$^6A_1$ radiative transition of the Mn^{2+} impurity. The well-known green emission of Zn vacancies (at around 480 nm) has not been clearly observed in the ZnS:Mn^{2+} nanocrystals, indicating that this emission has been quenched by the energy transfer to the Mn^{2+} [48,49]. The fluorescence emission of dopant ions is more stable and controllable than the defect/vacancy-related emission, because the defects or vacancies in semiconducting nanomaterials are greatly affected by many factors such as synthesis procedures and environments.

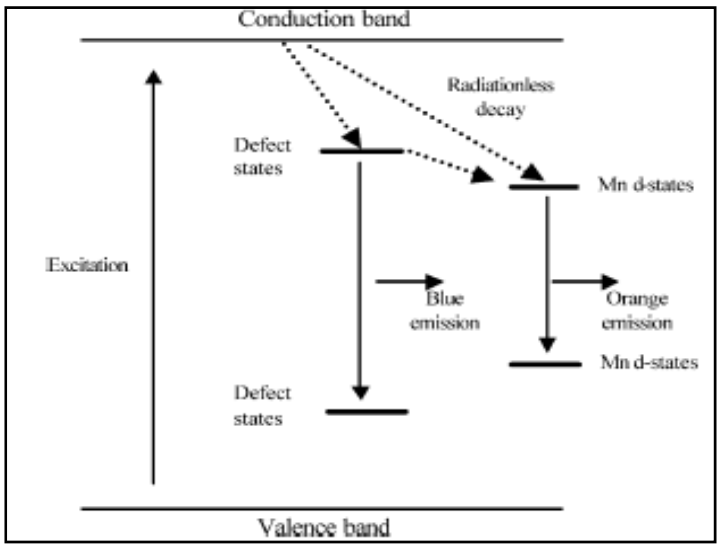

Figure 6.4 Energy transfer mechanism in ZnS:Mn nanophosphor under UV excitation

Photoluminescence spectra of Mn doped ZnS nanoparticles capped with chitosan and the aminoacids, L-citrulline, L-lysine, L-arginine, L-serine, L-histidine and glycine , recorded at room temperature under an excitation of 330 nm are shown in figure 6.5 (a). The PL spectra obtained from the capped ZnS:Mn samples show intense orange red emission [figure 6.5 (b)] peaks at 598 nm. The small broad peaks observed around 420 nm can be due to the presence of defect states arising from zinc ion vacancies in the ZnS crystal

lattice. The PL peak intensity of ZnS:Mn capped with L-citrulline and L-serine at 598 nm is found to be much higher than the peak intensity in other samples. Though the emission peak intensity at 598 nm of ZnS:Mn, capped with L-citrulline and L-serine are the same, the intensity of the peak at 420 nm is found to be less in the case of L-citrulline capped ZnS:Mn, compared to that in L-serine capped ZnS:Mn [50]. This indicates that L-citrulline is more effective as a fluorescent probe for biomedical applications.

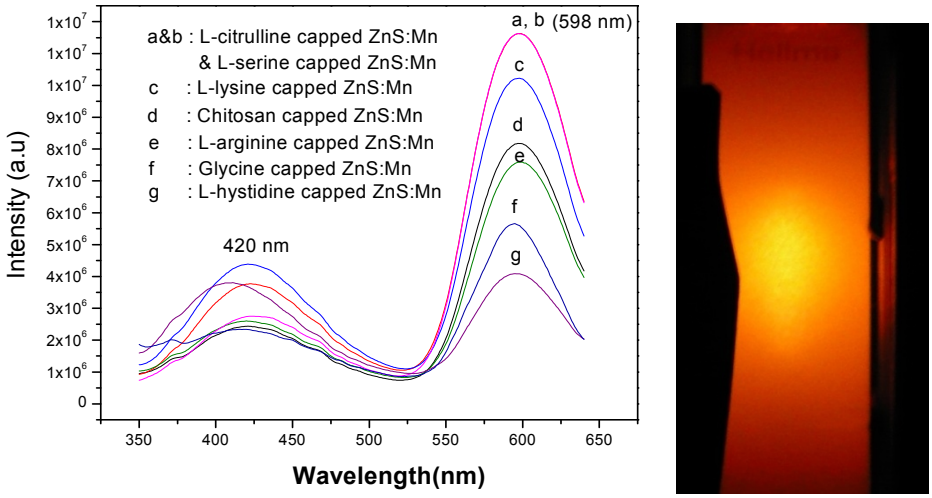

(a) (b)

Figure 6.5 (a) PL spectra of ZnS:Mn nanoparticles capped with chitosan, L-citrulline, L-lysine, L-arginine, L-serine, L-histidine and glycine and (b) orange red emission observed from capped ZnS:Mn nanoparticles.

6.4.5 Cytotoxicity assessment

Cytotoxicity of uncapped ZnS:Mn nanoparticles and ZnS:Mn nanoparticles capped with L-citrulline, L-lysine, chitosan, L-arginine, L-serine, L-histidine and glycine was evaluated using MTT assay in mouse fibroplast L929 cells for 24 hrs and the results are shown as bar diagram in figure 6.6. Studies carried out on the activity of cells (%) at different

concentrations of these ZnS:Mn nanocrystals show that nanocrystals capped with L- citrulline are 100% non toxic and hence highly bio-compatible for 0.1nM concentration. L-arginine is also found to be an efficient capping agent to make ZnS:Mn nanocrystals bio-compatible for 1nM concentration.

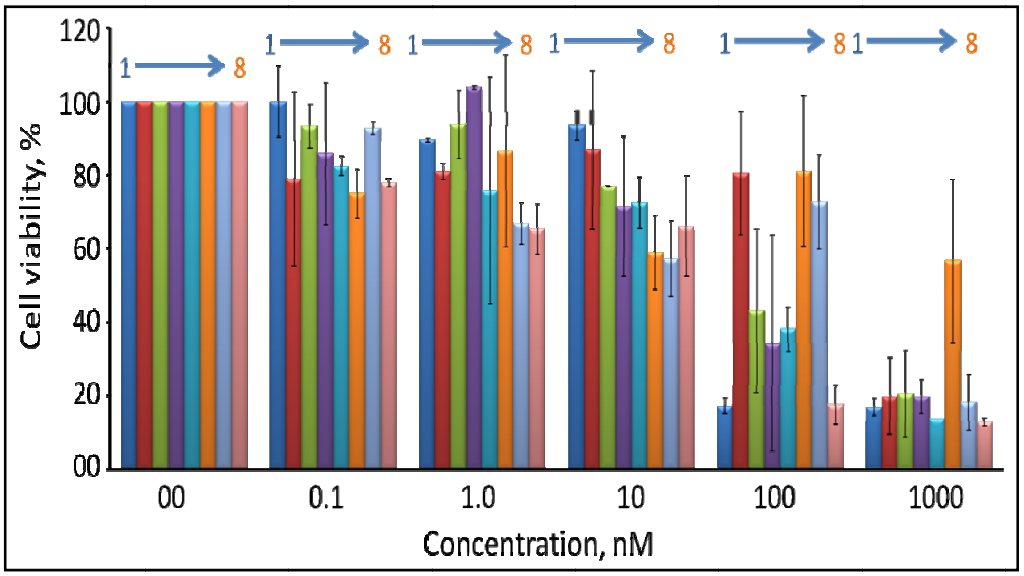

Figure 6.6 Bar diagram showing cell viability (%) at different concentrations of ZnS:Mn capped with L-citrulline (1), L-lysine (2), chitosan (3), L-arginine (4), L-serine (5), L-histidine (6) and glycine (7) and uncapped ZnS:Mn (8).

6.4.6 Cellular uptake studies

In vitro cellular uptake study in HEK293T cells was carried out using ZnS:Mn nanocrystals biofunctionalized with L-arginine, L-citrulline, L-histidine and chitosan and the cells were observed using fluorescent microscope and the images are shown in figure 6.7. The results show that ZnS:Mn nanoparticles capped with L-arginine has the maximum uptake compared to L-citrulline, L-histidine and chitosan for 1nM concentration.

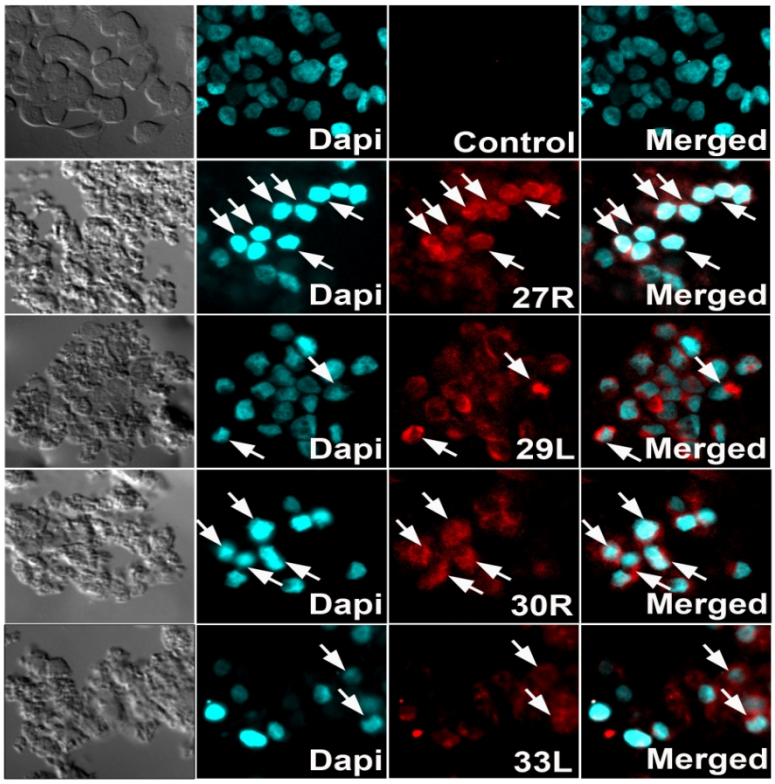

Figure 6.7 In vitro cellular uptake in ZnS:Mn nanocrystals capped with L-arginine (27R), L-citrulline (29L), L-histidine (30R) and chitosan (33L)

6.5 Conclusions

Biofunctionalized ZnS:Mn nanocrystals have been synthesized using chitosan and amino acid ligands as capping materials.These nanocrystals show orange emission at 598 nm and the emission intensity of L- citrulline capped ZnS:Mn is found to be the maximum. The toxicity of these nanocrystals has been assessed in mouse fibroblast L929 cells using the colorimetric MTT *in vitro* assay and effects on human cells have also been investigated.

Studies on the cytotoxicity of uncapped and capped ZnS:Mn nanocrystals with chitosan, L-citrulline, L-lysine, L-arginine, L-serine,

L-histidine and glycine as capping agents, show that nanocrystals capped with L- citrulline are 100% non toxic for 0.1 nM concentration and those capped with L-arginine for 1nM concentration and hence highly bio-compatible. With a host of opportunities for nanomaterial use in medical and pharmaceutical applications, a thorough awareness of associated systemic toxicity is mandatory.

In vitro cellular uptake studies in HEK293T cells using these biofunctionalized ZnS:Mn nanocrystals show that ZnS:Mn nanoparticles capped with L-arginine (1nM concentration) show the maximum uptake. These results highlight the importance of using appropriate amino acids for the bioconjugation of ZnS:Mn nanocrystals. These bioconjugated nanocrystals have safe physico-chemical properties which will enable them to be utilized as ideal agents for intracellular tracking and biomedical imaging.

References

[1] M. Bruchez, M. Moronne, P. Gin, S. Weiss and A. P. Alivisatos, *Science*, 281 (1998) 2013

[2] W. C. W. Chan and S. Nie, *Science*, 281 (1998) 2016

[3] R. Elghanian, J. J. Storhoff, R. C. Mucic, R. L. Letsinger and C.A. Mirkin, *Science*, 277 (1997) 1078

[4] F. V. D. Rijke, H. Zijlmans, S. Li, T. Vail, A. K. Raap, R. S. Niedbala and H. J. Tanke, *Nat. Biotechnol*.,19 (2001) 273

[5] Gerion, D.; Pinaud, F.; Williams, S. C.; Parak, W. J.; Zanchet,D.; Weiss, S.; Alivisatos, A. P. *J. Phys. Chem. B*195 (2001) 8861

[6] Jun, Y. W.; Jang, J. T.; Cheon, J. W. *Bull. Kor. Chem. Soc.*27 (2006) 961

[7] Y. Xing, Q. Chaudry, C. Shen, K. Y. Kong, H. E. Zhau, L. W. Chung, J. A. Petros, R. M. O'Regan, M. V. Yezhelyev, J. W. Simons, M. D.Wang, and S. Nie, *Nat. Protoc.* 2 (2007)1152

[8] I. L. Mednitz, H. T. Uyeda, E. R. Goldman, and H. Mattoussi, *Nat.Mater.* 4 (2005)435

[9] A. R. Clapp, E. R. Goldman, and H. Mattousi, *Nat. Protoc.* 1 (2006) 1258

[10] H. Mattoussi, J. M. Mauro, E. R. Goldman, T. M. Green, G. P.Anderson, V. C. Sundar, and M. G. Bawendi, *Phys. Status Solidi B* 224 (2001) 277

[11] E. R. Goldman, G. P. Anderson, P. T. Tran, H. Mattoussi, P. T. Charles, and J. M. Mauro, *Anal. Chem.*74 (2002) 841

[12] E. R. Goldman, E. D. Balighian, H. Mattoussi, M. K. Kuno, J. M. Mauro, P. T. Tran, and G.P. Anderson, *J. Am. Chem. Soc.* 124 (2002) 6378

[13] W. J. Parak, D. Gerion, D. Zanchet, A. S. Woerz, T. Pellegrino,C. Micheel, S. C. Williams, M. Seitz, R. E. Bruehl, Z. Bryant, C. Bustamante, C. R. Bertozzi, and A. P. Alivisatos, *Chem.Mater.*14 (2002) 2113

[14] X. Wu, H. Liu, J. Liu, K. N. Haley, J. A. Treadway, J. P. Larson, N. Ge, F. Peale, and M. P. Bruchez, *Nat. Biotechnol.* 21 (2002) 41

[15] J. K. Jaiswal, E. R. Goldman, H. Mattoussi, and S. M. Simon, *Nat.Methods*1 (2004) 73

[16] S. Lin, X. Xie, M. R. Patel, Y. H. Yang, Z. Li, F. Cao, O. Gheysens, Y. Zhang, S. S. Gambhir, J. H. Rao, and J. C. Wu, *BMC Biotechnol.*7 (2007) 67

[17] W. A. Hild, M. Breunig, and A. Goepferich, *Eur. J. Pharm. Biopharm.* 68 (2008) 153

[18] H. Wang, H. Jiang, H. Zhang, Y. Zhou, C. Wu, J. Zhao, C. Wu, L. Ba, and X. Wang, *J. Nanosci. Nanotechnol*. 11 (2011) 1117

[19] H. Li, M. Li, W. Y. Shih, P. I. Lelkes, and W. Shih *J. Nanosci.Nanotechnol.* 11 (2011)3543

[20] S. Kim, Y. T. Lim, E. G. Soltesz, A. M. D. Grand, J. Lee, A. Nakayama, J. A. Parker, T. Mihaljevic, R. G. Laurence, D. M. Dor, L. H. Cohn, M. G. Bawendi, and J. V. Frangioni, *Nat. Biotechnol.*22 (2004) 93

[21] X.Gao, Y. Cui, R. M. Levenson, L. W. K. Chung, and S. Nie, *Nat.Biotechnol.* 22 (2004) 969

[22] A. M. Smith, H. Duan, A. M. Mohs, and S. Nie, *Adv. Drug Deliv. Rev.* 60 (2008) 1226.

[23] M. Han, X. Gao, J. Z. Su, and S. Nie, *Nat. Biotechnol.* 19 (2001) 631

[24] W. C. W. Chan, D. J. Maxwell, X. Gao, R. E. Bailey, M. Han, and S. Nie, *Curr. Opin. Biotechnol.* 13 (2002) 40

[25] J. K. Jaiswal, H. Mattoussi, J. M. Mauro, and S. M. Simon, *Nat. Biotechnol.* 21 (2002) 47.

[26] NandananErathodiyil, Jackie Y. Ying, *Acc. Chem. Res*. 44 (2011) 925–935

[27] Cheong-Soo Hwang, Narae Lee, Young-Ah Kim, Youn Bong Park, *Bull. Korean Chem. Soc*. 27 (2006) 1809-1814

[28] Hoon Young Kong,Song-Yi Kim,JonghoeByun,and Cheong-Soo Hwang, *Bull. Korean Chem. Soc.* 32 (2011) 53-58

[29] Ju Ho Lee, Yong Ah Kim, Kimoon Kim, Young Duk Huh, June Won Hyun, H. S. Kim, S. J. Noh, Cheong-Soo Hwang, *Bull. Korean Chem. Soc.* 28 (2007) 1091-1096

[30] Baruah, S.; Warad, H.C.; Chindaduang, A.; Tumcharern, G.; Dutta, J. *Journal of Bionanoscience*, 2 (2008) 42-48

[31] R.S. Juang, F.C. Wu, R.L. Tseng, *Adv*. *Environ*. *Res.* 6 (2002) 171-177

[32] Z. Li, R. Jin, C.A. Mirkin, R.L. Letsinger, *Nucleic Acids Res*. 30 (2002) 1558.

[33] A.P. Alivisatos, *Nature*, 382 (1996) 609

[34] X. Gao, W.C.W. Chan, S. Nie, *Science* 281(1998) 2016

[35] S.R. Whaley, D.S. English, E.L. Hu, P.F. Barbara, A.M. Belcher, *Nature* 405 (2000) 665

[36] W. Chen, R. Sammynaiken and Y. N. Huang, *J. Appl. Phys*., 88 (2000) 5188

[37] P. B. Xie, W. P. Zhang, M. Yin, H. T. Chen, W. W. Zhang,L. R. Lou and S. D. Xia, *J. Colloid Interface Sci*., 229 (2000) 534

[38] W. Chen, R. Sammynaiken, Y. Huang, J. O. Malm, R.Wallenberg, J. O. Bovin, V. Zwiller and N. A. Kotov, *J. Appl.Phys*., 89 (2001) 1120

[39] M. F. Bulanyi, Y. A. Gulevskii and B. A. Polezhaev, *Inorg.Mater*., 36 (2000) 997

[40] A. D. Dinsmore, D. S. Hsu, S. B. Qadri, J. O. Cross,T. A. Kennedy, H. F. Gray and B. R. Ratna, *J. Appl. Phys*., 88 (2000) 4985

[41] Chithrani BD, Ghazani AA, Chan WCW. *Nano. Lett.* 6 (2006) 662–668

[42] Murphy CJ, Gole AM, Stone JW *et al. Acc. Chem. Res.* 41 (2008) 1721–1730

[43] Hussain SM, Hess KL, Gearhart JM, Geiss KT, Schlager JJ. *Toxicol. In vitro* 19 (2005)975–983

[44] Oberdörster G, Stone V, Donaldson K. *Nanotoxicology* 1 (2007) 2–25

[45] Nan A, Bai X, Son SJ, Lee SB, Ghandehari H. *Nano. Lett.* 8 (2008) 2150–2154

[46] Abdulaziz Anas, Tetsuya Okuda, Nagako Kawashima, Kenichi Nakayama, TamitakeItoh, Mitsuru Ishikawa, Vasudevanpillai Biju. *ACS Nano*. 3 (2009) 2419–2429

[47] Vasudevanpillai Biju, TamitakeItoh, Abdulaziz Anas, Athiyanathil Sujith, Mitsuru Ishikawa. *Anal Bioanal Chem*. 39 (2008) 12469–2495

[48] Sapra. S, Prakash .A, Ghangrekar .A, Periasamy. N and Sarma D. D, *J.Phys. Chem. B,* 109 (2005) 1663

[49] Biswas. S, Kar. S and Chaudhuri .S *„J.Phys. Chem. B*,109 (2005) 17526

[50] Aswathy Jayasree, Sajith Sasidharan, Manzoor Koyakutty, Shantikumar Nair, Deepthy Menon, *Carbohydrate Polymers* 85 (2011) 37-43

Chapter 7

IMMOBILIZATION OF TRYPSIN ON BIO-COMPATIBLE, CHITOSAN CAPPED ZnS:Mn NANOCRYSTALS FOR THERAPEUTIC APPLICATIONS

Contents

This chapter gives an account of the studies carried out on the immobilization of trypsin on chitosan capped, manganese doped zinc sulphide nanoparticles, synthesized by chemical capping co-precipitation method, using glutaraldehyde (GA) as cross-linker. Results indicate that the activity of trypsin, immobilized onto chitosan modified ZnS:Mn nanoparticles has been improved upon cross-linking, which suggests that the immobilized trypsin has become more stable and active. This investigation highlights the prospects of potential applications of immobilized trypsin in therapeutic and diagnostic fields.

7.1 Introduction

Advancements in the synthesis of water- dispersible nanometer sized fluorescent semiconductor materials and the understanding of their optical properties have accelerated their practical applications in several fields. These bio-compatible nanocrystals have received much attention because of their potential biomedical applications in imaging, drug targeting and delivery. The

conjugation of tiny nanoparticles with specific biomolecules allows researchers to target the desired location, reduce overall toxicity, and enhance the efficiency of the imaging probes [1]. Rational modification in the composition and structure of the nanoparticles, using safer materials, increases the prospects of their usefulness in protein delivery and transport [2].

Major research issues in protein delivery include the stabilization of proteins in delivery devices and the design of appropriate protein carriers [2]. Immobilization is an important step in commercial and fundamental enzymology for repetitive economic utilization of enzymes [3]. The immobilization of enzymes onto the nanoparticles offers prospects of applications of these nanoparticles as biosensors and biocatalysts [4]. In particular, bio-compatible nanoparticles upon which enzyme has been immobilized are considered to be novel therapeutic and diagnostic agents [5]. Moreover, these nanoparticles make them safe for human applications, help to increase the shelf-life of the proteins and to protect them over a longer period of time [6].

Chitosan is safe and non-toxic and therefore widely used in food and bioengineering industries, enzyme immobilization, and as a carrier for controlled drug delivery [7-9]. The presence of reactive amine and –OH groups in chitosan makes it a good candidate for biomedical and pharmaceutical applications. The passivation layer of chitosan on the surface of nanocrystals makes them bio-compatible so that they can be attached to biomolecules such as DNA [10], RNA, protein [11, 12], peptides [13] etc. In the present work, nanoparticle encapsulation with chitosan, its size dependent optical properties and immobilization of trypsin with the encapsulated nanoparticle are discussed, together with the future prospects of such systems.

Several studies have been conducted on chitosan capped ZnS:Mn nanoparticles [14-17] . However, no reports are available on the applicability of these bio-compatible nanoparticles in protein immobilization.

Proteins immobilized on bio-compatible nanoparticles have wide applications in drug targeting and delivery, the isolation of protein inhibitors, peptide mass fingerprinting (PMF) [18], and studying protein-protein interactions. Though proteins are vulnerable to degradation, immobilization helps to prevent denaturation of proteins. The fluorescence of nanoparticles, attached to the immobilized trypsin also helps to locate the position of protein inhibitors during the isolation process. Therefore, The present work is novel since, there are no previous reports on the application of chitosan capped, fluoresecent, ZnS:Mn nanoparticles in protein immobilization.

7.2 Experimental Details

7.2.1 Synthesis of chitosan capped ZnS:Mn nanoparticles

ZnS nanoparticles doped with manganese (Mn) were prepared by a chemical capping co-precipitation method in which zinc acetate [Zn $(CH_3COO)_2.2H_2O$] (Merck Specialities Private Limited, Mumbai, >98%), manganese acetate [$Mn(CH_3COO)_2.4H_2O$] (Merck Specialities Private Limited, Mumbai, >99.5%) and sodium sulphide $Na_2S.9H_2O$ (Merck Specialities Private Limited, Mumbai, 98%) were used as the reactants. These nanoparticles were stabilized by steric hindrances upon using chitosan as a capping agent. The synthesis was carried out at room temperature in water for all of its inherent advantages of being simple and cost effective. This method

is similar to that described by Bhargava et al [19] with a suitable modification. With Mn doping high luminescence occurs at around 597 nm [20, 21]. Chitosan is a bio-compatible capping agent which prohibits the diffusion of ions from the solution and restricts the growth of nanocrystals. In this experiment, 0.1mol L^{-1} zinc acetate and 0.01mol L^{-1} manganese acetate were mixed in 50 ml of water along with 0.001% of chitosan to which 0.1mol L^{-1} sodium sulphide was added drop wise to form chitosan capped ZnS:Mn nanoparticles. The mixture was kept under constant stirring for one and a half hours and then filtered and dried in an oven at 40^{o}C. A set of samples was prepared by varying the molarity of sodium sulphide from 0.125 to 0.01mol L^{-1}.

7.2.2 Trypsin assay using BAPNA

Trypsin activity was measured using the synthetic substrate α-N-benzoyl-DL-arginine-p-nitroanilide (BAPNA, Sigma) [22]. For this 25 µl of 0.1 mg/ml trypsin was diluted in 425 µl of 0.01mol L^{-1} phosphate buffer with pH 7.5. Then 50 µl of 2 mmol L^{-1} freshly prepared BAPNA was added and incubated at 37 ^{o} C for 30 minutes. The reaction was stopped by the addition of 500µl of 30% acetic acid. The optical absorbance of p-nitroaniline released by the reaction was read at 410 nm. One unit of trypsin activity (U) was defined as 1µmol of p-nitroaniline released per ml per minute at pH 7.5 and at 37^{o}C.

7.2.3 Immobilization of Trypsin

Trypsin was immobilized using the cross-linker glutaraldehyde [23]. Glutaraldehyde (0.1%) was added to I ml of the nano solution in 0.01 mol L^{-1} phoshate buffer (pH 7.5) and gently stirred for 2h at room temperature. The colloidal nano particles were collected by centrifuging at 3000 rpm for 15 minutes at 25 °C. The excess amount of glutaraldehyde was washed off with water until extinction at 220 and 280 nm approached zero and equilibrated with 0.01 mol L^{-1} phosphate buffer (pH 7.5). Glutaraldehyde attached nanoparticles were suspended in 1 ml of 0.1mg/ml trypsin solution for cross-linking. The mixture was stirred at room temperature for 1hr and kept in a refrigerator at 4°C overnight. The immobilized enzyme was collected by centrifugation and washed three times with distilled water until extinction at 280 nm approached zero. This immobilized trypsin was used for further studies.

7.3 Sample Characterization

The X-ray powder diffraction (XRD) pattern of the chitosan capped ZnS:Mn nanoparticles was recorded on a Rigaku X-ray diffractometer with CuKα radiation (1.5418 Å) operating at 30 kV and 20 mA. Scanning was carried out in the 2θ range from 20^o - 60^o at a scan speed of 2^o per minute. Transmission electron microscope (TEM) image of the synthesized nanocrystals was taken in order to estimate the particle size. Fourier transform infrared (FT-IR) spectra of the samples were obtained with AVTAR 370 DTGS FTIR spectrophotometer in the wave number range 400–4000 cm^{-1}.

UV-Visible spectra in transmission mode were recorded on a Jasco-V 500 spectrophotometer in the wavelength range 200-800 nm. The PL emission spectra of the samples were obtained with Fluoromax-3 Spectrofluorimeter using Xe lamp as excitation source.

7.4 Results and discussion

7.4.1 X-ray powder diffraction (XRD) studies

The XRD patterns of the synthesized Mn doped ZnS nanoparticles capped with chitosan for sodium sulphide concentrations 0.01, 0.05, 0.075, 0.1 and 0.125mol L^{-1} are shown in figure 7.1. The samples are having cubic crystal structure and the diffraction data are in agreement with the JCPDS data for ZnS (JCPDS card No.050566). The XRD patterns are quite broad with three main peaks corresponding to the reflections from (111), (220) and (311) planes which suggest zinc blende crystal structure. The particle size is determined from the full width at half maximum (FWHM) of the diffraction peaks, using Debye- Scherrer formula

$$d = 0.9\lambda/\beta \cos\theta \qquad (1)$$

where d, λ, β and θ are the average particle size, the wavelength of the X-ray, full width at half maximum intensity expressed in radians and diffraction angle respectively.

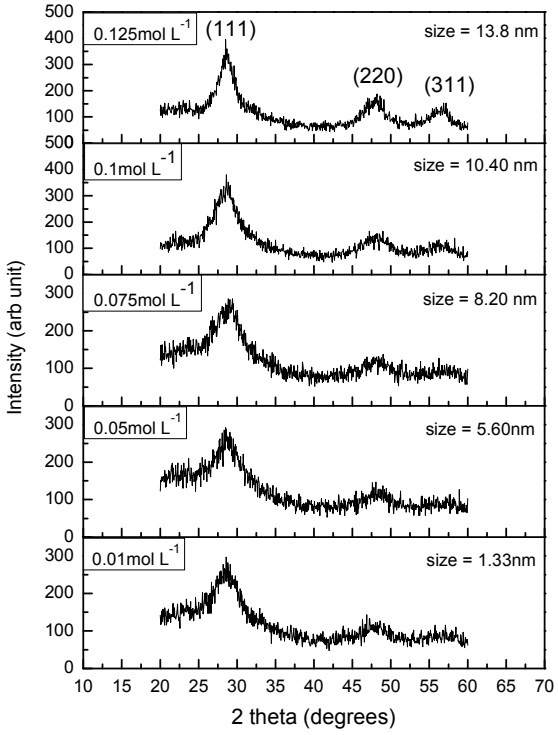

Figure 7.1 XRD patterns of chitosan capped ZnS:Mn for various concentrations (0.125 to 0.01mol L^{-1}) of sodium sulphide

The grain size is found to decrease with decrease in sodium sulphide concentration. The peaks get broadened as the size decreases and the extent of broadening is used to calculate the average size of the particles. The decrease in precursor concentration from 0.125to 0.01mol $L^{-1}$is accompanied by a decrease in average particle size from 13.8 to 1.33 nm (Table 7.1).

7.4.2 Transmission electron microscope (TEM) studies

The morphological analysis was carried out using Transmission Electron Microscopy (TEM) studies on chitosan capped ZnS:Mn sample synthesized for a stochiometric concentration 0.1mol L^{-1} of sodium sulphide and the TEM image is shown in figure 7. 2 (a). The TEM image reveals that

the particles are polycrystalline and have an average crystallite size of approximately 10 nm. The Energy Dispersive X-ray Spectroscopy (EDXS) diagram of the sample is shown in figure 7.2 (b), which provides the elemental composition of the sample. The presence of zinc, sulphur and manganese besides that of carbon and oxygen confirms the formation of chitosan capped ZnS:Mn nanocrystals in the powder sample.

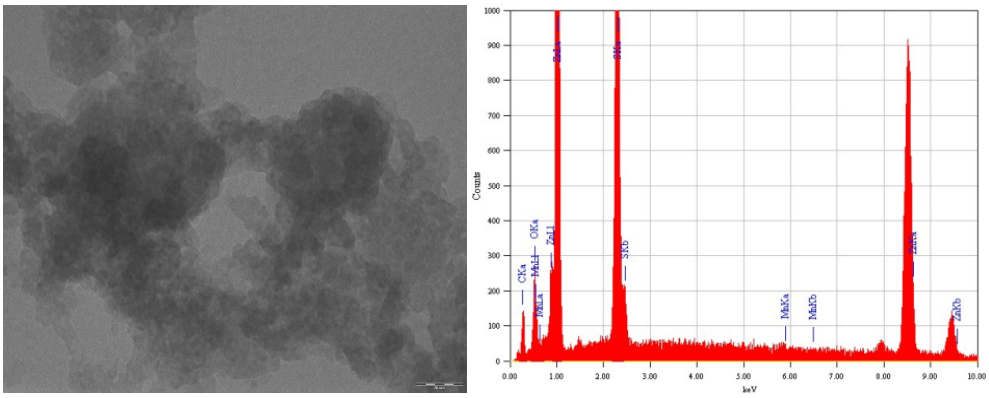

(a) (b)

Figure 7.2 (a) TEM image [scale bar: 20 nm] and (b) EDX spectrum of chitosan capped ZnS:Mn, synthesized for 0.1mol L^{-1} concentration of sodium sulphide

7.4.3 UV-Visible absorption spectra

The UV-Visible absorption spectra of Mn doped ZnS capped with chitosan for various molar concentrations of sodium sulphide from 0.125 to 0.01mol L^{-1} were recorded and the spectra are shown in figure 7.3. With the decrease in particle size of ZnS:Mn nanocrystals, the excitonic peak is found to be blue shifted from 327 to 294 nm as given in Table 7.1, which can be attributed to the confinement effects [24]. The extent of confinement in a low dimensional structure is judged by the value of the exciton Bohr radius. Quantum confinement effects arise as soon as the dimension of a nanocrystal

becomes comparable to the Bohr radius (2.5 nm), leading to significant changes in the electronic and optical properties.

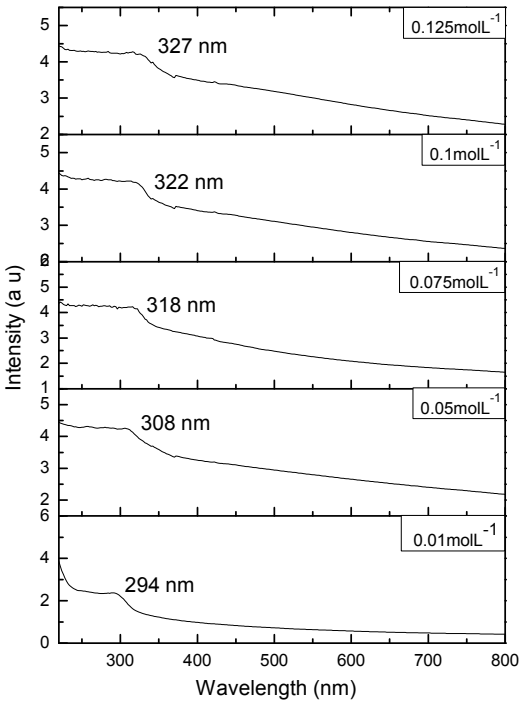

Figure 7.3 Absorption spectra of chitosan capped ZnS:Mn nanoparticles with molar concentrations of sodium sulphide from 0.125 to 0.01mol L^{-1}

Table 7.1 Spectral characteristics of chitosan capped ZnS:Mn nanocrystals

Sodium sulphide concentration (mol L^{-1})	Particle size (nm)	Excitonic peak (nm)
0.010	1.33	294
0.050	5.60	308
0.075	8.20	318
0.100	10.4	322
0.125	13.8	327

7.4.4 Photoluminescence (PL) emission spectra

Photoluminescence (PL) emission spectra of chitosan capped ZnS:Mn nanoparticles , for various molar concentrations of sodium sulphide were recorded at room temperature and the spectra are shown in figure 7.4. In general, the PL emission spectrum of ZnS:Mn shows a broad, orange emission peak around 597 nm. In the present work, under an excitation wavelength of 330 nm, similar peaks are observed in the PL spectra of ZnS:Mn which confirms the incorporation of manganese ions within the Zn S nanocrystals [25]. In the PL spectra shown in figure 7.4, the small broad peaks observed at about 420 nm can be due to defect states arising from zinc vacancies in the ZnS crystal lattice. The stochiometric concentration of sodium sulphide is 0.1 mol L^{-1}, corresponding to which the intensity of orange emission is high and that of the defect related emission at 420 nm is low. Hence the chitosan capped ZnS:Mn nanoparticles with sodium sulphide concentration of 0.1mol L^{-1} is used for the protein immobilization studies.

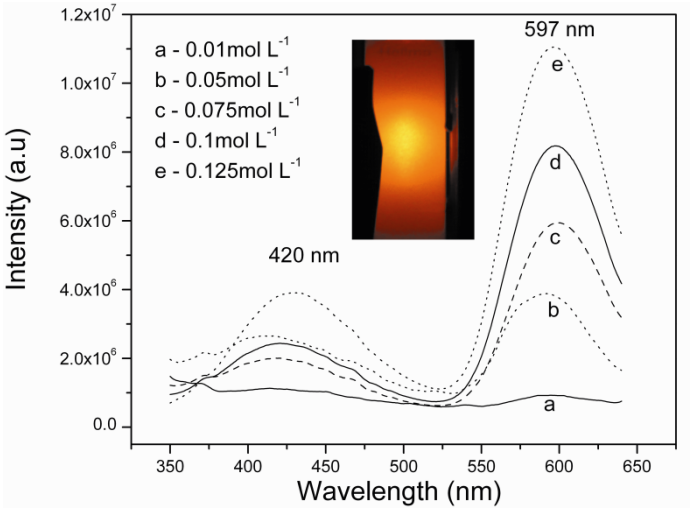

Figure 7.4 PL spectra of chitosan capped ZnS:Mn nanoparticles with sodium sulphide concentrations varying from 0.125 to 0.01mol L^{-1}

The PL emission spectra of chitosan capped ZnS:Mn (synthesized using 0.1mol L^{-1} concentration of sodium sulphide), free trypsin and trypsin immobilized on chitosan capped ZnS:Mn, are shown in figure 7.5. The orange red emission from chitosan capped ZnS:Mn at 597 nm can be observed in figure 7.5(a). Free trypsin shows an emission peak at 341 nm [figure 7.5(b)] which gets shifted to 418 nm [figure 7.5(c)] after cross-linking with chitosan capped ZnS:Mn. The observed shift in the PL spectrum of immobilized trypsin confirms the cross-linking of trypsin with the nanoparticles.

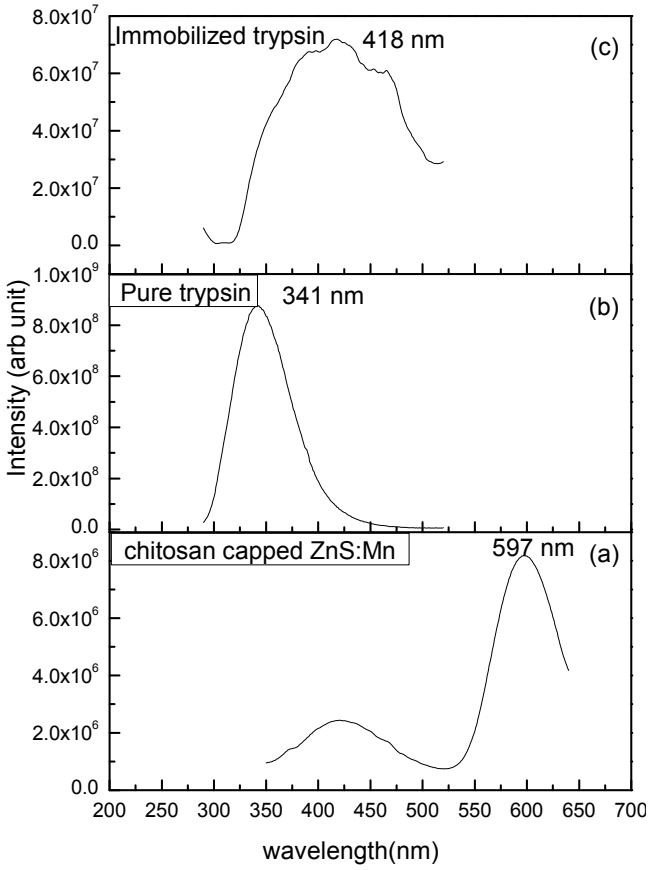

Figure 7.5 PL spectra of (a) chitosan capped ZnS:Mn, (b) pure trypsin and (c) immobilized trypsin

Photographs of emissions observed from (A) immobilized trypsin, (B) chitosan capped ZnS:Mn nanoparticles for 0.1mol L^{-1}concentration of sodium sulphide and (C) pure trypsin, when exposed to UV radiation are shown in figure 7.6.

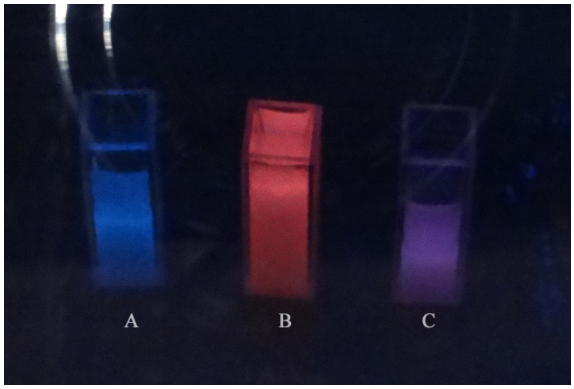

Figure 7.6 Emission observed from (A) immobilized trypsin, (B) chitosan capped ZnS:Mn and (C) pure trypsin

7.4.5 Fourier transform infrared (FT-IR) spectral studies

The FT-IR spectra of (a) chitosan capped ZnS:Mn nanocrystals, (b) pure trypsin and (c) trypsin immobilized onto chitosan capped ZnS:Mn nanocrystals are shown in figure 7.7. The major peaks observed at 656 cm^{-1}, 1008 cm^{-1} and 1400 cm^{-1}in figure 7.7(a) are attributed to the characteristic vibrations of ZnS:Mn sample. The strong peak observed at 1560 cm^{-1} and the weak one at 656 cm^{-1} are indicative of the presence of attached amine groups onto the nanoparticles [26]. The spectrum confirms the attachment of chitosan onto ZnS:Mn nanoparticles. The characteristic peak of trypsin is observed at 1644 cm^{-1} as shown in figure 7.7(b). Characteristic peaks of trypsin and chitosan capped ZnS:Mn nanoparticles can be observed in figure 7.7(c) with a shift towards shorter wavelength region, which is due to the strong van der Waals interaction of the dense assembly of trypsin on the surfaces of

nanoparticles. This result indicates that trypsin has been adsorbed on the surfaces of chitosan capped ZnS:Mn nanoparticles [27-31].

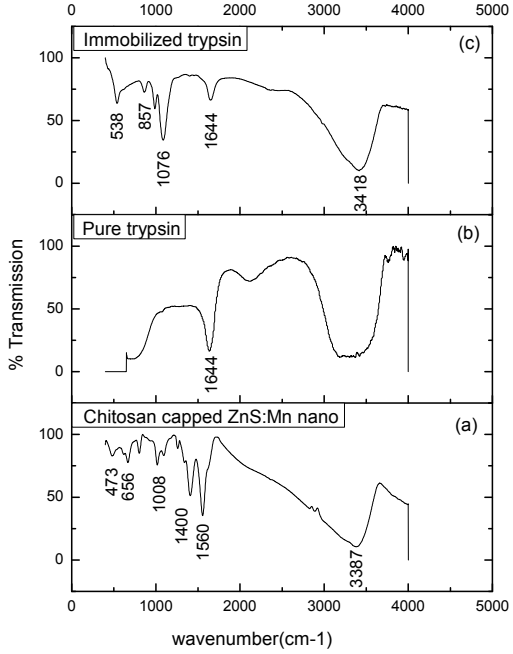

Figure 7.7 FT-IR spectra of (a) chitosan capped ZnS:Mn, (a) pure trypsin and (c) immobilized trypsin

7.5 Activity assessment of trypsin and immobilized trypsin

Activity of trypsin and trypsin immobilized with ZnS:Mn nano particles was assessed using BAPNA as substrate (Shimadzu UV-Vis spectrophotometer). Activity of trypsin immobilized on nano particle surface was found to be 1.9 units, which is higher compared to that of unimmobilized trypsin 1.37 units. Bar diagram showing the activity of trypsin and immobilized trypsin is depicted in figure 7.8. The increase in the activity of the immobilized trypsin compared to that of pure trypsin suggests that the trypsin has now become stable and more active due to immobiliazation with the nanoparticles.

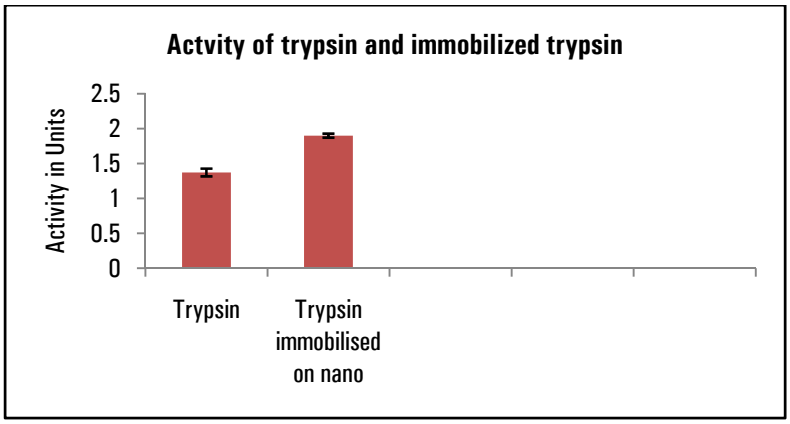

Figure 7.8 Bar diagram showing the activity of trypsin and immobilized trypsin

7.6 Conclusions

The chitosan capped ZnS:Mn nanocrystals were synthesized by chemical capping co-precipitation method at room temperature, which is a reproducible and comparatively simple method. It allows control on the size of the particles through variations in precursor concentration. The synthesized nanoparticles were structurally characterized by XRD, TEM, and EDXS. They were characterized for their optical properties by UV/Vis absorption and PL emission spectroscopic techniques.

The PL spectra show intense orange red emission around 597 nm and the intensity of emission is found to increase with increase in sodium sulphide concentration. The stoichiometric sodium sulphide concentration of 0.1mol L^{-1} is found to be the optimum precursor concentration to achieve the best PL emission characteristics. These chitosan capped, water-dispersible ZnS:Mn semiconductor nanocrystals can be attached to many biomolecules including DNA, RNA, and proteins so that they can be used for a variety of biomedical applications.

As an application, trypsin was immobilized on the surfaces of chitosan capped ZnS:Mn of average size 10 nm, using glutaraldehyde. The immobilization was confirmed by the shift in the photoluminescence (PL) emission spectra and FT-IR spectroscopic analysis. Trypsin activity was measured before and after cross linking and it has been observed that the immobilized trypsin shows increase in its activity compared to free trypsin. The potential of immobilized trypsin in therapeutic applications has to be explored in detail.

References

[1] NandananErathodiyil, Jackie Y. Ying, *Acc. Chem. Res*. 44 (2011) 925–935

[2] A. Vila, A. Sanchez, M. Tobıo, P. Calvo, M.J. Alonso, *J. Controlled Release* 78 (2002) 15 –24

[3] Givanildo Bezerra Oliveira, Jose ´ Luiz Lima Filho, Maria Elizabeth Cavalcante Chaves ,Walter Mendes Azevedo, Luiz Bezerra Carvalho Jr., *React. Funct. Polym*. 68 (2008) 27–32

[4] J. Felipe Diaz, Kenneth J. Balkus Jr, *J. Mol. Catal. B: Enzym*. 2 (1996) 115 -126

[5] M.J. Alonso, Nanoparticulate drug carrier technology, In: S.Cohen, H. Bernstein (Eds.), New York, (1996) 203–242

[6] Pooja M. Tiwari, KomalVig, Vida A. Dennis , Shree R. Singh, *Nanomaterials* 1 (2011) 31-63

[7] R.S. Juang, F.C. Wu, R.L. Tseng, *Adv. Environ. Res.* 6 (2002) 171-177

[8] Li-Ming Zhao, Lu-E Shi, Zhi-Liang Zhang, Jian-Min Chen, Dong-Dong Shi, Jie Yang, et al. *Braz. J. Chem. Eng*.28 (2011) 353 – 362

[9] G.F. Payne, W.Q. Sun, *Appl. EnViron. Microbiol*. 60 (1994) 397-401

[10] Z. Li, R. Jin, C.A. Mirkin, R.L. Letsinger, *Nucleic Acids Res*.30 (2002) 1558

[11] A.P. Alivisatos, *Nature*, 382 (1996) 609

[12] X. Gao, W.C.W. Chan, S. Nie, *Science* 281(1998) 2016

[13] S.R. Whaley, D.S. English, E.L. Hu, P.F. Barbara, A.M. Belcher, *Nature* 405 (2000) 665

[14] AswathyJayasree, SajithSasidharan, ManzoorKoyakutty, Shantikumar Nair, DeepthyMenon, *Carbohydrate Polymers* 85 (2011) 37-43

[15] Mathew, M. E., Mohan, J. C., Manzoor, K., Nair, S. V., Tamura, H., &Jayakumar, R. *Carbohydrate Polymers*, 80 (2010) 443-449

[16] Sharma Manoj, Singh Sukhvir, O. P Pandey, *Journal of Applied Physics,* 107 (2010) 104319-104319-8

[17] S. Baruah, H. C. Warad, A. Chindaduang, G. Tumcharern, and J. Dutta *Journal of Bionanoscience* 2 (2008) 1–7

[18] YuhoNajimaetal, *J. Biol. Chem*. 280 (2005) 27523-27532

[19] R.N. Bhargava, D.Gallangher, *Phys.Rev.Lett*. 72 (1994) 416

[20] R.N. Bhargava, D. Gallagher, X. Hong, and A. Nurmikko, *Phys. Rev. Lett*. 72 (1994) 416–419

[21] H.C. Warad, S.C. Ghosh, B. Hemtanona, C. Thanachayanontb, J. Dutta, *Sci. Technol. Adv.Mater* 6 (2005) 296–301

[22] M.L. Kakade, J. J. Rackis, J.E. McGhee, G. Puski, *Cereal chem*. 51 (1974) 376-382

[23] M.A. Abdel Naby, S.I. Abdel-Mohsen, A.M. Abdel-Fattah, A.F. Abdel-Fattah, *Process Biochem.* 34 (1999) 391-398

[24] DebasisBera, Lei Qian, Teng-Kuan Tseng, Paul H. Holloway, *Materials* 3 (2010) 2260-2345

[25] R. Kripal, A. Kumar Gupta, *ChalcogenideLett*. 7 (2010) 203 – 209

[26] S. Baruah, H.C. Warad, A. Chindaduang, G. Tumcharern, J. Dutta, *Journal of Bionanoscience*2 (2008) 1–7

[27] Linmei Li and JianWeng, *Nanotechnology* 21 (2010) 305603

[28] HuiminBao, Qiwen Chen, Luyan Zhang and Gang Chen* *Analyst* 136 (2011) 5190

[29] J.L. Luque-Garcia, G. Zhou, D.S. Spellman, T.T. Sun, T.A.Neubert, *Mol. Cell. Proteomics* 7 (2008) 308−314.

[30] Y. Lin,Y. Li, Y. Liu, W.J. Han, Q.Z. He, J.L. Li, P. Chen, X.C. Wang, S.P. Liang, *Electrophoresis* 30 (2009) 3626−3635

[31] S. Bornemann, B. Rietschel, S. Baltruschat, M. Karas, B. Meyer, *Electrophoresis* 31 (2010) 585−592

Chapter 8

L-CITRULLINE CAPPED, LUMINESCENT ZnS:Mn FOR RAPID SCREENING OF *LYSINIBACILLUS FUSIFORMIS* BACTERIA

Contents

This chapter illustrates the work on bio-compatible and highly luminescent manganese doped zinc sulphide (ZnS:Mn) nanocrystals of average particle size 10 nm, synthesized by capping with the aminoacid ligand, L-citrulline. The study is focussed on the detection of a special type of metal accumulating bacteria, Lysinibacillus fusiformis. This bacterium has significant applications in the disposal of metal components from industrial effluents. In this context, the detection of this bacterium is quite important and the present work demonstrates a novel technique for this bacterial detection. The synthesized nanocrystals were attached to Lysinibacillus fusiformis and characteristics of the bioconjugated system were studied by UV-Visible absorption and photoluminescence (PL) spectroscopy. The study of relative growth of Lysinibacillus fusiformis in the presence of L-citrulline capped ZnS:Mn, proves the bio-compatible nature of these nanocrystals and their tunable colour properties under different excitation wavelengths, make them ideal for bio-labeling applications.

M. Sajimol Augustine et al.

Journal of Biological and Chemical Luminescence (accepted)

"Highly luminescent and bio-compatible, L-citrulline capped ZnS:Mn nanocrystals for rapid screening of metal accumulating *Lysinibacillus fusiformis* bacteria"

8.1 Introduction

Water-dispersible nanometer sized fluorescent semiconductor materials, used as bio-labels have attracted considerable attention in recent years, due to their unique physical, chemical and optical properties [1–5]. Compared to common organic dyes, nanometer-sized fluorescent materials are more stable with high luminescent intensity, low photobleaching effects and large Stokes'shift [2]. Water dispersible semiconductor nanocrystals have been developed for fluorescent labeling technologies, especially to be applied in biomedical area [6, 7]. More recently, amino acid ligands have been developed as surface capping agents for semiconductor nanocrystals. They are found to be very effective capping ligands in the synthesis of semiconductor nanocrystals with controllable size distribution.

Zinc Sulphide (ZnS) is a semi-conducting luminescent material, which has a wideband gap of 3.70 eV [8, 9]. Luminescent, semi-conducting nanophosphors have received much attention, particularly for their life time shortening and enhanced emission efficiencies [10, 11]. Manganese doped zinc sulphide (ZnS:Mn) is a favorable phosphor which exhibits excellent optical properties such as high luminescence intensity, narrow emission bands etc [12–16]. Modification of the surface of these nanocrystals by suitable capping agents such as aminoacid ligands makes these nanocrystals bio-compatible. This orange light emitting, manganese ion doped nanocrystallite, is of special interest due to its high photoluminescence efficiency and stability at ambient temperatures, which are critical properties required for commercial bio-imaging applications.

The synthesis and optical characterization of ZnS:Mn nanocrystals capped with aminoacid ligands such as L-valine, L-cysteine , L-histidine, L-arginine, methionine etc have already been reported earlier [17-19]. The present work is aimed at synthesizing ZnS:Mn nanocrystals, using the aminoacid ligand, L-citrulline, which is a novel and effective capping material for the synthesis of bio-compatible semiconductor nanocrystals. Since ZnS is a toxic material, capping with aminoacids make these nanocrystals more bio-compatible and less toxic. The presence of reactive amine and –OH groups in the aminoacid makes them bio-compatible and hence good candidates for biological applications.

Heavy metals constitute a major hazard for the human health and ecosystem [20]. Some metals including iron, zinc, copper and manganese are micronutrients used in the redox processes, regulation of osmotic pressure, enzyme cofactors and are also important in the maintenance of the protein structure [21]. Even essential metals such as zinc and copper are toxic at high concentration levels. Among the different techniques employed for metal removal from multi elemental systems, biosorption has been found to be highly selective [22]. Furthermore, metal accumulating bacteria can be used to remove, concentrate and recover metals from industrial wastes [23, 24]. This could be generally explained by the fact that the negatively charged groups (carboxyl, hydroxyl and phosophryl) of bacterial cell wall absorb metal cations through various mechanisms such as electrostatic interaction, van der Waals forces, covalent bonding or combination of such processes [25]. Due to the metal uptaking ability of *Lysinibacillus fusiformis,* it can be used for the removal of metals like zinc, boron etc. Hence the detection of this bacterium is an important, interdisciplinary research field. Out of the various possible

detection techniques, a novel technique using bio-compatible and highly luminescent L-citrulline capped ZnS:Mn nanocrystals have been used in the present work, for detecting *Lysinibacillus fusiformis* bacteria.

8.2 Experimental Details

8.2.1 Synthesis of L-citrulline capped ZnS:Mn nanoparticles

In the present work, L-citrulline capped manganese doped zinc sulphide nanoparticles were sythesized by a simple and cost effective wet chemical co-precipitation method[26]. The chemicals used were, Zn $(CH_3COO)_2.2H_2O$ (Merck Specialities Private Limited, Mumbai, >98%), $Mn(CH_3COO)_2.4H_2O$ (Merck Specialities Private Limited, Mumbai, >99.5%), $Na_2S.9H_2O$ (Merck Specialities Private Limited, Mumbai, 98%), and L- citrulline ($C_6H_{13}N_3O_2$) (Loba Chemie Private Limited, Mumbai, 99%). In a typical experiment, 0.1 mol L^{-1} zinc acetate, 0.01mol L^{-1} manganese acetate and 0.025mol L^{-1}citrulline were mixed in 50 ml of water to which 0.1mol L^{-1} aqueous solution of sodium sulphide was added dropwise to form L-citrulline capped ZnS:Mn nanoparticles. The mixture was kept under constant stirring for one and a half hour and then filtered and dried in an oven at 40^0C. The powder so obtained was used for further detailed studies.

8.2.2 Bioconjugation of L-citrulline capped ZnS:Mn with *Lysinibacillus fusiformis* bacteria

Log phase cells of *Lysinibacillus fusiformis* bacteria were grown in 10 ml of nutrient broth in an orbital shaker at 37^0C and 120 rpm for 24 hrs in the presence of 2.5% (v/v) of L-citrulline capped ZnS:Mn nanoparticles. The cells were centrifuged at1000 rpm to remove the traces of nanoparticles in the

medium and then the supernatant was taken and the process was repeated twice. The cells were washed in saline by centrifugation at 10000 rpm. Pure *Lysinibacillus fusiformis bacteria* (Control) were also grown in the absence of nanoparticles. *Lysinibacillus fusiformis* bacteria were grown in the presence of different concentrations of L-citrulline capped ZnS:Mn (2.5%, 5%, 7.5%, 10%; v/v) in10 ml nutrient broth and incubated at 37^{o}C in a rotary shaker. All the experiments were conducted in triplicates.

8.3 Sample Characterization

The X-ray powder diffraction (XRD) pattern of the L-citrulline capped ZnS:Mn nanoparticles was recorded on a Rigaku X-ray diffractometer with CuKα radiation (1.5418 Å) operating at 30 kV and 20 mA. Scanning was carried out in the 2θ range from 20^{o} - 60^{o} at a scan speed of 2^{o} per minute. Transmission electron microscope (TEM) image of the synthesized nanocrystals was taken in order to estimate the particle size. Fourier transform infrared (FT-IR) spectra of the samples were obtained with AVTAR 370 DTGS FTIR spectrophotometer in the wave number range 400–4000 cm^{-1}. UV-Visible spectra in transmission mode were recorded on a Jasco-V 500 spectrophotometer in the wavelength range 200-700 nm. The PL emission spectra of the samples were obtained with Fluoromax-3 Spectrofluorimeter using Xe lamp as excitation source. Fluorescence Microscope (Olympus BX 51) provided with a CCD camera and 40X and 100X objectives was used for observing fluorescence emission.

8.4 Results and Discussion

8.4.1 X-ray powder diffraction (XRD) studies

The XRD patterns of the uncapped ZnS:Mn nanoparticles and L-citrulline capped ZnS:Mn nanoparticles synthesized by chemical co-precipitation method are shown in figure 8.1 (a) and (b). The samples have cubic crystal structure and the diffraction data are in agreement with the JCPDS data for ZnS (JCPDS card No.050566). The spectra show three main peaks corresponding to reflections from the (111), (220) and (311) planes which suggest zinc blende crystal structure. The major peaks in the XRD pattern of L-citrulline capped ZnS:Mn nanoparticles are found to be broadened due to decrease in particle size upon capping. The particle size is determined from the full width at half maximum (FWHM) of the diffraction peaks, using Debye- Scherrer formula

$$d = 0.9\lambda/\beta \cos\theta \qquad (1)$$

where d, λ, β and θ are the average particle size, the wavelength of the X-rays, full width at half maximum intensity expressed in radians and diffraction angle respectively. The average crystallite size of the uncapped ZnS:Mn nanoparticles and L-citrulline capped ZnS:Mn nanoparticles calculated from the diffraction peaks is around 4.6 nm and 2 nm respectively.

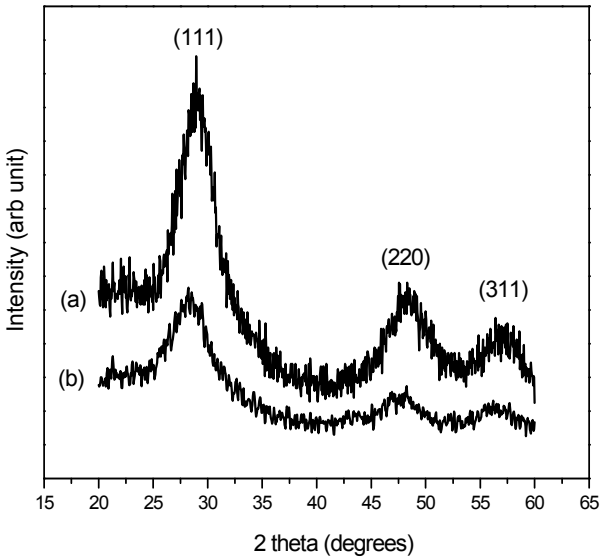

Figure 8.1 XRD patterns of (a) uncapped ZnS:Mn nanoparticles and (b) L-citrulline capped ZnS:Mn nanoparticles

8.4.2 Energy dispersive X-ray spectrum (EDXS) analysis

The energy dispersive X-ray spectrum (EDXS) of the synthesized manganese doped ZnS nanoparticles capped with L-citrulline is shown in figure 8.2, which provides the elemental composition of the sample. The presence of zinc, sulphur and manganese can be confirmed besides that of carbon and oxygen in the powder sample. The diagram confirms the formation of the ZnS:Mn nanocrystals in solid state, capped with L-citrulline. The L-citrulline capping is confirmed from the presence of carbon and oxygen in the EDX spectrum.

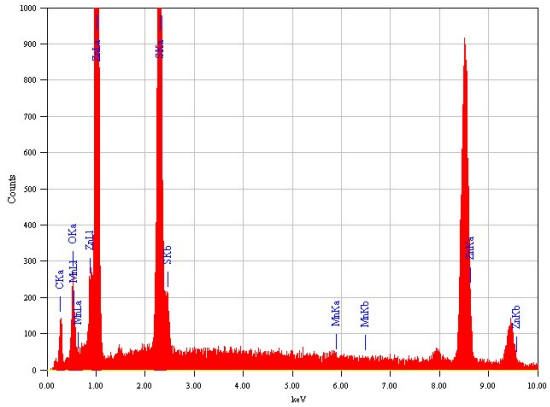

Figure 8.2 EDX Spectrum of ZnS:Mn nanoparticles capped with L- citrulline

8.4.3 Transmission electron microscope (TEM) studies

Transmission electron microscope (TEM) image of the synthesized nanocrystals was taken in order to estimate the particle size and is shown in figures 8.3. The TEM image reveals that the particles have an average crystallite size of approximately 10 nm. The average particle size obtained from TEM analysis is found to be slightly bigger than that determined from the XRD peaks using the Debye-Scherrer formula due to some extent of agglomeration.

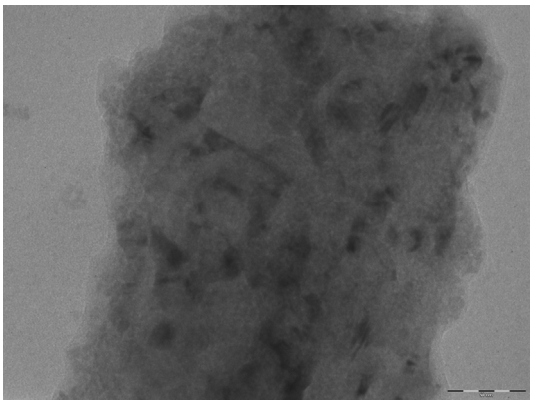

Figure 8.3 TEM image (scale bar:50 nm) of L-citrulline capped ZnS:Mn nanoparticles

8.4.4 Fourier transform infrared (FT-IR) spectral studies

The FT-IR spectrum of manganese doped ZnS nanocrystals is shown in figure 8.4. The peak at 3430 cm^{-1} is assigned to O-H stretching vibration and the peak at 1625 cm^{-1} corresponds to O-H bending . The sharp peaks observed at 2080 and 2929 cm^{-1} are due to the presence of carbon which is an instrumental error. The band centered at 1415 cm^{-1} is attributed to the stretching vibration of C=C group in the acetate species used to synthesize ZnS. The band at 1250 cm^{-1} is due to the characteristic frequency of the dopant manganese ions. The peak observed at1041 cm^{-1} indicates the presence of resonance interaction between vibrational modes of sulphide ions in the crystal. The peak at 668 cm^{-1} is assigned to the Zn-S vibrational modes.

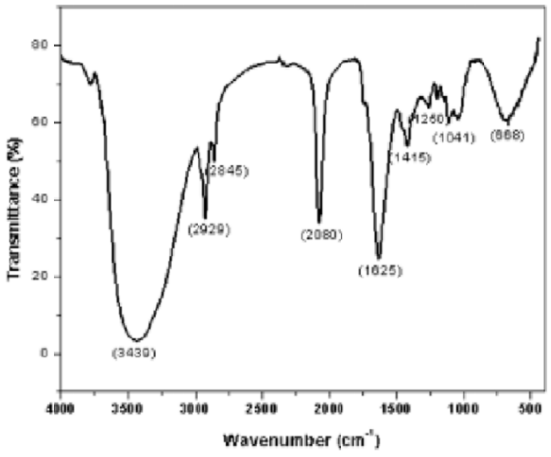

Figure 8.4 FT-IR spectrum of manganese doped ZnS nanocrystals

The FT-IR spectra of (a) *Lysinibacillus fusiformis*, (b) L-citrulline capped ZnS:Mn nanocrystals and (c) *Lysinibacillus fusiformis* attached to L-citrulline capped ZnS:Mn nanocrystals are shown in figure 8.5. The spectrum of *Lysinibacillus fusiformis* [figure 8.5 (a)] shows typical absorption

bands for carbohydrates (a broad OOH elongation band in the 3,145 to 3,620 cm^{-1} range and band at 1,075 cm^{-1} assigned to COO elongation), as well as bands characteristic of proteins (elongation of amide at 1,653 cm^{-1} and bending NOH amide band at 1,550 cm^{-1}) [27, 28]. The major peaks appearing at 662 cm^{-1}, 1014 cm^{-1} and 1400 cm^{-1} in figure 8.5 (b) are attributed to the characteristic vibrations of the ZnS:Mn sample. The strong peaks appearing around 3385 cm-1 and 1563 cm^{-1} are assigned to zinc coordinated -NH_2 and –COO groups of the aminoacid [29, 30]. However, the peak appearing around 3385 cm^{-1} overlaps with that for C-H stretching in the aminoacid molecule [31, 32]. The spectral data provides the confirmation that the aminoacid ligands are attached onto the surface of the ZnS:Mn nanocrystals to provide a water dispersible nature for ZnS:Mn nanocrystals. On comparing the IR spectrum of ZnS:Mn shown in figure 8.4 with that of aminoacid capped ZnS:Mn shown in figure 8.5, it is observed that the vibrational bands corresponding to both ZnS:Mn and the aminoacid, L-citrulline are present in figure 8.5(b), whereas the vibrational bands of only ZnS:Mn are seen in figure 8.4. Characteristic peak of *Lysinibacillus fusiformis* and peaks corresponding to L-citrulline capped ZnS:Mn nanoparticles can be observed in figure 8.5(c). This indicates that *Lysinibacillus fusiformis* has been adsorbed onto the surface of L-citrulline capped ZnS:Mn nanoparticles.

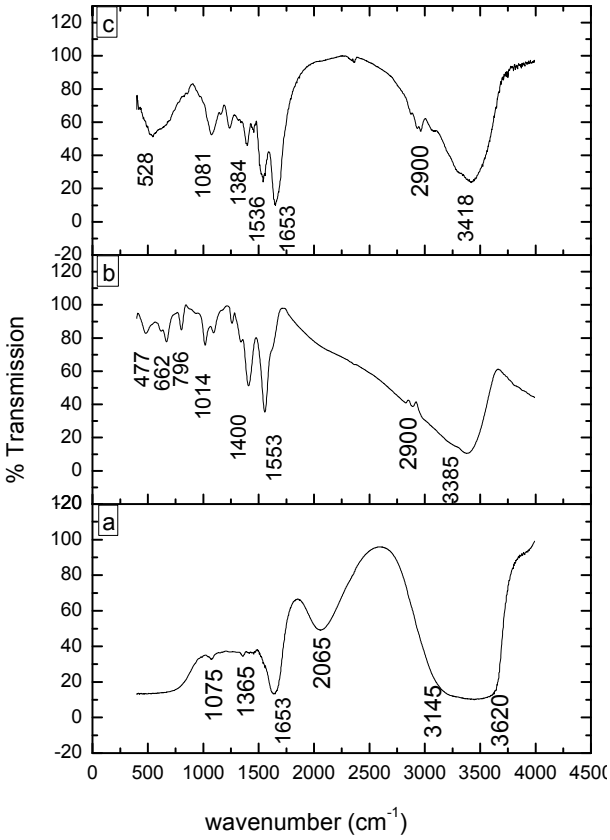

Figure 8.5 FT-IR spectra of (a) *Lysinibacillus fusiformis,* (b) L-citrulline capped ZnS:Mn nanocrystals and (c) *Lysinibacillus fusiformis* attached with L-citrulline capped ZnS:Mn nanocrystals.

8.4.5 UV-Visible absorption spectra

The UV-Visible absorption spectra of *Lysinibacillus fusiformis*, L-citrulline capped ZnS:Mn attached *Lysinibacillus fusiformis* and L-citrulline capped ZnS:Mn nanoparticles are shown in figures 8.6 (a), (b), and (c) respectively. The values of absorption edge corresponding to *Lysinibacillus fusiformis* sample, L-citrulline capped ZnS:Mn nanoparticles and L-citrulline capped ZnS:Mn attached *Lysinibacillus fusiformis* sample are 418nm, 542 nm and 475 nm respectively. These values are calculated by extrapolating the

linear portion of the corresponding absorption spectrum to the X-axis (wavelength axis). A blue shift of 67 nm is observed for the absorption edge of the L-citrulline capped ZnS:Mn attached *Lysinibacillus fusiformis* sample compared to L-citrulline capped ZnS:Mn.

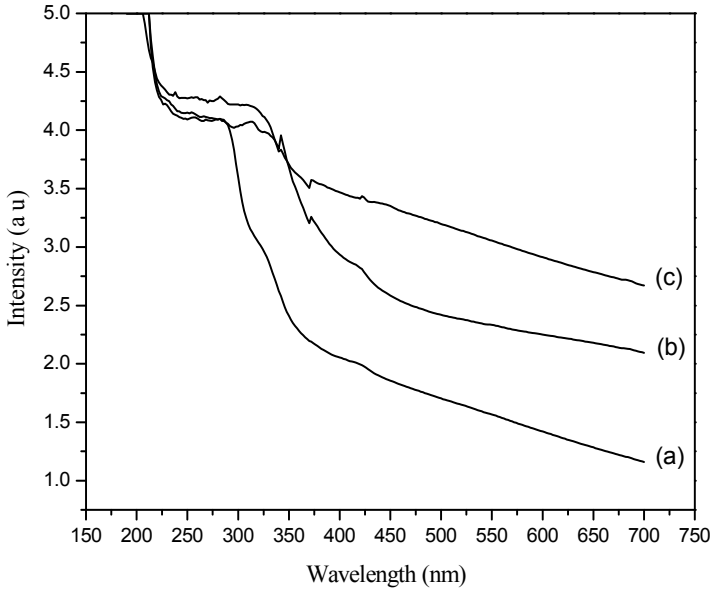

Figure 8.6 Absorption spectra of (a) *Lysinibacillus fusiformis* bacteria, (b) L-citrulline capped ZnS:Mn nanoparticles attached *Lysinibacillus fusiformis* bacteria and (c) L-citrulline capped ZnS:Mn nanoparticles

8.4.6 Photoluminescence (PL) emission spectra

Photoluminescence (PL) emission spectra of samples prepared in water were recorded at room temperature. The PL spectra of Mn doped ZnS nanocolloid capped with L-citrulline for various manganese concentrations (0.5%,1%,5%,10% and 20%) show broad, orange emission peaks at around 598 nm as depicted in figure 8.7. The small broad peaks observed at 420 nm can be due to defect states arising from zinc ion vacancy in the ZnS crystal lattice and the intensity of these peaks is found to be decreased with increasing

manganese concentration. The PL intensity at 598 nm gradually increases with manganese concentration and the maximum intensity is observed for 20% manganese doping. Since there is not much difference in emission intensity between 10% and 20% manganese concentrations, ZnS:Mn nanocrystals with a manganese concentration of 10% is used for further studies.

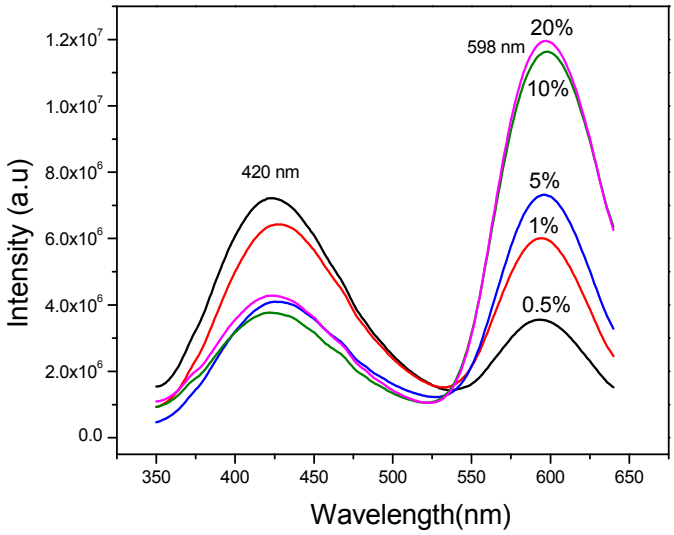

Figure 8.7 PL spectra of nanocolloids of L-citrulline capped ZnS:Mn for various manganese concentrations

The PL emission spectra obtained from L-citrulline capped ZnS:Mn nanoparticles, *Lysinibacillus fusiformis* bacteria and L-citrulline capped ZnS:Mn nanoparticles attached *Lysinibacillus fusiformis* bacteria are shown in figure 8.8. The photoluminescence spectrum of *Lysinibacillus fusiformis* bacteria shows an emission peak at 316 nm. A blue shift of 214 nm from 598 nm to 384 nm has been observed for the PL emission peak of the ZnS:Mn attached *Lysinibacillus* sample compared to L-citrulline capped ZnS:Mn nanoparticles. This distinct blue shift is a confirmed indication of the attachment of *Lysinibacillus* bacteria with the L-citrulline capped ZnS:Mn nanoparticles.

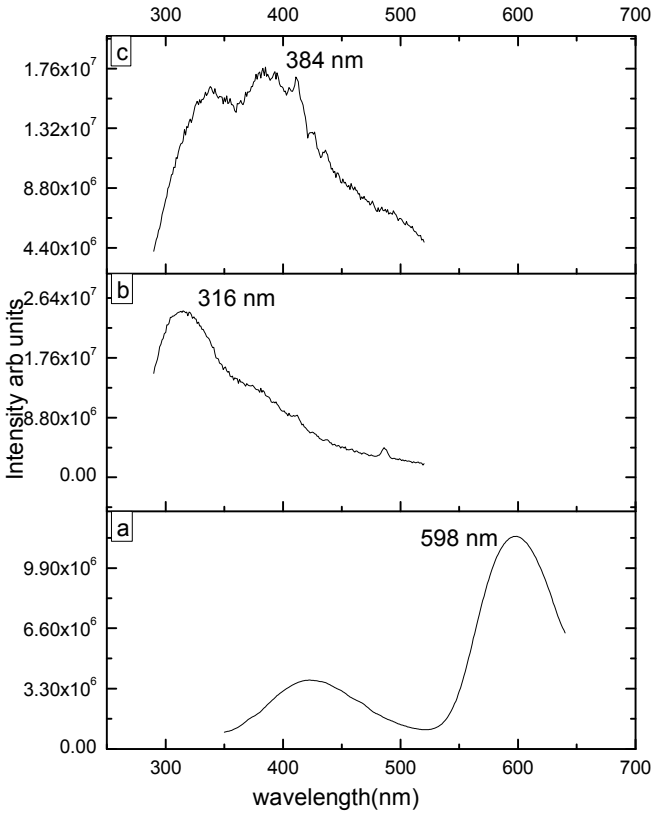

Figure 8.8 PL spectra of (a) L-citrulline capped ZnS:Mn nanoparticles, (b) *Lysinibacillus fusiformis* and (c) L-citrulline capped ZnS:Mn nanoparticles attached *Lysinibacillus fusiformis*

The luminescence emission observed from (a) L-citrulline capped ZnS:Mn nanoparticlesand (b) *Lysinibacillus fusiformis* bacteria attached to L-citrulline capped ZnS:Mn,when exposed to UV radiation are shown in figure 8.9. The emission from L-citrulline capped ZnS:Mn nanocolloid displays bright orange fluorescence whereas the emission observed from the bioconjugated system depicts blue emission. The observed blue shift in the fluorescence emission further confirms the bioconjugation of the bacteria with the citrulline capped ZnS:Mn.

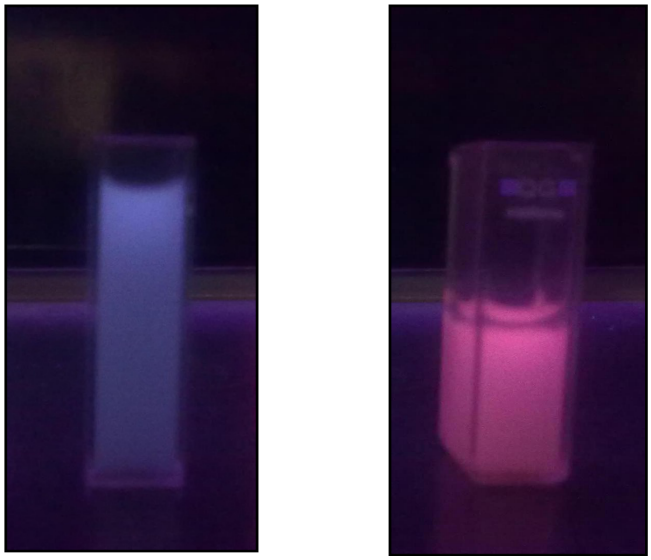

(a) (b)

Figure 8.9 Emission observed from (a) L-citrulline capped ZnS:Mn nanoparticles and (b) *Lysinibacillus fusiformis* bacteria attached to L-citrulline capped ZnS:Mn nanoparticles, when exposed to UV light

8.4.7 Fluorescent microscope images

For confirmation of attachment of *Lysinibacillus fusiformis* bacteria to L-citrulline capped ZnS:Mn nanoparticles, the samples have been observed with fluorescent microscope under both bright field and UV light as shown in figure 8.10. Bright field image of pure *Lysinibacillus fusiformis* bacteria (control) is shown in figure 8.10(a). The same sample is observed under UV light and no fluorescence is observed, which shows that *Lysinibacillus fusiformis* bacteria has no autofluorescence. The bacteria attached to L-citrulline capped ZnS:Mn nanoparticles were observed under fluorescent microscope with excitation wavelengths 365.4 nm (UV), 435.8 nm (blue) and 546.1 nm (green), and fluorescence emissions were obtained in yellow [figure 8.10 (b)], green [figure 8.10(c)], and red regions [figure 8.10(d)], respectively. One can thus confirm the attachment of *Lysinibacillus fusiformis* bacteria to

L-citrulline capped ZnS:Mn nanoparticles, which also demonstrates that different emission colours can be observed from the same sample as reported earlier [33], by changing the excitation wavelength.

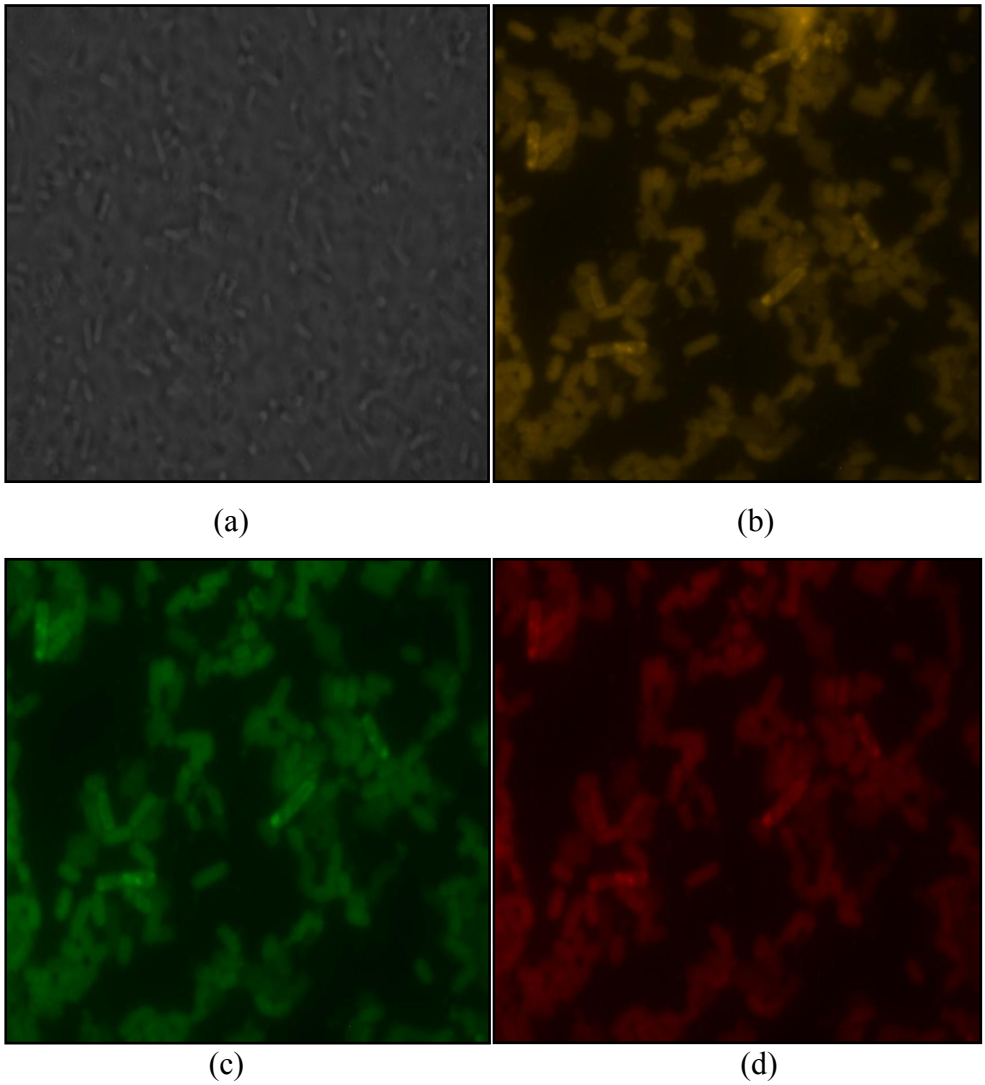

Figure 8.10 Fluorescent images of *Lysinibacillus fusiformis* bacteria attached to L-citrulline capped ZnS:Mn nanoparticles (a) bright field image, (b), (c) and (d) fluorescence images under different excitation wavelengths 365.4 nm, 435.8 nm and 546.1 nm (Magnification:100X)

8.5 Studies on relative growth of bacteria

The relative growth of bacteria was evaluated by adding different concentrations of L-citrulline capped ZnS:Mn nanocolloid into the nutrient broth in which log phase cells of the bacteria were added. The growth was monitored by finding Optical Density (OD) at 600 nm in a UV-visible spectrophotometer with uninoculated broth as control. Relative growth was expressed as the percentage of growth obtained in untreated control which was taken as 100% [34] and the details are depicted in Table 8.1. From the table it is evident that bacteria can grow even upto 10% (v/v) addition of L-citrulline capped ZnS:Mn. This shows the bio-compatible nature of ZnS:Mn nanoparticles capped with L-citrulline.

Table 8.1 Relative growth of bacteria for different concentrations of L-citrulline capped ZnS:Mn nanocolloid.

	Concentration of nanocolloid (v/v)	OD at 600nm (average value)	Relative growth
1	2.5%	1.8	100 %
2	5.0%	1.8	100 %
3	7.5%	1.79	99.4 %
4	10%	1.78	98.8 %
6	Control	1.8	100 %

8.6 Conclusions

Water dispersible and bio-compatible ZnS:Mn nanocrystals capped with a novel, aminoacid ligand, L-citrulline have been successfully synthesized using a simple chemical co-precipitation method. The synthesized nanocrystal powder was structurally characterized by XRD, TEM, EDXS and

FT-IR spectroscopic techniques. The optical properties of these nanocrystals were investigated by UV-Visible absorption and photoluminescence (PL) spectroscopy. The intense orange red emission observed at 598 nm offers prospects of applications of these bio-compatible nanocrystals in the fields of biosensing and bioimaging. The blue shift observed in the UV-Visible absorption and photoluminescence emission peaks shows that bacteria have been effectively attached to the L-citrulline capped ZnS:Mn nanoparticles. FT-IR spectra and fluorescent microscopic images provide further evidence for the attachment of bacteria with these nanoparticles. The study of relative growth of *Lysinibacillus fusiformis* in the presence of L-citrulline capped ZnS:Mn nanoparticles shows that even in the environment of 10% (v/v) of nanocolloid, there is no significant retardation in the growth of bacteria, which further confirms the bio-compatibility of these nanocrystals. L-citrulline capped ZnS:Mn nanoparticles can hence be used as efficient biosensors to mark the presence of the metal accumulting bacteria, *Lysinibacillus fusiformis.*

References

[1] M. Bruchez, M. Moronne, P. Gin, S. Weiss and A. P. Alivisatos, *Science*, 281 (1998) 2013

[2] W. C. W. Chan and S. Nie, *Science*, 281 (1998) 2016

[3] Milliron D.J, Alivisatos A.P, Pitois.C, Edder.C and Fréchet J.M, *J. Adv. Mate,*15 (2003) 58

[4] Brus L. E, *Appl. Phys.A*, 53 (1991) 465

[5] R. Elghanian, J. J Storhoff, R. C Mucic, R. L Letsinger and C.A Mirkin, *Science*, 277 (1997) 1078

[6] Gerion D, Pinaud F, Williams S. C, Parak W. J, Zanchet D, Weiss S and Alivisatos A. P, *J.Phys Chem.B*, 195 (2001) 8861

[7] Jun Y. W, Jang J. T and Cheon J. W, *Bull.Kor.Chem. Soc*.,27 (2006) 961

[8] D. Denzler, Mlschewski and K. Sattler, *J.Appl.Phys*., 84 (1998) 2841

[9] Zou B.S, Little R.B, Wang J.P and E.L-Sayed M.A, *Int .J. Quantum Chem*., 72 (1999) 439

[10] R.N Bhargava and D.Gallangher, *Phys.Rev.Lett*, 72 (1994) 416

[11] T .Igarashi, T. Isobe and M. Senna, *Phys.Rev.B*, 56 (1995) 6444

[12] W. Chen, R. Sammynaiken and Y. N. Huang, *J. Appl. Phys*., 88 (2000) 5188

[13] P.B Xie, W.P Zhang, M.Yin, H.T Chen, W.W Zhang, L.R Lou and S.D Xia, *J.Colloid Interface Sci.,* 229 (2000) 534

[14] W.Chen, R.Sammynaiken, Y.Huang, J.O Malm, R.Wallenberg, J.O Bovin, V.Zwiller and N.A Kotov, *J. Appl.Phys*,. 89 (2001) 1120

[15] M.F Bulanyi, Y.A Gulevskii and B.A Polezhaev, *Inorg.Mater*,. 36 (2000) 997

[16] A.D Dinsmore, D.S Hsu, S.B Qadri, J.O Cross, T.A Kennedy, H.F Gray and B.R Ratna, *J.Appl.Phys*., 88 (2000) 4985

[17] Cheong-Soo Hwang, Narae Lee, Young-Ah Kim, Youn Bong Park. *Bull. Korean Chem. Soc*. 27 (2006) 1809-1814

[18] Hoon Young Kong,Song-Yi Kim,Jonghoe Byun,Cheong-Soo Hwang. *B. Korean Chem. Soc.* 32 (2011) 53-58

[19] Lee JH, Kim YA, Kim K, Huh YD, Hyun JW, Kim HS, Noh SJ, Cheong-Soo H. *B. Korean Chem.Soc*. 28 (2007)1091

[20] Boopathy.R, *Bioresource Technology*, 74 (2000) 63-67

[21] Vallee B.L and Auld D.S, *Biochemistry*, 29 (1990) 5647-5659

[22] Knauer M.F, Kridel S.J, Hawley S.B and Knauer D.J, *J.Biol. Chem*,. 272 (1997)29039–29045

[23] Malekzadeh.F, Farazmand .A, Ghafourian.H, Shahamat.M, Levin.M and Colwell R.R, *J. Microbiol.Biotechnol*, 18(4) (2002) 295-302

[24] Chowdhury .S, Mishra .M, Adarsh V. K, Mukherje A, Thakur A. R and Chadhuri S. R, *American Journal of biochemistry and biotechnology*, 4 (2008) 255-264

[25] Chojnacka. K, Chojnacki .A and Gorecka .H, *Chemosphere,* 59 (2005) 75-84

[26] Nanda .J, Sapra .S, Sarma D. D, Chandrasekharan .N and Hodes. G, *Chem. Mater*.,12 (2000) 1018

[27] Fabienne François et al, *Applied and Environmental Microbiology*, 78 (2012)1097–1106

[28] Ulrike Jankowski, Mohamed L. Merroun, Sonja Selenska-Pobell and Karim Fahmy *Spectroscopy* 24 (2010) 177-181.

[29] Moszczenski C .W and Hooper R. J, *Inorg. Chim. Acta*, 70 (1983) 71

[30] Nakamoto. K, Infrared and Raman Spectra of Inorganic and Coordination Compounds Part B, 5th Ed, (1997) Wiley: p 59

[31] Pandiarajan.S, Umadevi.M, Rajaran R.K and Ramakrishinan.V, *J. Spectrochim. Acta A,* 62 (2005) 630

[32] Pawlukojic.A, Leciejewicz J, Ramirez-Cuesta and A. J Nowicka Sciebe, *J. Spectrochim. Acta A,* 61 (2005) 2474

[33] Manoj Sharma, Sukhvir Singh and O.P Pandey, *J. Appl. Phys*., 107 (2010) 104319

[34] Munees Ahemad and Abdul Malik, *Bacteriology Journal*, 2 (2012) 12-21

Chapter 9

SUMMARY AND FUTURE PROSPECTS

Nanotechnology is a multidisciplinary field of applied science and technology, which aims at controlling of matter on the atomic scale and the designing of atomic and molecular scale devices. Nanotechnology has already influenced all walks of human life. The integration of nanotechnology with biotechnology is an attractive trend, as the former provides the analytical tools and platforms for the investigation of biological systems. The role of semiconductor nanostructures on the present status of nanotechnology and nanobiotechnology is unfathomable. The technological developments in the synthesis of semiconductor quantum dots and the understanding of their optical properties have opened new application arenas from optical devices to biomedical detection and imaging. Fluorescent semiconductor quantum dots have become indispensable in biomedical and pharmaceutical research, especially for multiplexed, quantitative and long-term fluorescence imaging and detection.

Generally nanostructured materials do exhibit properties quite different from their bulk analogue due to quantum confinement effects. In the nanometre regime the size dependence of the material properties allows the desired tunability of properties over a wide range of particle size. Polymer nanocomposites consisting of a polymer host and a nanostructured semiconductor filler material find extensive applications in optoelectronics, magneto-optics, nanophotonics and biophotonics. In the first phase of the

work, polymer/inorganic nanocomposites and their films that offer attractive properties have been investigated, which include zinc oxide (ZnO) and iron disulfide (FeS_2) based polymer nanocomposites suitable for photonic applications. Nanometer sized fluorescent semiconductor materials have attracted considerable attention due to high luminescence intensity, low photobleaching, large Stokes' shift and high photochemical stability. The unprecedented optical and spectroscopic features of these nanomaterials make them very convincing alternatives to traditional fluorophores in a range of applications. In the second phase of the present work, bio-compatible and fluorescent, manganese doped zinc sulphide (ZnS) nanocrystals suitable for bio-imaging applications have been developed and assessed for cytocompatibility.

One-dimensional nanostructured materials, such as nanorods, nanowires, nanotubes, and nanobelts, have recently attracted much attention because of their special physical properties and widespread potential applications in optoelectronics and photonics. In the present study, the well known transparent conducting oxide, zinc oxide (ZnO) has been synthesized by wet chemical method at room temperature with and without oleic acid. Modification with oleic acid is found to result in the growth of long and well separated ZnO nanorods of approximately 25 nm in diameter. Highly transparent, ZnO/PVA nanocomposite films could be realized using spin-coating technique from pristine and OA modified ZnO nanorods.

One of the highlights of the present work is that, small amounts of oleic acid modified ZnO nanorods (1 weight%) are sufficient as the filler material to suitably modify the optical absorption characteristics of the ZnO/PVA nanocomposite. Such nanocomposites are quite significant from the view point

of the production cost. The excellent UV absorption around 300 nm of OA modified ZnO/PVA nanocomposite films offers prospects of making efficient UV filters, or UV protectors for the UV shielding in plastics, textiles, paints, cosmetics, and packaging in a cost effective way.

Photoluminescence studies of ZnO/PVA nanocomposite films with and without oleic acid modification have brought about significant results. The intensity of PL emission observed at 364 nm is found to be higher in films prepared from OA modified ZnO nanorods. Oleic acid can be absorbed on to the surfaces of ZnO nanorods via electrovalent bonds which can affect the homogeneous dispersion of nanorods in the PVA matrix. The better dispersion of OA modified ZnO nanorods in the PVA matrix can be the prime factor contributing towards the higher PL intensity in the ZnO/PVA nanocomposite films prepared from OA modified ZnO. Another interesting aspect is the significant extent of surface modification of ZnO nanorods, brought about by the PVA matrix. The surface modification results in the removal of defect states within ZnO and the quenching of the PL emission in the visible region. The combined effect of oleic acid and PVA modification considerably reduces the PL emission in the visible region and confines the emission entirely to the UV region.

Among conducting polymers, polyaniline (PANI) is the most promising material because of its tunable electrical and optical properties, environmental stability, low cost of production and high yield of polymerization. Oleic acid modification has already been found to work wonders with the inorganic semiconductor ZnO. As part of the present investigations, attempts have been hence made to explore in detail, the effect of oleic acid modification on the structural and optical properties of the organic semiconductor, polyaniline.

In the present study, highly luminescent orthophosphoric acid doped PANI has been developed by treating with oleic acid, without considerably affecting its structural properties. This work highlights the enhanced photoluminescence emission observed in oleic acid modified PANI compared to PANI. The enhanced emission intensity in oleic acid modified PANI is the effect of capping of oleic acid on each PANI molecule resulting in the formation of nanostructured PANI. The band gap of oleic acid modified PANI is found to be blue shifted considerably from that of PANI which is another signature of the creation of nanostructured PANI samples upon modification with oleic acid. From FESEM studies, the oleic acid modified PANI is found to have rod like structure of diameter less than 100 nm, compared to the PANI sample without oleic acid, where the PANI molecules are found to have more agglomeration.

The second category of polymer nanocomposites investigated in the present work makes use of nanostructured iron disulfide (FeS_2) as the filler material. Nanocomposites of pyrite FeS_2 with polyvinyl pyrrolidone (PVP) and PVA as templates have been successfully synthesized using thiourea-mediated solvothermal process at 150^{o}C. The XRD analysis confirms the formation of nanostructured FeS_2 particles of size around 20 nm. A simple and effective solution casting approach has been used to realize thin films of these nanocomposites on glass and flexible substrates.

The highlight of the work on FeS_2/polymer nanocomposites is the identification of the excellent UV shielding efficiency (almost zero transmittance) of these nanocomposite films in the wavelength range 200 to 400 nm. It is also observed that free standing films of FeS_2/PVA nanocomposite can be easily obtained by peeling the films off from the

substrate with the additional advantage that these transparent and flexible films can be directly attached as UV protective layers. The present work on FeS_2/PVA and FeS_2/PVP nanocomposite films, opens new opportunities for developing good quality, transparent and flexible films for UV-shielding applications by controlling the reaction time, temperature and also by employing other soft templates.

With a multitude of opportunities for nanomaterial use in medical and pharmaceutical applications, a thorough understanding of associated systemic toxicity is critical. In this context, the synthesis of bio-compatible ZnS:Mn nanocrystals functionalized with capping agents like chitosan and aminoacid ligands is extremely important. The second phase of the present work is devoted to the studies on highly luminescent, manganese doped zinc sulphide (ZnS:Mn) nanocrystals, biofunctionalized with chitosan and various aminoacids such as L-citrulline, L-lysine, L-arginine, L-serine, L-histidine and glycine, synthesized by chemical capping co-precipitation method at room temperature, which is a simple and cost effective technique. The biofunctionalized ZnS:Mn nanocrystals possess high colloidal stability and show strong orange red photoluminescence emission at 598 nm.

Taking into consideration the prospects of these highly luminescent, biofunctionalized ZnS:Mn nanocrystals in bio-imaging applications, cytotoxicity studies have been conducted to identify the capping combination suitable for achieving minimum toxic effects. ZnS:Mn nanocrystals biofunctionalized with L-citrulline, glycine, chitosan, L-artginine, L-serine and L-histidine show least toxicity up to 10 nM concentrations in mouse fibroblast L929 cells, which further confirms their cytocompatibility. In particular, L-citrulline capped ZnS:Mn is found to be 100% nontoxic for 0.1 nM

concentration and L-arginine capped ZnS:Mn, for 1 nM concentration. The ZnS:Mn nanocrystals biofunctionalized with L-arginine show maximum uptake in *in vitro* studies carried out in human embryonic kidney cells, HEK293T. In conclusion, the present study proposes aminoacid conjugated ZnS:Mn nanocrystals, to be promising candidates for biomedical and pharmaceutical applications.

The immobilization of proteins with bio-compatible nanoparticles has drawn considerable interest, as it expands the range of potential applications that includes the delivery of proteins and vaccines to the systemic circulation and to the immune system. In the present study, trypsin has been immobilized on chitosan conjugated zinc sulphide nanoparticles doped with manganese (ZnS:Mn) using glutaraldehyde (GA) as cross-linker. The bioconjugation of trypsin with ZnS:Mn has been confirmed by photoluminescence (PL) and Fourier transform infrared (FTIR) spectroscopic studies. Results indicate that the activity of trypsin, immobilized on chitosan modified ZnS:Mn has improved upon cross-linking, which suggests that the immobilized trypsin has become more stable and active. The present work highlights the prospects of potential applications of immobilized trypsin in therapeutic and diagnostic fields.

Part of the present investigations is devoted to the detection of a special type of metal accumulating bacteria, *Lysinibacillus fusiformis.* This bacterium has significant applications in the disposal of metal components from industrial effluents. The L-citrulline conjugated ZnS:Mn nanocrystals (size 10 nm) could be attached to *Lysinibacillus fusiformis* and characteristics of the bioconjugated system have been studied. The blue shift observed in the UV-Visible absorption and photoluminescence (PL) spectra of the

bioconjugated system, confirms the conjugation of the *Lysinibacillus fusiformis* with the L-citrulline capped ZnS:Mn. Analysis of FT-IR spectra and fluorescent microscopic images provides further evidence for the attachment of bacteria with L-citrulline conjugated ZnS:Mn and the latter can hence be used as an efficient biosensor to mark the presence of the metal accumulating bacteria, *Lysinibacillus fusiformis.* The study of relative growth of *Lysinibacillus fusiformis* in the presence of L-citrulline modified ZnS:Mn, shows that even in the environment of 10% (v/v) of the nanocolloid, there is no significant retardation in the growth of bacteria, which further confirms the bio-compatibility of these nanocrystals. The bio-compatible nature of these nanocrystals and, their tunable colour properties under different excitation wavelengths, make them ideal for bio-imaging applications.

Future prospects

The present investigations offer ample scope for further research in these areas. Vertically grown ZnO nanorods for solar cell applications can be developed using hydrothermal techniques. ZnS:Mn nanocrystals conjugated with cancer- targeting ligands like folic acid can be developed and investigated for targeted cancer imaging. The nature of binding of ZnS:Mn nanoparticles with different types of biomolecules is to be investigated in depth. ZnS:Mn quantum dots with extremely small size for therapeutic applications can be developed by methods like laser ablation. The present investigations highlight the significance of using suitable amino acids for the bioconjugation of ZnS:Mn nanocrystals. Continued research in this field will provide a better understanding of bio-compatible capping agents and will undoubtedly help the design of safe and effective nanoparticle platforms for biomedical

applications. In addition, the potential of immobilized trypsin in therapeutic applications has to be explored in detail.

*"**The smaller we can get, the higher we can go"***

The part of the work described below could not be included in the main thesis since it was being assessed for patent filing during the completion of the thesis. The patent filing has now been completed and hence these results are included as an annexure to the main thesis.

Bio-compatible, L-citrulline modified ZnS:Mn nanocrystals as fluorescent probes for DNA visualization and for forensic finger print analysis.

Water dispersible, nanometer sized fluorescent semiconductor materials have attracted considerable attention in recent years due to their unique emission characteristics. The high luminescent intensity, low photobleaching, large Stokes' shift and high photochemical stability are some of their remarkable properties. Fluorescence is a powerful tool in biological research, the relevance of which relies greatly on the availability of sensitive and selective fluorescent probes. The routinely employed chemical fluorophores usually have some drawbacks, including susceptibility to chemical changes in the medium and to photobleaching, fixed emission spectra, and limited Stokes' shift. The unprecedented optical and spectroscopic features of nanostructured semiconductors make them very convincing alternatives to traditional fluorophores in a range of applications, including multiplex bioanalysis.

ZnS is a semi-conducting luminescent material with a wideband gap of 3.70 eV, which exhibits excellent emission characteristics with high luminescent intensity and narrow emission bands. The orange light emitting, manganese doped ZnS nanocrystallite, is of special interest due to its high

photoluminescence efficiency and stability at ambient conditions, which constitute the critical properties required for commercial electro-luminescent devices. Since ZnS is a moderately toxic material, capping with aminoacids make these nanocrystals more biocompatible and less toxic. The main advantage of biocompatible ZnS:Mn nanocrystals is that they can be attached to biomolecules such as DNA, RNA and protein for biosensing applications.

The present work deals with the synthesis and luminescent properties of manganese doped ZnS (ZnS:Mn) nanocrystals capped with L-citrulline, an aminoacid ligand, and the applicability of these capped nanocrystals as DNA-staining dye , by replacing ethidium bromide.

The L-citrulline capped ZnS:Mn nanocrystals were prepared by a chemical capping co-precipitation method in which zinc acetate, manganese acetate, L-citrulline and sodium sulphide were used as the reactants. The synthesized nanocrystal of average particle size 10 nm was structurally characterized by TEM, XRD, EDXS and FT-IR spectroscopic techniques. The binding of DNA with the biofunctionalized ZnS:Mn, was confirmed from FTIR spectral analysis. The photoluminescence (PL) spectrum of L-citrulline capped ZnS:Mn nanocrystals in aqueous solution shows intense, orange emission centered around 598 nm. The shift observed in the photoluminescence peak is used as the confirmatory evidence for the binding of DNA with the capped nanocrystals.

A variety of nucleic acid binding dyes have been developed, mostly for agarose gel staining, of which ethidium bromide (EtBr) is the most common, sensitive and easy stain for DNA. The major drawback to EtBr use is that it is a potent mutagen. Solutions are to be handled with extreme caution, and

decontaminated prior to disposal. According to Material Safety Data Sheet, ethidium bromide is hazardous. The ZnS:Mn nanocrystals capped with L-citrulline have been used as a substitute for EtBr in the present study, by incorporating them into an agarose gel for electrophoresis. The *in vitro* toxicological analysis of these capped ZnS:Mn nanocrystals in mouse fibroblast L929 cells shows that ZnS:Mn nanocrystals capped with L-citrulline are 100% non toxic and hence highly bio-compatible. The highlight of the present work is the identification of L-citrulline capped Zns:Mn as a cost effective and non-hazardous alternative to ethidium bromide for DNA staining applications.

Sensitivity of DNA staining method using L-citrulline capped ZnS:Mn nanocrystals is highly comparable to ethidium bromide based methods and is found to be ideal for applications requiring rapid DNA band visualization in a safe and non-hazardous environment. The DNA visualization employing the conventional dye, ethidium bromide and using L-citrulline capped ZnS:Mn nanocrystals is illustrated in figure1 (a) and figure 1 (b) respectively.

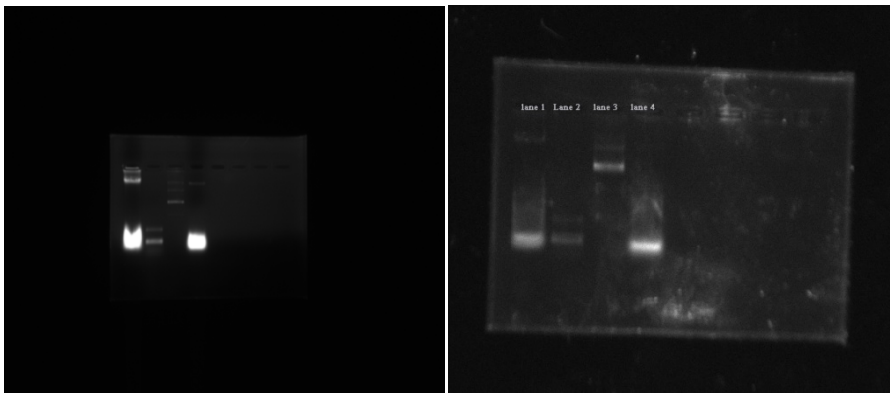

Figure 1(a) DNA visualization using ethidium bromide and 1(b) DNA visualization using L-citrulline capped ZnS:Mn nanocrystals (Lane-1 DNA marker, Lane-2 PCR product, Lane -3 plasmid DNA and Lane-4 genomic DNA)

The L-citrulline capped ZnS:Mn, has the prerequisites to be used as a powder for forensic finger printing analysis. The capped ZnS:Mn in powder form, which is white in colour becomes orange red (fluoresces) when exposed to UV radiation. The powder is found to be fine enough to show the details of the fingerprint. It has been observed that finer powders are theoretically more capable of displaying finer finger print details than coarser powders. The L-citrulline capped ZnS:Mn displays the right level of adhesion, so that it can adhere well to the residue of the fingerprint (often oils) and not to the rest of the surface where it would obscure the view of the print. This powder can flow more effectively and it does not 'cake' into a solid block, which would render it useless. In addition, the capability of the powder to fluoresce under UV light can be used to advantage in this application. The photograph of finger print, dusted with the L-citrulline capped ZnS:Mn powder is shown in figure 2.

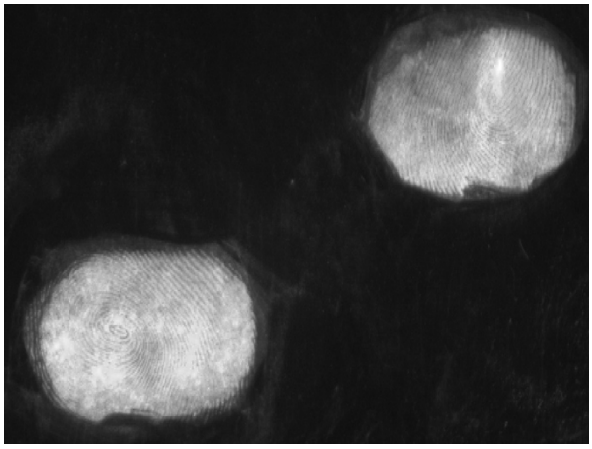

Figure 2 The photograph of finger print, dusted with L-citrulline capped ZnS:Mn powder.

The work described above has been submitted for patent filing with file number **4900/CHE/2012.**